AN EXPERIMENTAL INVESTIGATION OF CIRCULAR PLATES, BEAMS AND STIFFENED CIRCULAR PLATES SUBJECTED TO IMPULSIVE LOADING

by

DM LUMPP

1990

Submitted to the University of Cape Town
in partial fulfilment of the requirements for
the degree of Master of Science

DECLARATION

I, DIRK MANFRED LUMPP, declare that this thesis is essentially my own work and has not been submitted in this or in a similar form for a degree at this or any other university.

ABSTRACT

This primarily experimental investigation describes a series of experiments on fully-clamped circular plates, rectangular beams and stiffened circular plates. These test specimens were subjected to a uniformly distributed impulse.

The impulse was provided by plastic explosive. This was arranged in such a way that a uniformly distributed impulse was imparted to the test specimens. The impulse was measured by means of a ballistic pendulum to which the test specimens were attached. The final mid-point deflections of the plates and beams were measured.

The plate and beam results were compared to previous experimental work. A non-dimensional number for plates was modified to include an experimental mass scaling factor due to the ballistic pendulum mass. A non-dimensional number for rectangular beams was developed, including a similar experimental mass scaling factor. Comparing the beam and plate results from this study with those of previous work, using the respective non-dimensional numbers, showed good correlation.

The results for the stiffened plates are compared with the plate results.

ACKNOWLEDGEMENTS

The author wishes to thank the following:

Assoc Prof GN Nurick : for his guidance, advice, encouragement and his time spent preparing and detonating the explosive charges.

Ranval Engineering (Pty) Ltd. for making the clamping rig.

Prof LP Adams and Miss A Tregidga: for their assistance in measuring the deformed plates.

Mr V Appleton: for taking the photographs.

Somchem (Pty) Ltd. for providing the explosive material.

The Department of Mechanical Engineering and the Centre for Research in Computational and Applied Mechanics for their financial assistance.

TABLE OF CONTENTS PAGE

PAGE

LIST OF FIGURES

PAGE

PAGE

PAGE

LIST OF TABLES PAGE

NOMENCLATURE

E	Energy
E_p	Total plastic strain energy
I	Total impulse
M	Total mass of ballistic pendulum
R	Plate radius
R_o	Plate radius over which impulse is imparted
V_o	Impact velocity
b	Stiffener/beam width
h	Stiffener/beam thickness
l	Stiffener/beam length
m	Mass of test specimen
m_e	Mass of explosive
n	Material constant
r	Distance in radial direction
t	Plate thickness
u	Displacement in radial direction
z	Distance from plate middle surface
α	Johnson's damage number
β	Geometry number
δ	Test specimen mid-point deflection
$\dot{\varepsilon}$	Strain rate
$\dot{\varepsilon}_o$	Strain rate material constant
$\phi(r)$	Mode shape function
ϕ_b	Modified damage number for beams
ϕ_c	Damage number for circular plates
ϕ_c^1	Modified damage number for circular plates
ω	Vertical displacement of test specimen
μ	Experimental mass scaling factor
ω_o	Maximum displacement of the centre of the test specimen
υ	Poisson's ratio

ρ	Test material density
σ_d	Damage stress
σ_y	Yield stress
σ_o	Uniaxial static yield stress
σ_o^1	Dynamic yield stress
$\sigma_{\theta\theta}$, $\varepsilon_{\theta\theta}$	Stress and strain in circumferential direction
σ_{rr}, ε_{rr}	Stress and strain in radial direction
χ	bending strain in plate per unit length

GLOSSARY

Series I tests:	Preliminary tests
Series P tests:	Plate tests
Series B tests:	Beam tests
Series PS tests:	Stiffened plate tests

P	Plate test
B-x	Beam test where x denotes the beam thickness in mm
PS-x	Stiffened plate test where x denotes the stiffener thickness in mm
PS-xS	Plate stiffener where x denotes the stiffener thickness in mm
PS-xP	Plate component of stiffened plate where x denotes the stiffener thickness in mm

CHAPTER 1 - INTRODUCTION

This study presents a primarily experimental investigation into the dynamic response of impulsively loaded thin circular plates stiffened by rectangular beams. Several studies have been performed on either beams or plates, but not on a combined structure. A number of experiments on plates and beams were also performed in this study.

Chapter 2 begins by giving a summary of the previous experimental work performed on beams and plates. Various types of testing techniques have been used. These include underwater explosive forming, air-blast loading, impulsive loading using plastic sheet explosives and spring-loaded arms. The above work was primarily concerned with the final deformed shape and the deflection-time history of the test structure. Chapter 2 then continues by describing the technique used in this study. Plastic explosive was detonated against the test structures to simulate impulsive loading. A ballistic pendulum was used to measure the magnitude of the impulse. Measurements were taken to determine the final mid-point deflections and the final deformed shapes of the test specimens. Over 100 tests were performed.

The mild steel plates and beams were assumed to be rigid-viscoplastic. The Cowper-Symonds relation was used to determine the static and dynamic yield stresses for the analysis.

Chapter 2 concludes by commenting on two experimental observations: firstly a gap is observed between the stiffened plate and its stiffener and secondly the tearing that occurrs in the stiffener before tearing occurrs in the stiffened plate.

Chapter 3 presents the theoretical analysis in which an energy solution is used to determine the energy of deformation of the test structures. The energy formulation developed by Duffey [1] was

chosen. Since this method is dependent on a deformed shape approximation, several were investigated. The strain-rate sensitivity and the work hardening effect of the mild steel material are also considered, and a method developed by Symonds and Wierzbicki [2] is given to determine the dynamic yield stress of plates.

The experimental and theoretical results are presented in Chapter 4. The circular plate and beam results are compared with previous experimental work. Non-dimensional damage numbers, which include an experimental mass scaling factor due to the mass of the ballistic pendulum, are given for both plates and beams. The stiffened plate experimental results are given and a deformation energy comparison for different stiffener thicknesses is presented.

Chapter 5 presents a discussion of the results obtained in this investigation.

Chapter 6 concludes this thesis with recommendations for future work.

CHAPTER 2 - EXPERIMENTAL DETAILS

2.1 INTRODUCTION

The purpose of this investigation has been to determine the dynamic response of stiffened circular plates, which have been fully clamped. A stiffened plate consists of two components: a circular plate and a rectangular beam stiffener. The primary concerns were to measure the final mid-point deflections and to observe the final deformed shapes of the stiffened plates. From these the influence of the different stiffener thicknesses on the plates could be determined. Fig. 2.1 shows a typical stiffened plate, from this study, after being subjected to an impulsive load.

Only very few experimental studies have been attempted to determine the response and damage of stiffened plates. However several experimental studies have been carried out on plates and on beams individually, primarily to determine the deformed shapes and the deflection-time histories.

The experimental studies performed to determine the dynamic plastic behaviour of thin plates subjected to impulsive loading have been reviewed by Nurick and Martin [3]. In this review it is reported that four types of impulsive loading have been used.

The first type of loading subjects structures to underwater explosions. It is reported by Nurick and Martin [3] that the earliest studies of this type were by Taylor on large steel plates, which measured 1,83 × 1,22 m, in 1942. Subsequent investigations were carried out by Travis, Johnson, Finnie, Williams, Boyd and Bednarski on circular plates and diaphragms in the 1960's.

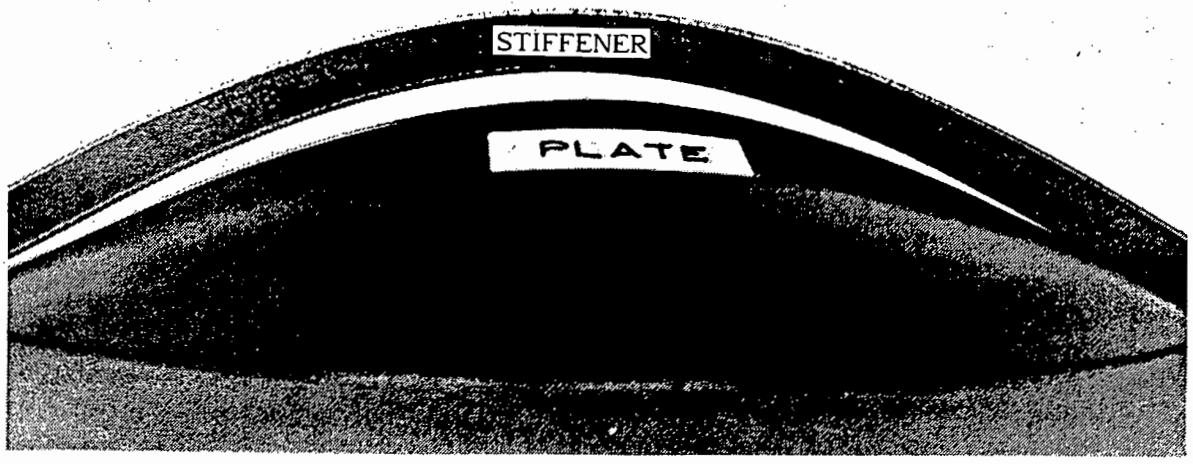

SIDE VIEW

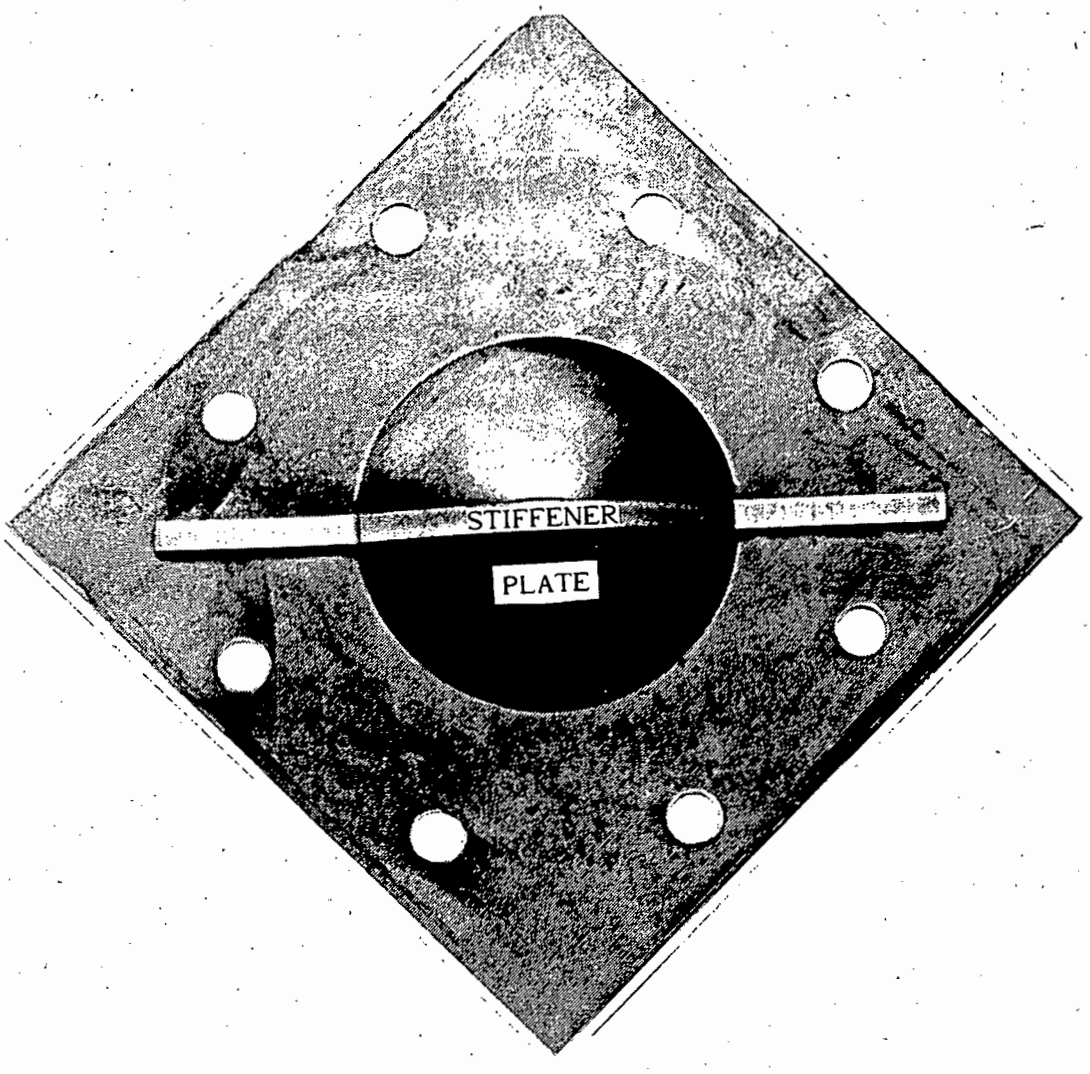

TOP VIEW

FIGURE 2.1 PHOTOGRAPH OF A STIFFENED PLATE

The second type of loading concerns air-blast loading, in which the explosive is detonated at a distance from the test specimen and the damage is then caused by the air pressure waves impinging on the specimen. Chong *et al.* [4] loaded rectangular plates, which were subject to in-plane compressive loading. Houlston and Slater [5] in 1989 exposed typical warship stiffened panels to air-blasts . The panels measured 2,44 × 4,57 m and were stiffened with 76 × 152 mm T-beams at 0,914 m spacing. In 1990 Slater *et al.* [6] reported on tests performed by them on similar panels as well as square plates.

Nurick and Martin [3] reported that the third type of impulsive loading was first described in 1965 by Humphreys [7], in his work on clamped beams. This type of loading involves sheet explosive and a ballistic pendulum. Humphreys [7] used Dupont sheet explosive and found that its burn rate was 6700 $m.s^{-1}$ and that this is greater than the speed of sound in carbon steel, 5200 ms^{-1} (Halliday and Resnick [8]). It was thus felt that a fair approximation to instantaneous uniform loading was obtained.

Humphreys [7] recorded the response using a high-speed camera and found that the explosion was completely over before the beam had noticeably moved at all. Subsequent motion takes place under no load, purely as a result of the inertia. Thus the assumption of an initial velocity condition is a reasonable one.

Nurick [9] confirmed Humphrey's proposal [7], when he found the response time of the deformation of thin mild steel plates to be 140 - 190 μs. The natural period of the pendulum was 3,20 s, thus all the plastic deformation takes place well before the beam has moved. The recorded pendulum deflection is a direct indication of the maximum potential energy of the system after the dissipation of energy in plastic work. The maximum velocity of the ballistic pendulum can be calculated from this potential energy and thus the applied impulse can be determined.

Nurick [9] used annular rings of sheet explosive to simulate uniform impulsive loading of circular, rectangular and square plates.

The ballistic pendulum enables the applied impulse to be easily and accurately determined. Another method of finding the impulse when using sheet explosive is to calibrate the explosive mass with the imposed impulse, as was done by Wierzbicki and Florence [10].

The fourth type of impulsive loading is described by Gosh *et al.* [11], in which a spring-loaded arm was used, which accelerates the test specimen to a maximum velocity of 55 $m.s^{-1}$ and strikes it against a rigid anvil, where the deformation of the diaphragm takes place under pure inertia forces.

2.2 EXPERIMENTAL MEASUREMENTS

Measurements taken from the experiments included: the impulse, which was measured using a ballistic pendulum; the final mid-point deflections of the plates and beams, as well as the shapes of the deformations. The uniaxial yield properties of the plate and beam materials were also determined. These measurements are discussed in more detail in the following section.

2.3 EXPERIMENTAL PROCEDURE

2.3.1 Introduction

The experiments performed can be grouped into four series, namely:

Series 1: initial set of tests using different stiffener materials and dimensions. 10 tests.
Series P: circular plates only. 8 tests.
Series B: beams only. 33 tests.
Series PS: stiffened plates. 62 tests.

The Series 1 experiments were performed in order to get an initial understanding of stiffened plates. From these it was decided which stiffener material and cross-sectional dimensions to use. The effectiveness of the clamping rig was also investigated.

Hot-rolled wrought iron and key steel stiffeners were experimented with. The key steel was found to be too brittle in that the stiffener broke for relatively small plate deflections. The wrought iron was found to be suitable for the proposed experiments, since it was able to withstand larger deflections. Stiffener widths and thicknesses of greater than 8 mm caused the plate to tear for relatively low impulse values, compared to those obtained by Nurick [9]. Fig. 2.2 shows the tearing caused when using a 10 mm × 10 mm stiffener.

From this series of tests it was decided to use stiffeners made from hot-rolled wrought iron bar with a width of 8mm and a thickness of 6mm and less.

Series P experiments were performed in order to obtain reference data to which the Series PS experiments could be compared. The Series B experiments were performed to determine beam-only behaviour.

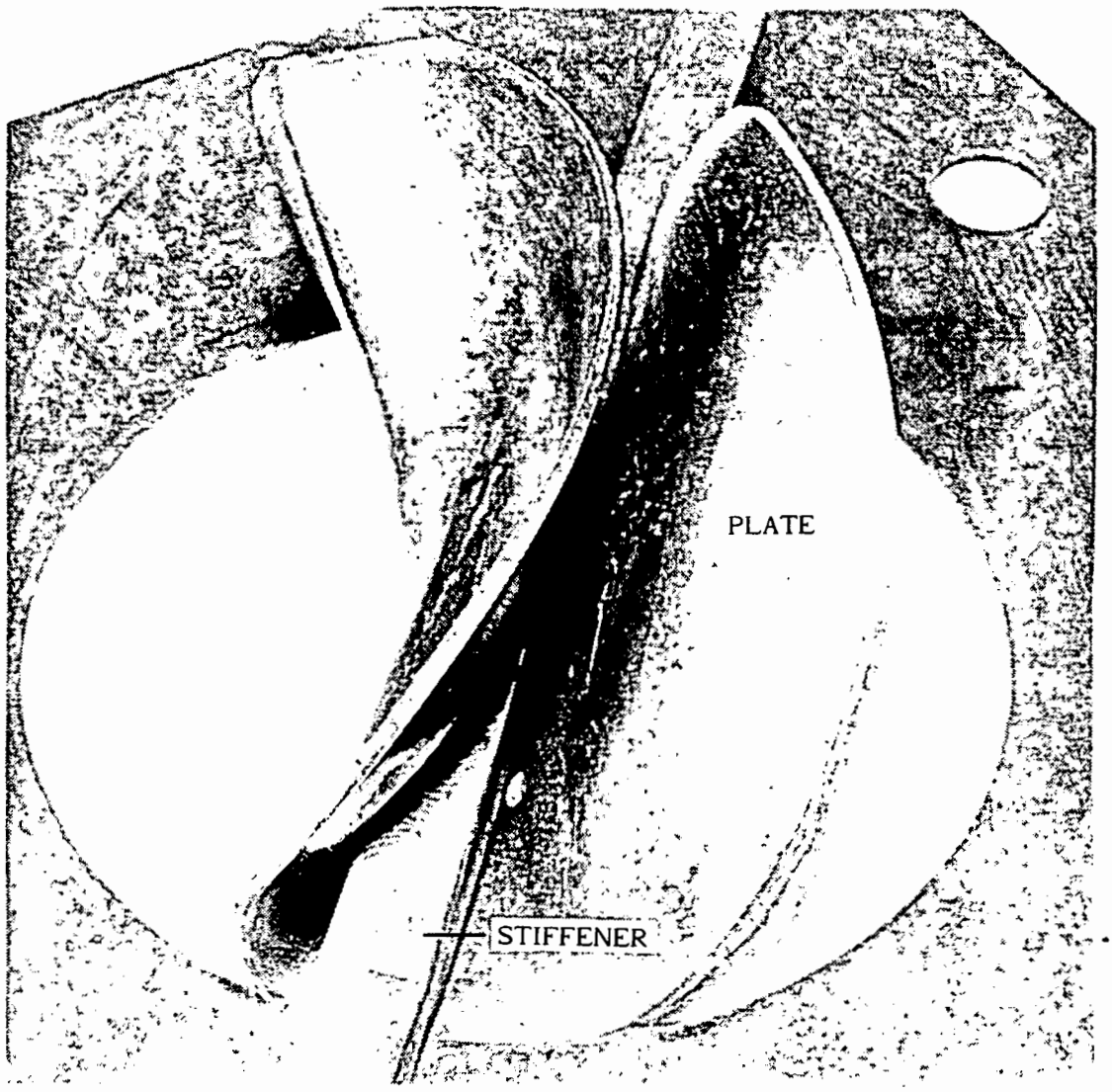

FIGURE 2.2 PHOTOGRAPH SHOWING TEARING CAUSED BY TOO STRONG A STIFFENER

2.3.2 Clamping Rig

The clamping rig was used to hold the test plates and beams in position during the impulsive loading. The rig itself was fixed to one end of the ballistic pendulum by four steel pillars.

Figs. 2.3(a) and 2.3(b) show the clamping rig. It consists of a 240 mm square mild steel base plate, two spacer plates and a securing ring. The test specimens are placed between the spacer plates and the base plate. The securing ring is used to clamp the spacer plates and the test specimens to the base plate by means of eight M12 high tensile bolts. The base plate is bolted to the four steel pillars.
The securing ring, spacer and base plates have 100 mm diameter holes in the centre through which the test specimens can deform when loaded.

The base plate and the securing ring are made of case-hardened mild steel, while the spacer plates are made of a high-alloy tool steel (AISI D2) which was hardened, air-quenched and then tempered to a hardness of 56 Rockwell. This was done to ensure that the clamping and boundary conditions for the test specimens remained the same throughout the series of tests.

The beams in the Series PS tests and the Series B tests are clamped by four M10 high tensile bolts. The M10 and M12 bolts were torqued to 80 N.m. and 130 N.m. respectively.

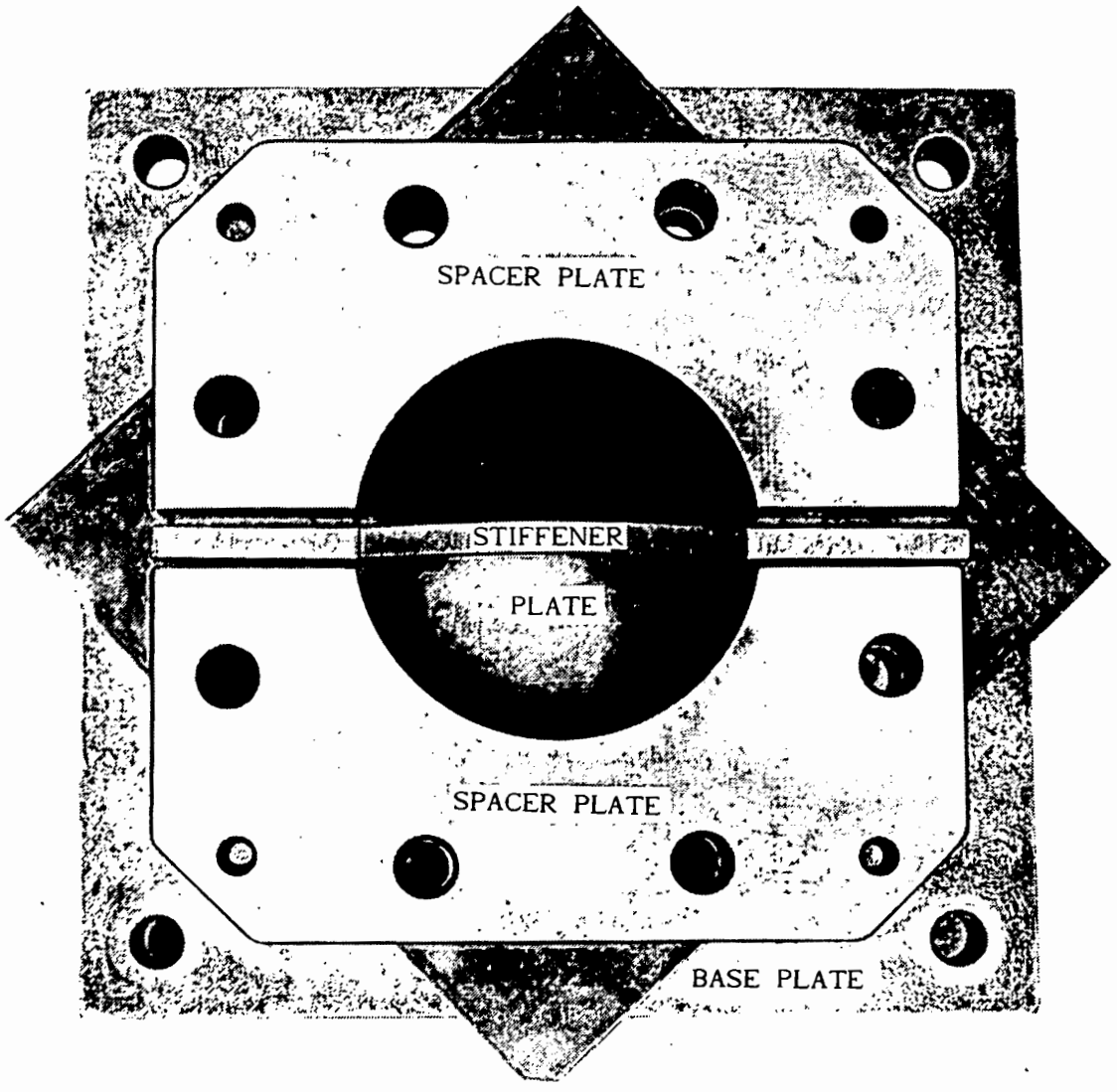

FIGURE 2.3(a) PHOTOGRAPH OF CLAMPING RIG WITHOUT SECURING RING

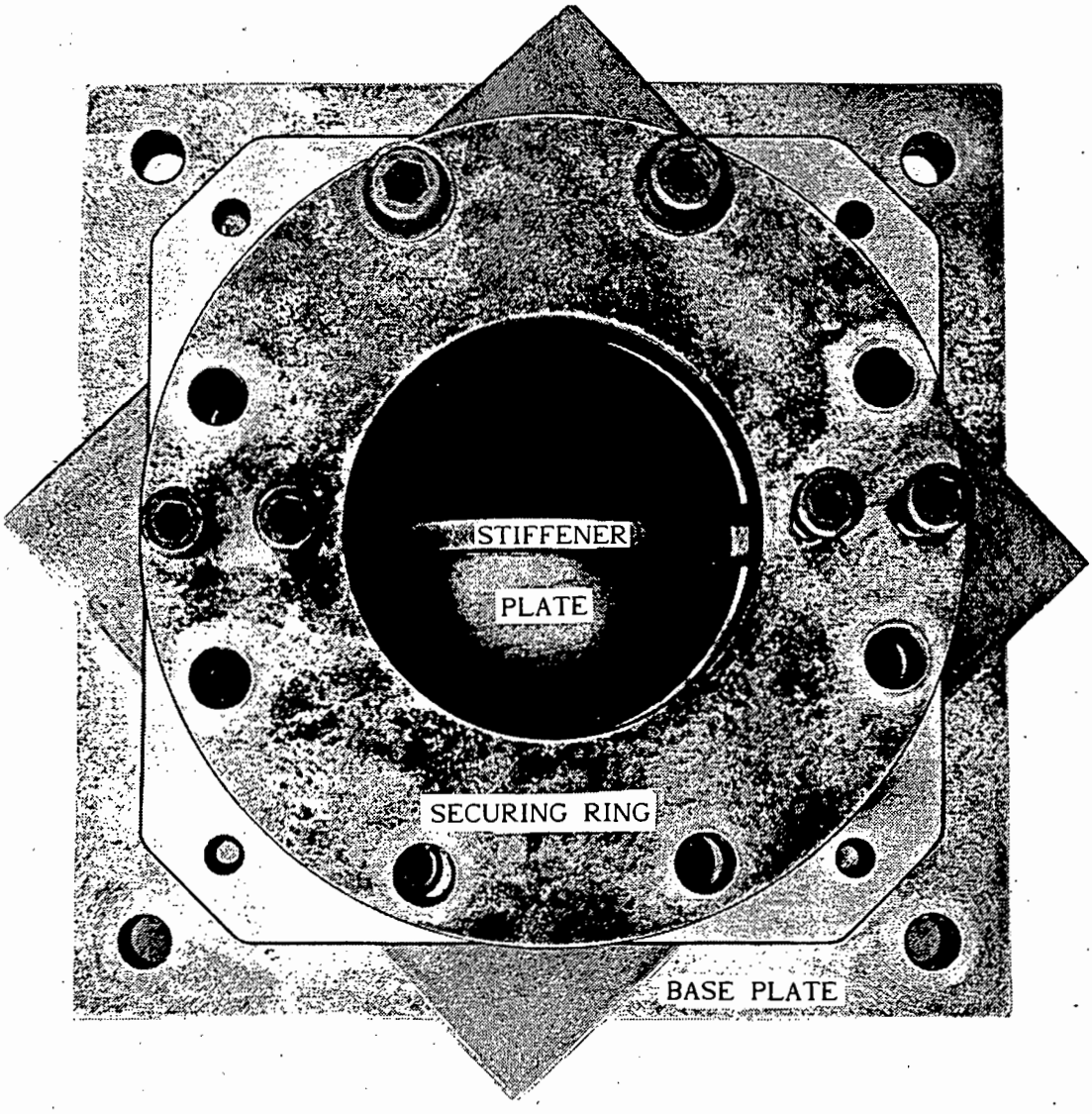

FIGURE 2.3(b) PHOTOGRAPH OF CLAMPING RIG WITH SECURING RING

2.3.3 Material Properties

The plate material used was cut from hot-rolled mild steel sheet and not annealed. The plate size was 200 mm square and 1,6 mm thick.

The beam material was cut from hot-rolled wrought iron bar. The beam length was 210 mm, the width was 8 mm and the thicknesses varied from 3 to 6 mm.

Tensile tests were performed on the the two materials at strain rates between $3{,}4 \times 10^{-4}\ s^{-1}$ and $1{,}4 \times 10^{-1}\ s^{-1}$. Typical stress-strain curves are shown in Figs. 2.4(a) and 2.4(b). Distinct yield stresses can be determined for both materials.

The Cowper-Symonds rigid-viscoplastic constitutive equation

$$\frac{\sigma_o^1}{\sigma_o} = 1 + \left(\frac{\dot{\varepsilon}}{\dot{\varepsilon}_o} \right)^{\frac{1}{n}}$$

where σ_o = static yield stress

σ_o^1 = dynamic yield stress

$\dot{\varepsilon}_o$ = uniaxial strain rate

$\dot{\varepsilon}$ = 40 sec^{-1}

n = 5

was used to calculate the static uniaxial yield stress. The choice of $\dot{\varepsilon}$ and n is discussed in section 3.3. The average static yield stress for the plates was 255 MPa and for the beams 427 MPa. The results for the tensile tests are given in Appendix A.

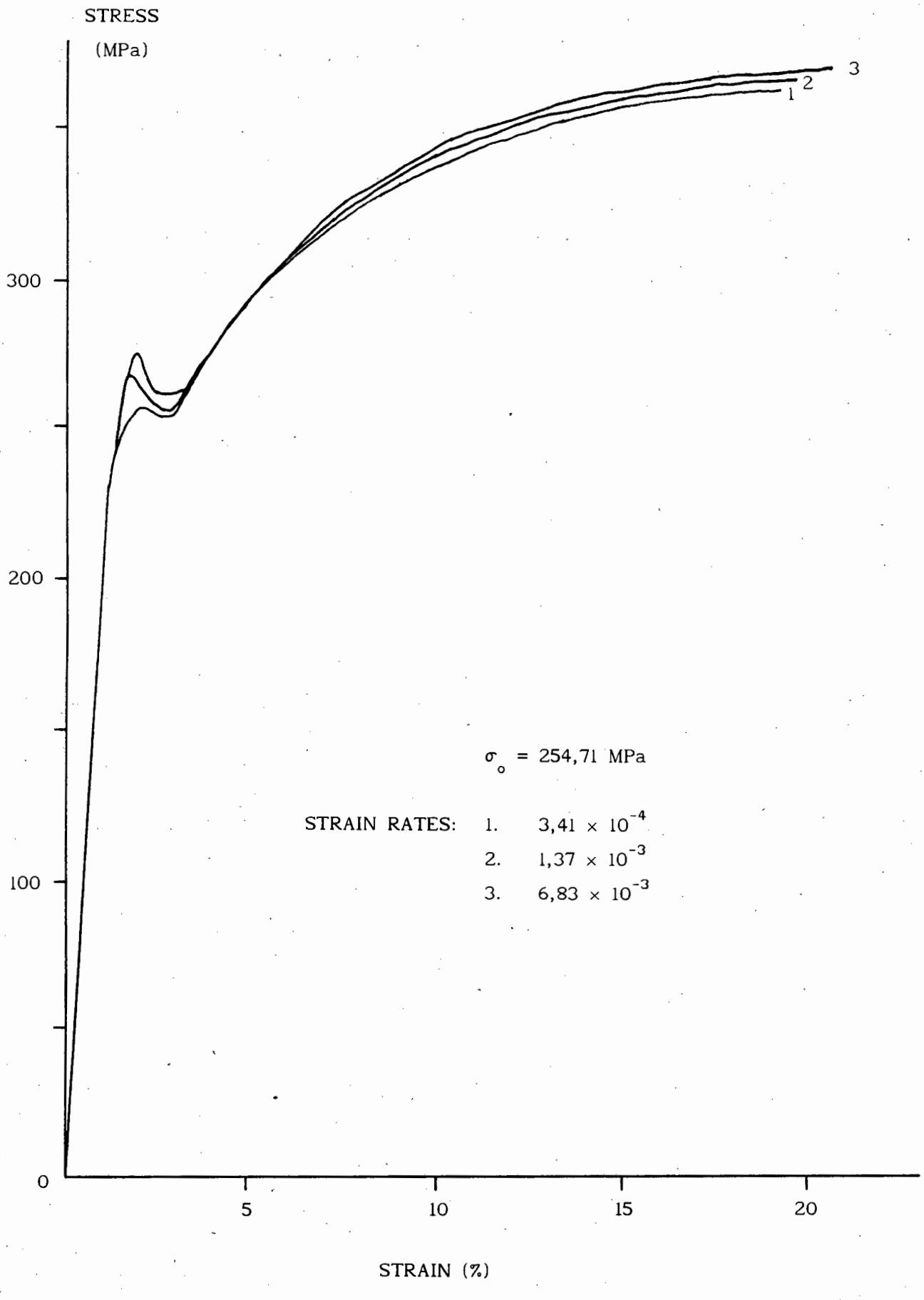

FIGURE 2.4(a) UNIAXIAL STRESS-STRAIN TENSILE TESTS FOR PLATE MATERIAL

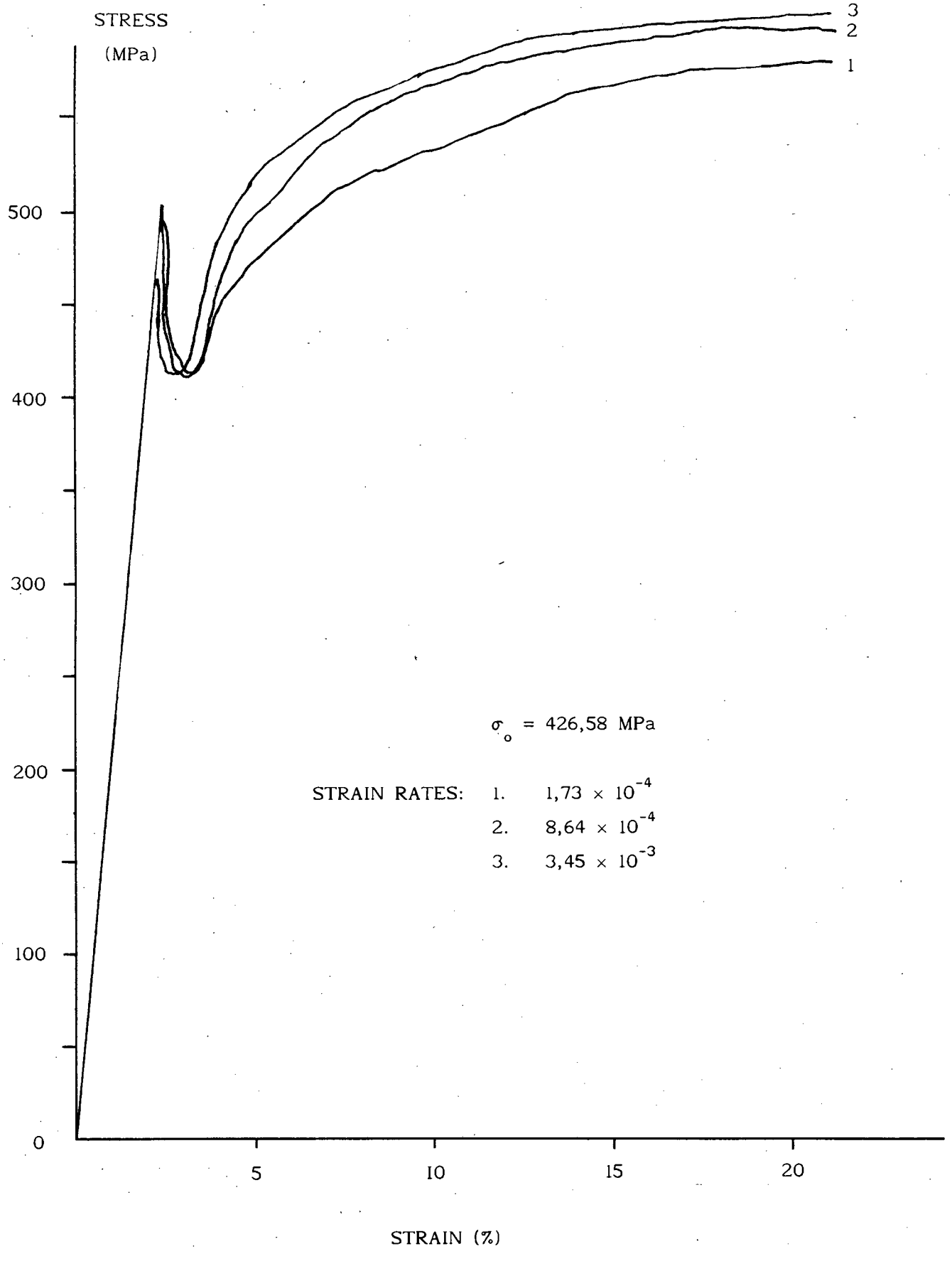

FIGURE 2.4(b) UNIAXIAL STRESS-STRAIN TENSILE TESTS FOR BEAM MATERIAL

2.3.4 Ballistic Pendulum

A ballistic pendulum as shown in Fig. 2.5 was used to measure the impulse imposed on the test specimens.

The pendulum was suspended from the concrete ceiling by four lengths of spring steel wire. Each of the four lengths had adjustable screws to allow the pendulum to be levelled. The experimental rig was attached to one end of the pendulum, while the balancing masses were bolted to the other end. The balancing masses ensured that each of the wire lengths carried approximately the same mass and that the impulse acted through the centroid of the pendulum. A pen at the balancing mass end recorded the pendulum oscillation. The amplitude of the initial swing is directly related to the impulse imposed on a test specimen.

The ballistic pendulum geometry is shown in Fig. 2.6.

The linearised equation of motion of the pendulum, assuming viscous damping, is

$$\ddot{x} + 2\beta\dot{x} + \omega_n^2 x = 0 \qquad (2.1)$$

where

$$\beta = \frac{C}{2M}, \quad \omega_n = \frac{2\pi}{T} \quad \text{and} \quad \omega_d = (\omega_n^2 - \beta^2)^{1/2}$$

and C is the damping coefficient, M is the total mass of the pendulum, experimental rig, balancing masses and explosive, and T is the natural period of the pendulum motion.

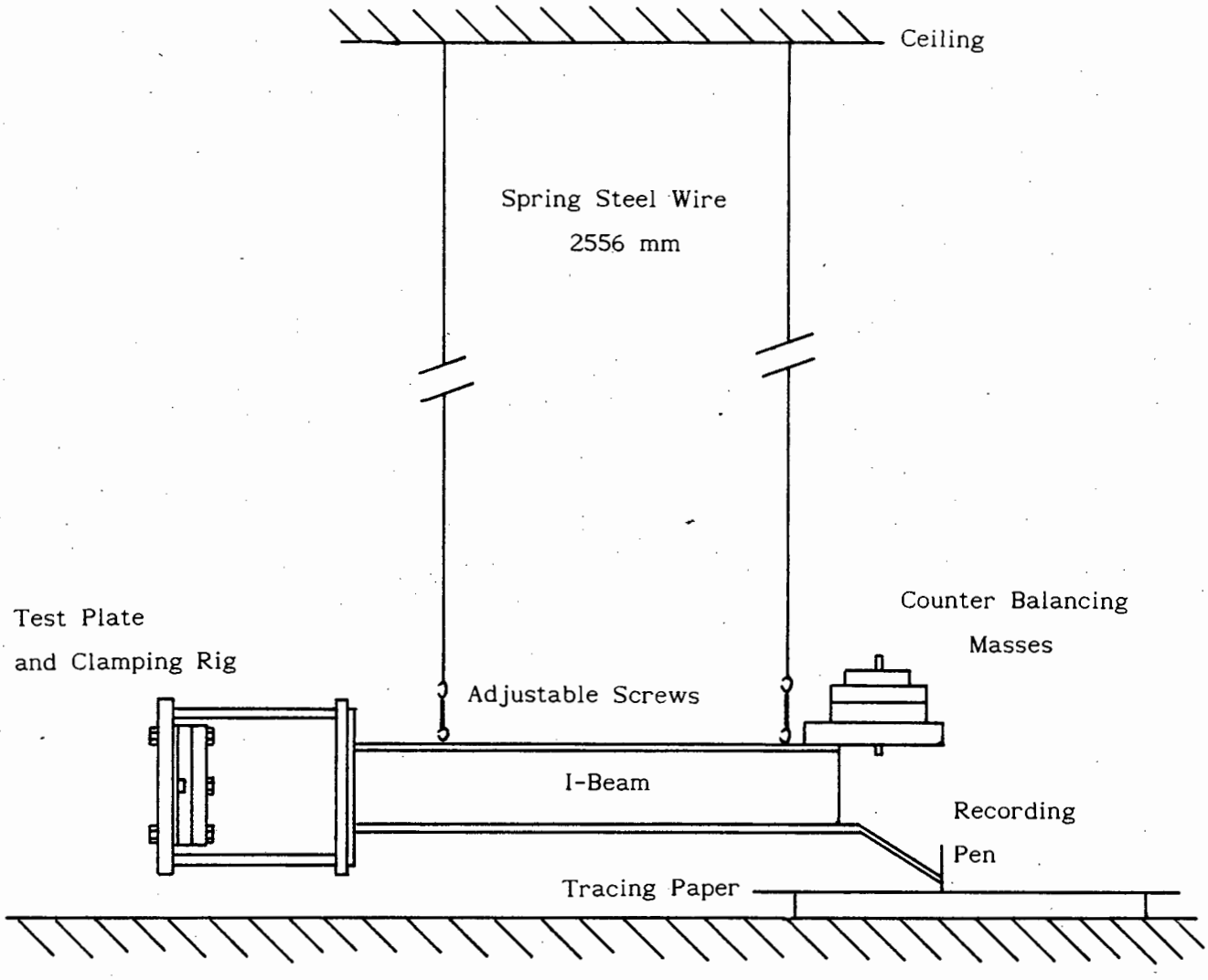

FIGURE 2.5 EXPERIMENTAL ARRANGEMENT

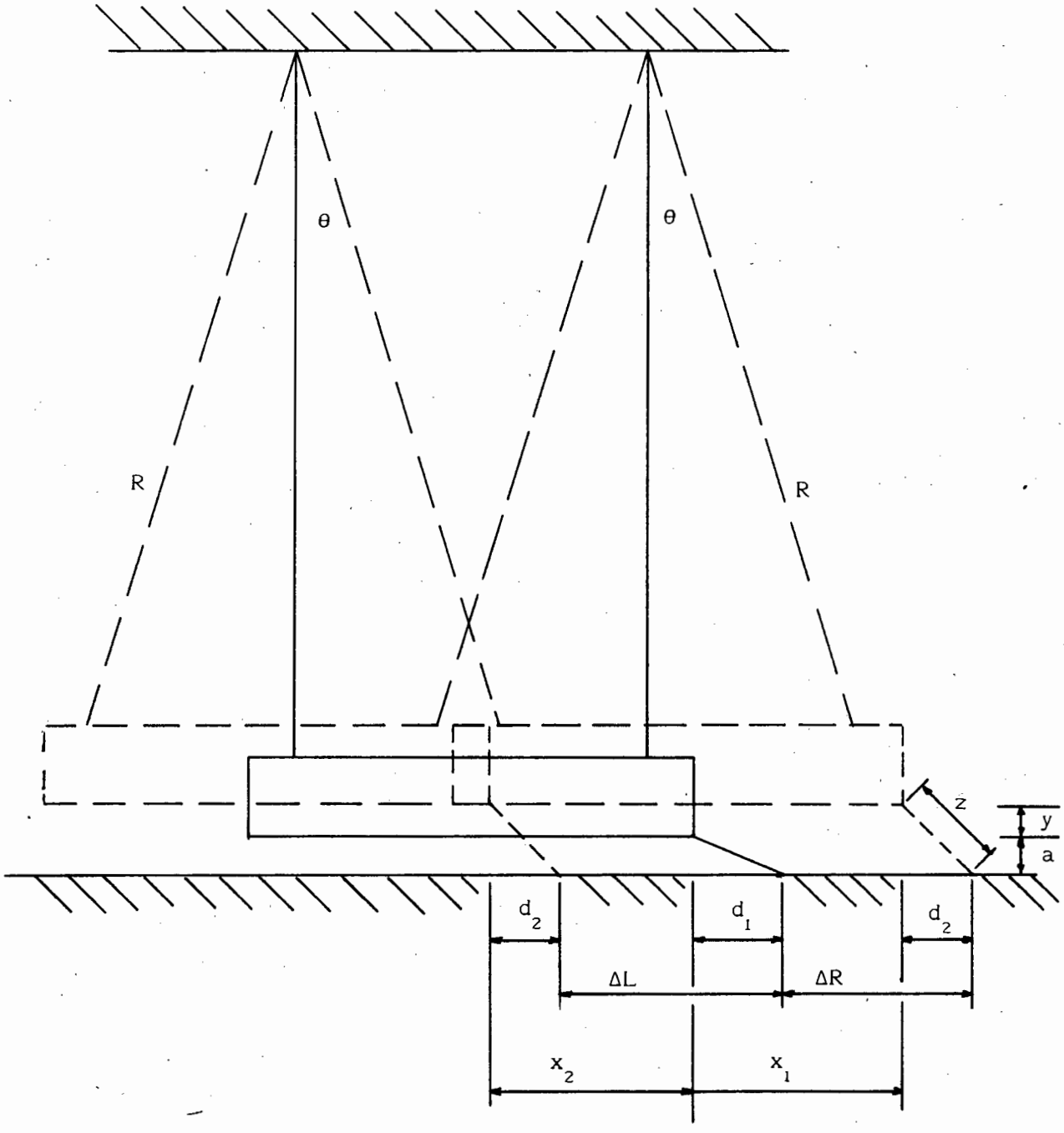

FIGURE 2.6 BALLISTIC PENDULUM GEOMETRY

The solution of equation (2.1) is given by

$$x = \frac{\left(e^{-\beta t} \right) \dot{x}_o \sin \omega_d t}{\omega_d} \tag{2.2}$$

where $\dot{x}_o$ is the initial velocity of the pendulum.

Let x_1 be the horizontal displacement at $t = \frac{T}{4}$ and

$-x_2$ be the horizontal displacement at $t = \frac{3T}{4}$

Substituting into equation (2.2) gives

$$x_1 = \frac{\dot{x}_o T}{2\pi} e^{-1/4(\beta T)} \tag{2.3}$$

$$x_2 = \frac{\dot{x}_o T}{2\pi} e^{-3/4(\beta T)} \tag{2.4}$$

Therefore

$$\frac{x_1}{x_2} = e^{1/2(\beta T)}$$

which gives

$$\beta = \frac{2}{T} \ln \frac{x_1}{x_2} \tag{2.5}$$

and

$$\dot{x}_o = \frac{2\pi}{T} x_1 e^{1/4(\beta T)}$$

The impulse can now be determined from

$$I = M \dot{x}_o \tag{2.6}$$

The period T is found by taking the average reading of a number of pendulum oscillations at full mass. The damping constant, β, is calculated from equation (2.5) where x_1 and x_2 are found from pendulum oscillations in which the pendulum is held away from the vertical and released.

The motion described by the pendulum, a circular arc, and the distance measured by the pen are not the same. This difference must be accounted for. Considering Fig. 2.6, the pendulum geometry, the horizontal distance from the end of the pendulum to the recording pen is given by

$$d_1 = \left(z^2 - a^2 \right)^{1/2} \tag{2.7}$$

while at peak oscillations the distance d_2 is given by

$$d_2 = \left(z^2 - \left(a + y \right)^2 \right)^{1/2} \tag{2.8}$$

The ballistic pendulum setup ensures that during testing the angle θ remains very small and therefore the assumption can be made that

$$x_1 \simeq R\,\theta \qquad \text{and} \qquad y \simeq \frac{R\,\theta^2}{2}$$

Therefore

$$y = \frac{x_1^2}{2R} \tag{2.9}$$

From Fig. 2.6

$$x_1 = \Delta R + d_1 - d_2$$

and

$$x_2 = \Delta L - d_1 + d_2$$

Substituting for d_1 and d_2, the corrected displacements become

$$x_1 = \Delta R + \left(z^2 - a^2 \right)^{1/2} - \left[z^2 - \left(a + \frac{x_1^2}{2R} \right)^2 \right]^{1/2} \qquad (2.11)$$

$$x_2 = \Delta L - \left(z^2 - a^2 \right)^{1/2} + \left[z^2 - \left(a + \frac{x_1^2}{2R} \right)^2 \right]^{1/2} \qquad (2.12)$$

where ΔL, ΔR, Z, a and R are measured and hence x_1 and x_2 can be calculated. Table 2.1 gives the constants of the ballistic pendulum as used for the experiments.

Table 2.1 Ballistic Pendulum Details

R	2556 mm	Mass of I-beam	22,0 kg
Z	170 mm	Mass of Test Rig	36,12 kg
a	52 mm	Mass of Counter Balance	37,94 kg
T	3,20 sec	Total Mass	96,06 kg
β	0,00547	Typical Pen Stroke	20 - 140 mm

2.3.5 Explosive Material

PE4 plastic explosive was used for all the experimental work. The explosive had the following specifications:

a) density: 1,545 $g.cm^{-3}$
b) detonation velocity: 7200 - 7500 $m.s^{-1}$

The detonation velocity is higher than the speed of sound in steel, 5200 $m.s^{-1}$ (Halliday and Resnick [8]), so the assumption that a good approximation to instantaneous uniform loading, ie. impulsive loading, was obtained seems reasonable.

A two-ring configuration, as used by Nurick [9], was used for all plate and stiffened plate experiments. Fig. 2.7 shows the explosive configuration. The two rings are connected to a cross-leader, which is connected by a main central leader to a shielded detonator. The cross-leader for the stiffened plates was placed at 90 degrees to the stiffener length. The explosive for the beam experiments was placed along the entire length of the beam and was detonated with a central leader from a shielded detonator.

In all the experiments the explosive was placed on a 16 mm thick polystyrene pad with the same dimension as the circular plate. This pad served as an attenuator to reduce the shock transmitted to the plate, to prevent spallation of the specimen and to provide a uniform impulse.

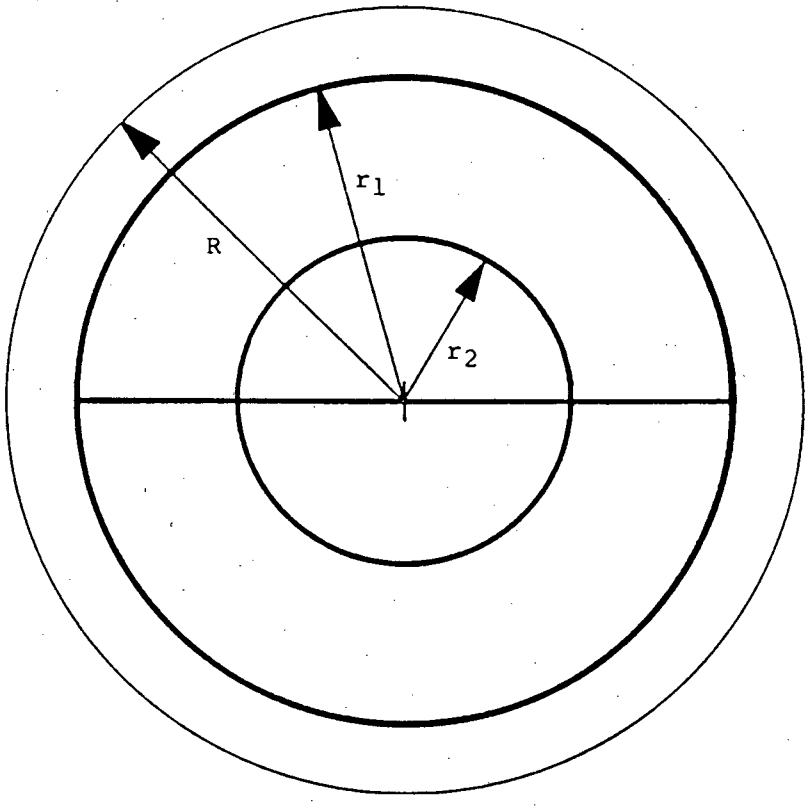

$r_1 = 0{,}82\ R$

$r_2 = 0{,}41\ R$

FIGURE 2.7 EXPLOSIVE CONFIGURATION

The ballistic pendulum's ability to measure the impulse for each test avoided the necessity of:

a) a separate series of calibration tests
b) the possible variation in the specified specific impulse of the explosive.
c) the variation that might occur because of factors such as variable plate and beam material, explosive geometry and boundary conditions.

Fig. 2.8(a) shows a plot of impulse versus explosive masses for the two-ring configuration used in the plate and the stiffened plate tests. It is apparent from this graph that there is no correlation in the data and that a ballistic pendulum is essential when using the PE4 explosive in the two-ring configuration.

Fig. 2.8(b) gives the plot of impulse versus explosive masses as used for the beam experiments. Although the correlation according to the least squares line is good, there are still significant variations justifying the use of a ballistic pendulum. The least squares line for the Series B tests is given by

$$I = 1{,}273\ m_e + 0{,}880 \quad \text{with} \quad r = 0{,}985$$

Metabel explosive was used in previous experimental work on plates using the two-ring configuration by Nurick [9] and Teeling-Smith [12]. Although the correlations to the least squares lines in these studies were good, it was noted that for equal explosive masses, the variations of impulse in some cases were quite large.

A probable reason for the inconsistency of the PE4 explosive in the two-ring configuration, is that the required impulsive loads resulted in the explosive needing to be rolled to thicknesses which were too

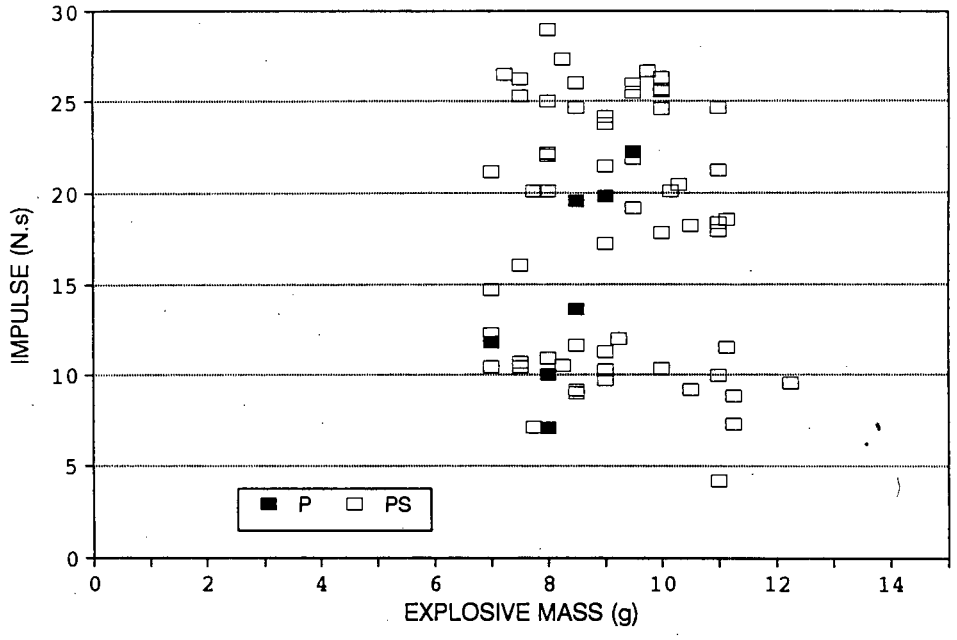

FIGURE 2.8(a) GRAPH OF IMPULSE vs. EXPLOSIVE MASS FOR PLATE AND STIFFENED PLATE TESTS

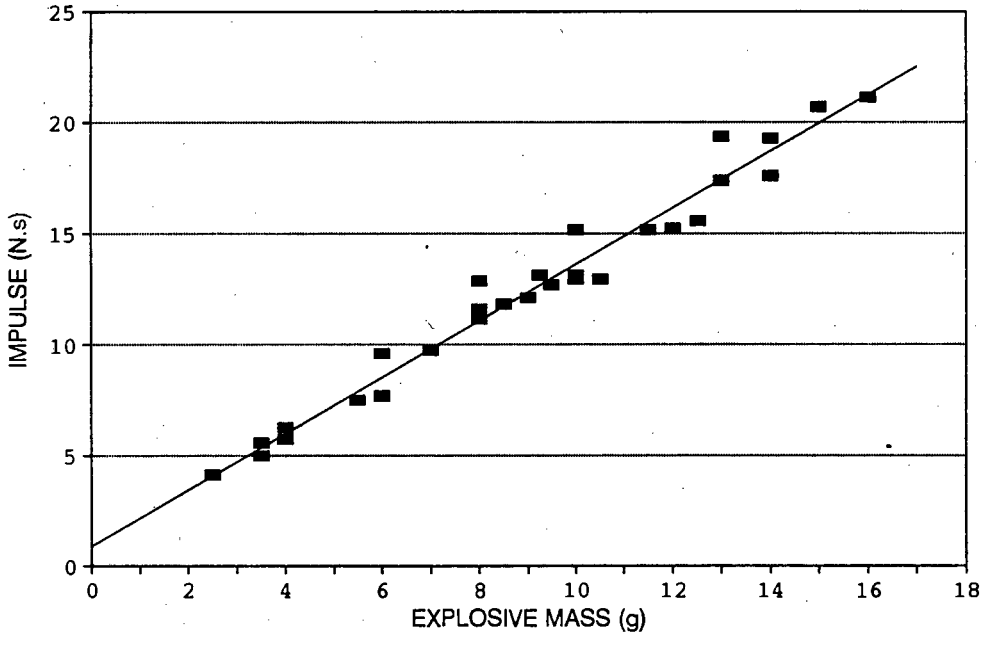

FIGURE 2.8(b) GRAPH OF IMPULSE vs. EXPLOSIVE MASS FOR BEAM TESTS

thin to effectively detonate. The fact that good correlation is evident in the beam-only experiments seems to substantiate this, since the explosive in this instance could be rolled to larger thicknesses.

2.4 TEST RESULTS

2.4.1 Introduction

Series 1 tests were conducted to obtain an initial understanding of the proposed experimental work. These tests were also used to determine the effectiveness of the clamping rig.

Eight Series P tests were done on plates only. One plate showed tearing on the cicumference and was not considered for the analysis.

62 Series PS tests were performed, of which 50 were used in the analysis. In 11 cases the plate tore and in one case the beam had not been clamped properly and slipped.

33 Series B tests were performed. In two cases no impulse reading was recorded, because the recording pen fell off and in three cases the beam broke.

In all, 103 tests were performed, of which 85 tests could be used in the analysis.

2.4.2 Test Readings

2.4.2.1 Impulse

The initial swing of the ballistic pendulum was measured and the impulse was determined from equation (2.6) in section 2.3.3.

2.4.2.2 Measured Deflection

Two methods were used to determine the final mid-point deflection of the test plates and beams. For all the test specimens the mid-point deflections were measured with a height vernier, while for selected plates and beams measurements were also made using a reflex microscope. This method enabled the complete deformed surfaces to be measured accurately. Approximately 350 points per plate and 45 points per beam were digitised. These were then interpolated and plotted using the Saclant graphics package. The plotted output consists of contour, profile and three-dimensional perspective plots. Typical contour and profile plots are shown in Figs 2.9(a,b,c,d,e) and the three-dimensional plots are shown in Figs. 2.10(a,b,c).

2.4.2.3 Test Results of Uniaxial Yield Tests

Typical stress-strain curves are shown in Figs. 2.4 (a,b). All the results are given in Appendix A.

2.4.2.4 Tables of Test Data

Tables 2.2, 2.3 and 2.4 list the test readings for the plate tests, the stiffened plate tests and the beam tests respectively.

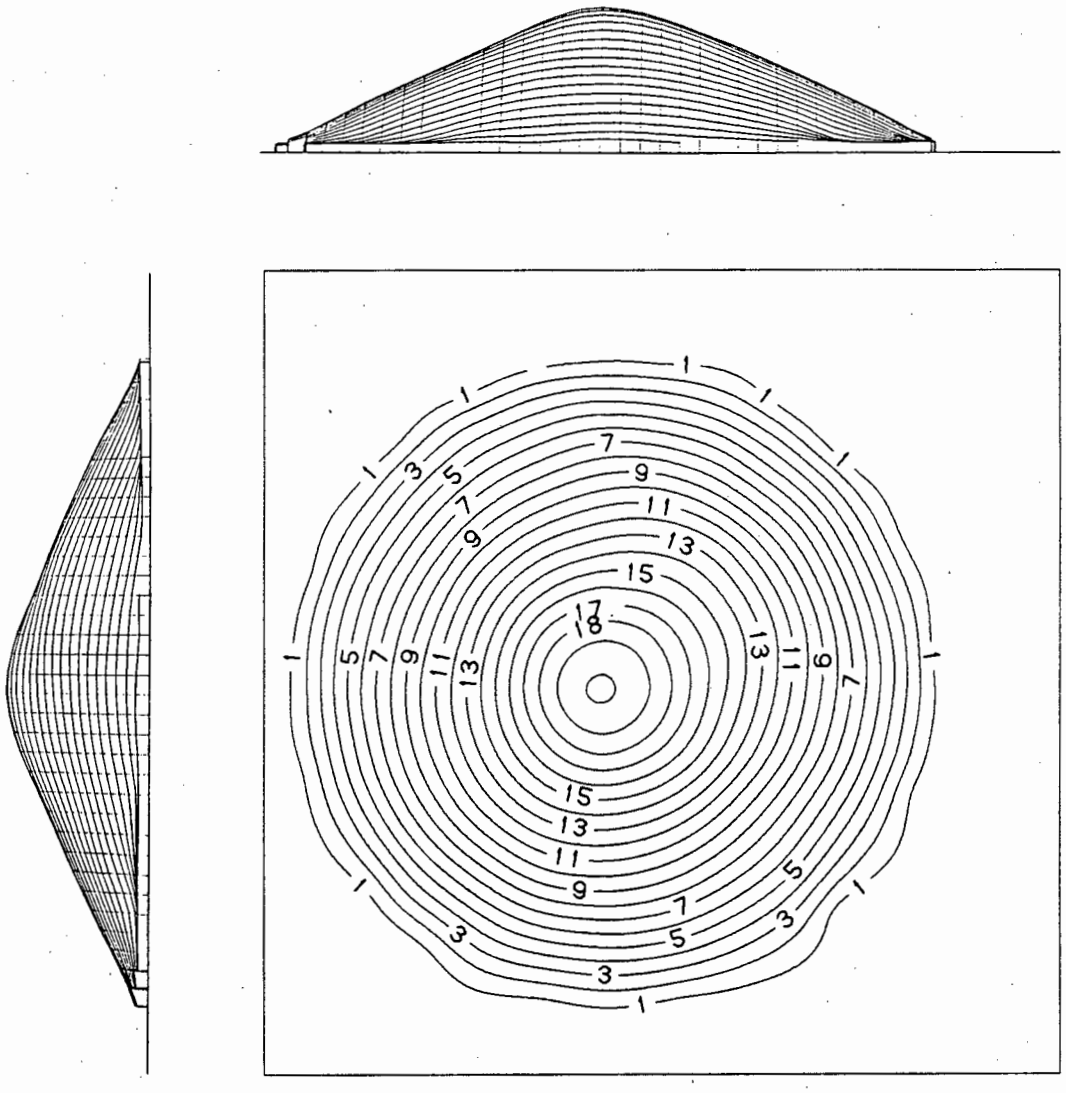

Test No : P5

Impulse - 22,24 N.s

Mid-point deflection - 20,43 mm

FIGURE 2.9(a) CONTOUR PLOT AND DEFORMED PROFILE OF A PLATE TEST

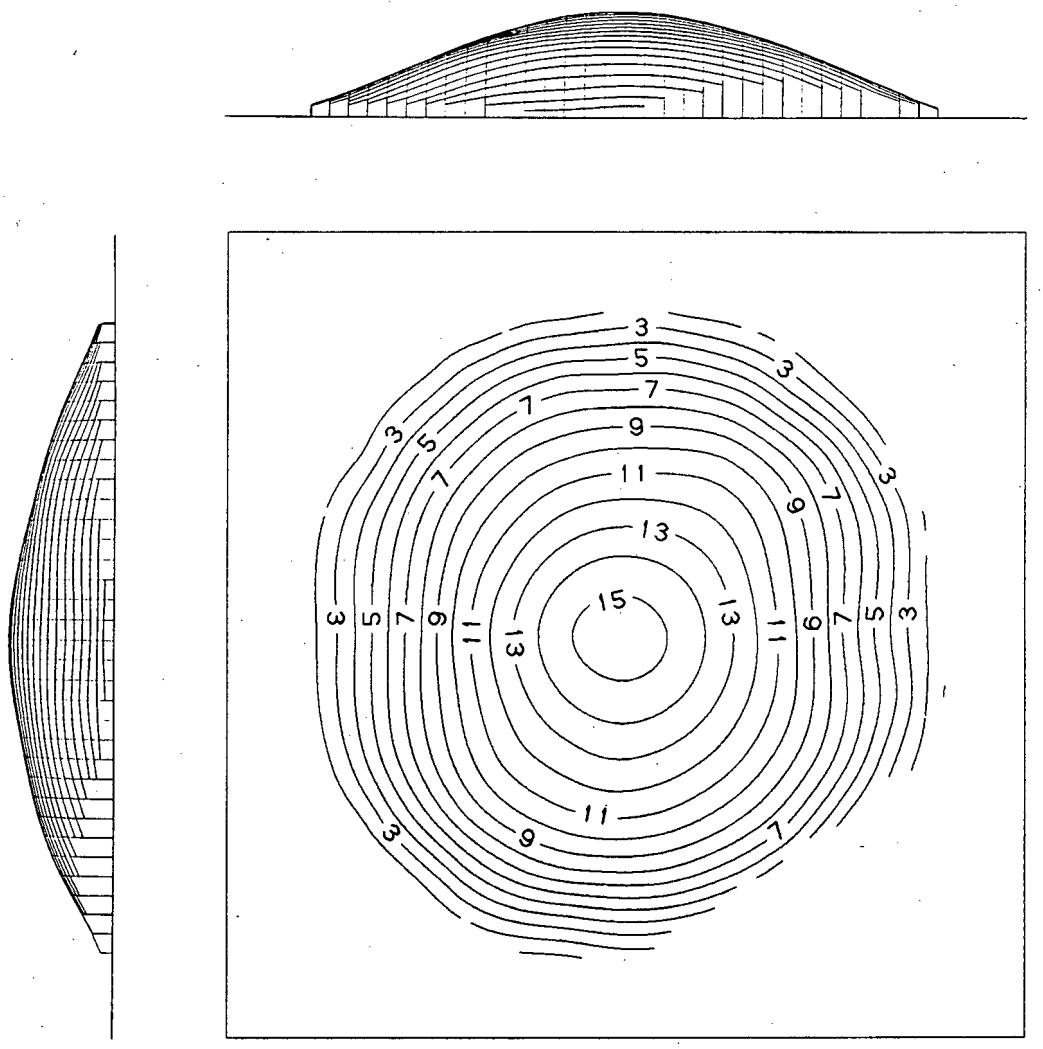

Test No : PS2

Impulse - 22,06 N.s

Mid-point deflection - 15,36 mm

FIGURE 2.9(b) CONTOUR PLOT AND DEFORMED PROFILE OF A STIFFENED PLATE TEST

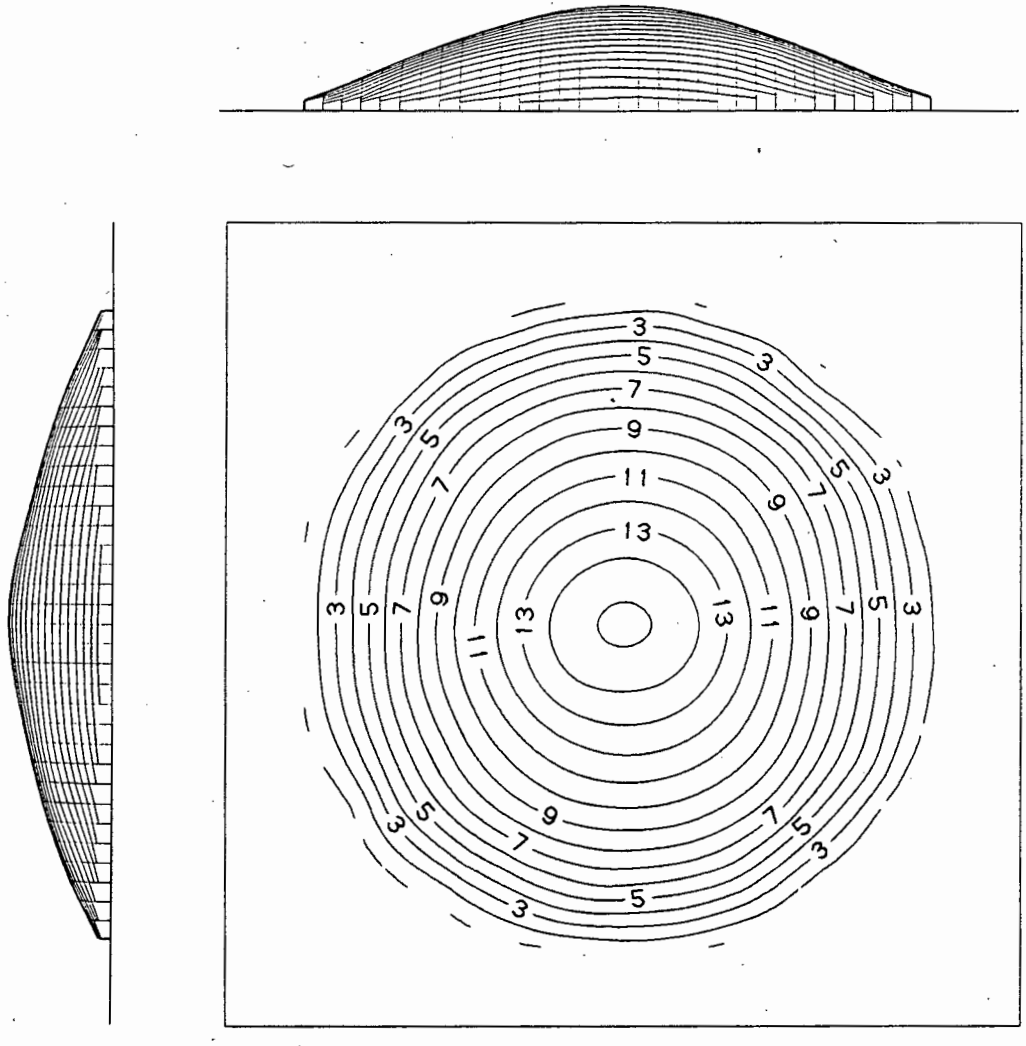

Test No : PS40

Impulse - 22,18 N.s

Mid-point deflection - 15,14 mm

FIGURE 2.9(c) CONTOUR PLOT AND DEFORMED PROFILE OF A STIFFENED PLATE TEST

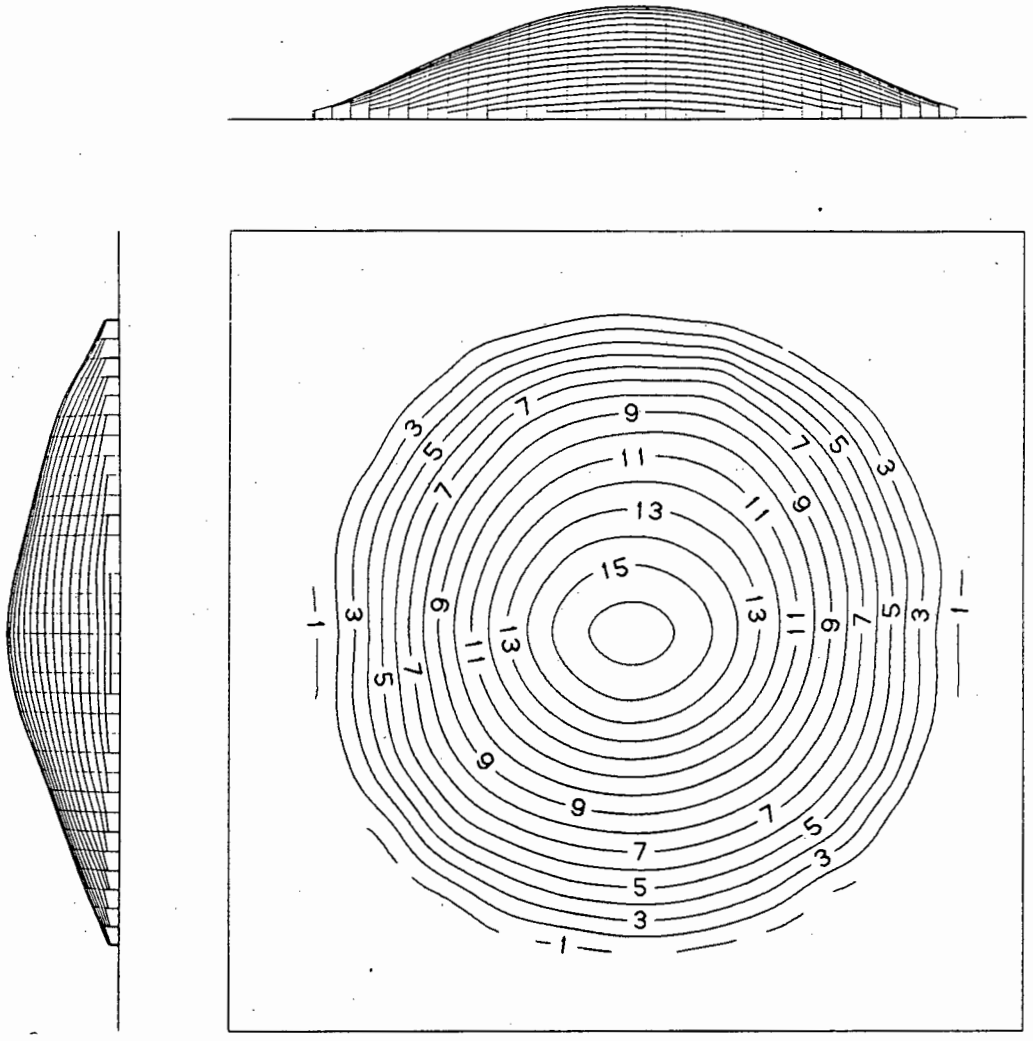

Test No : PS52

Impulse - 24,21 N.s

Mid-point deflection - 16,36 mm

FIGURE 2.9(d) CONTOUR PLOT AND DEFORMED PROFILE OF A STIFFENED PLATE TEST

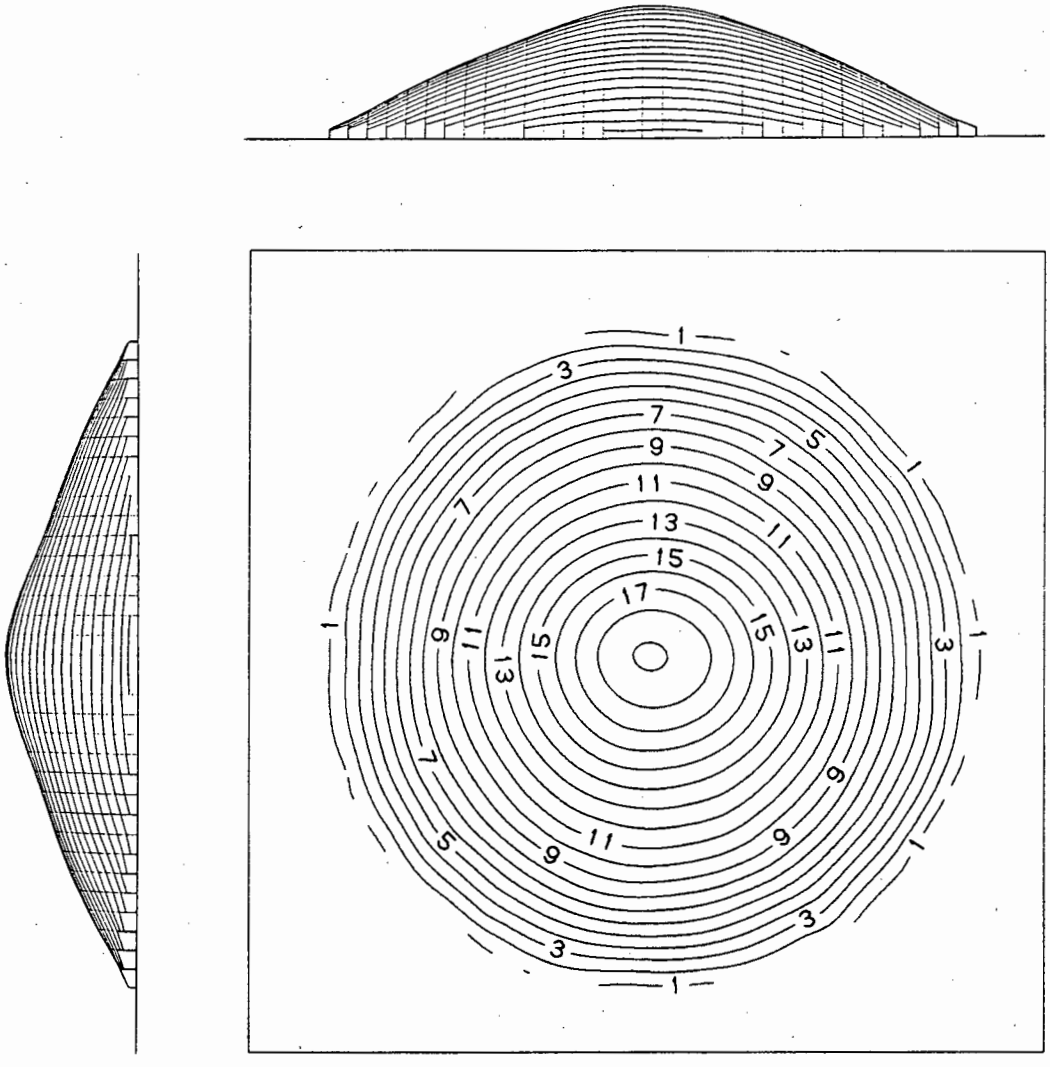

Test No : PS32

Impulse - 24,61 N.s

Mid-point deflection - 19,59 mm

FIGURE 2.9(e) CONTOUR PLOT AND DEFORMED PROFILE OF A STIFFENED PLATE TEST

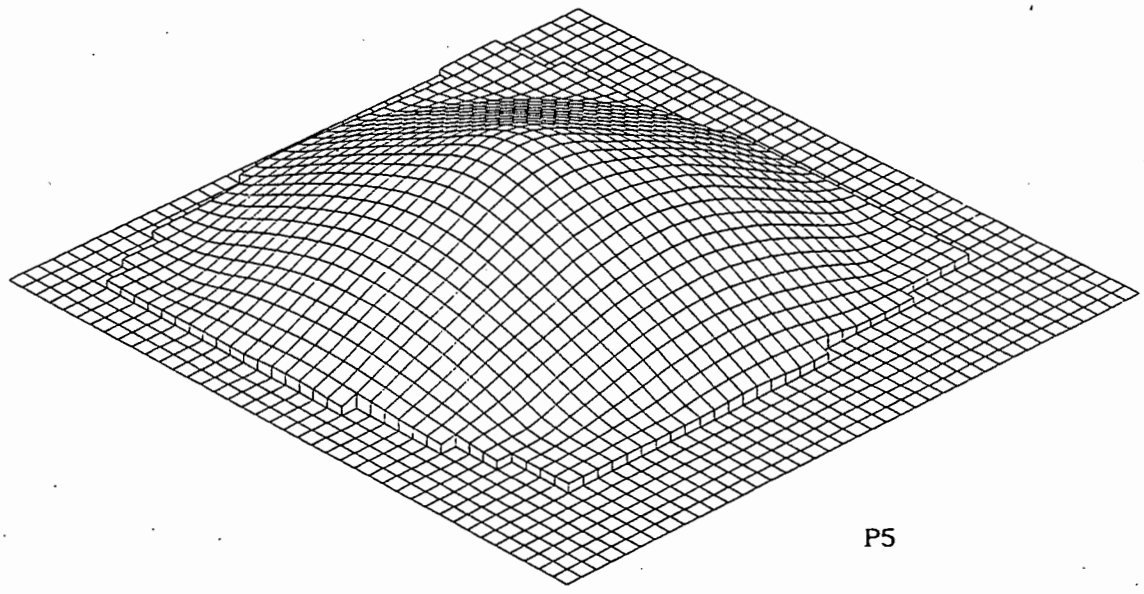

FIGURE 2.10(a) THREE-DIMENSIONAL PLOT OF A DEFORMED PLATE

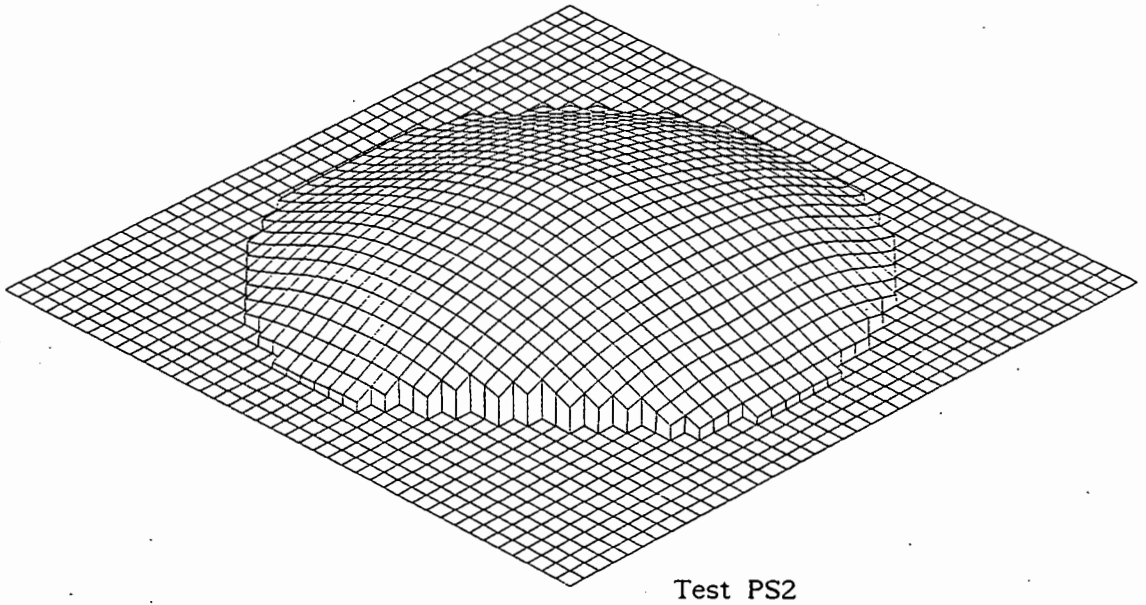

Test PS2

stiffener thickness = 6 mm

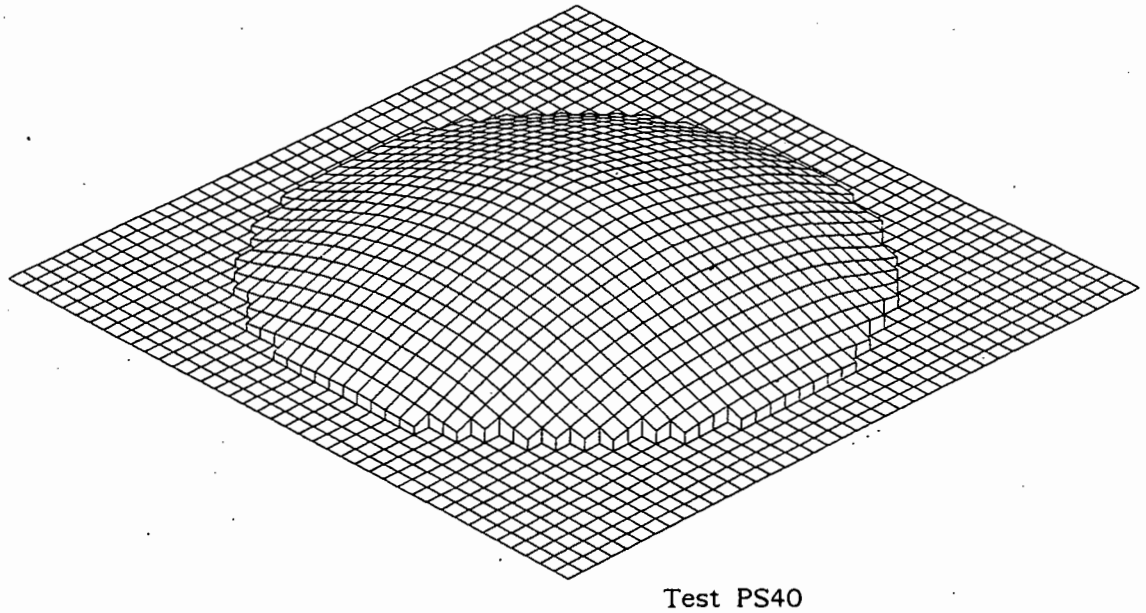

Test PS40

stiffener thickness = 5 mm

FIGURE 2.10(b) THREE-DIMENSIONAL PLOTS OF DEFORMED STIFFENED PLATES

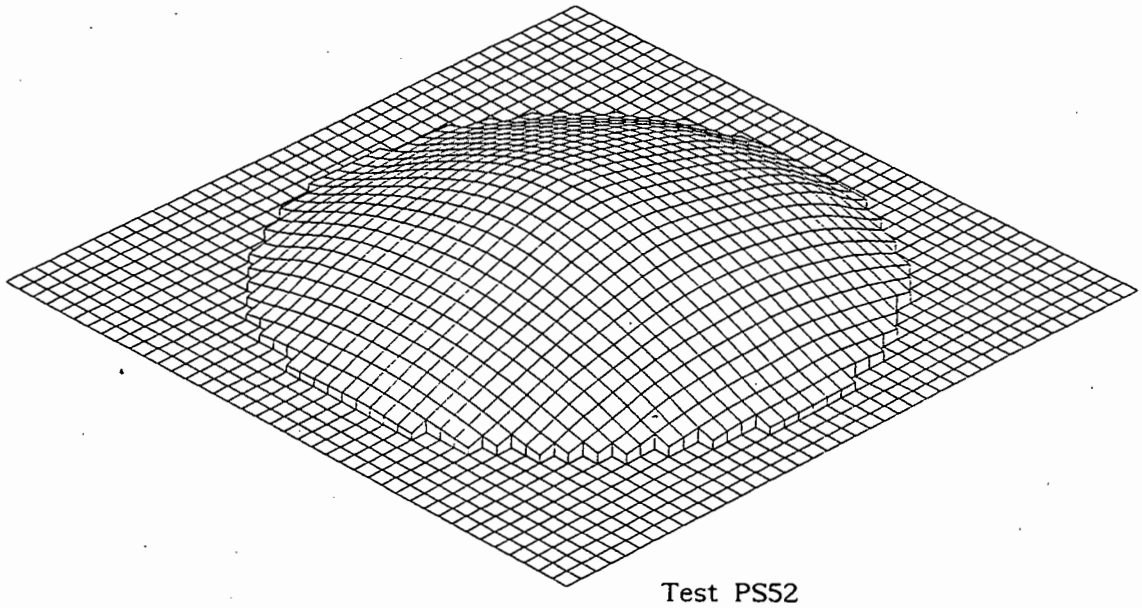

Test PS52

stiffener thickness = 4 mm

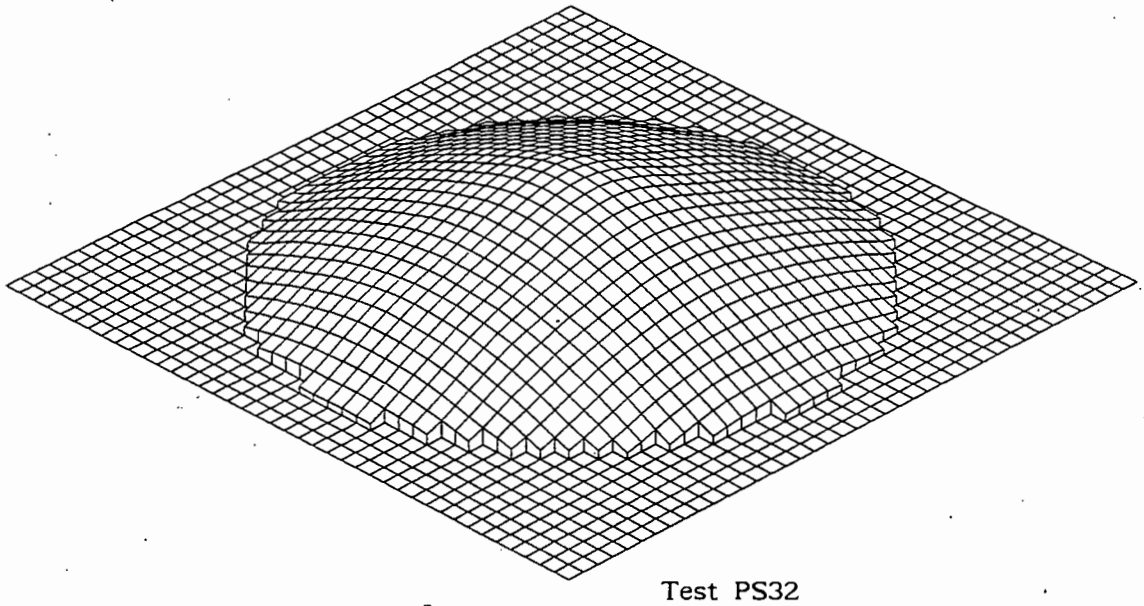

Test PS32

stiffener thickness = 3 mm

FIGURE 2.10(c) THREE-DIMENSIONAL PLOTS OF DEFORMED STIFFENED PLATES

Table 2.2 Plate test data

Test No.	Explosive Mass (g)	Impulse (N.s)	Measured Mid-point Deflection (mm)	Deflection -Thickness Ratio
P1	7,0	11,79	10,65	6,66
P2	8,0	7,03	7,26	4,54
P3	9,0	19,83	19,09	11,93
P4	8,0	10,00	9,97	6,23
P5	9,5	22,24	20,43	12,77
P6	8,5	13,61	13,81	8,63
P7	9,5	21,94	Tearing of plate	
P8	8,5	19,55	19,89	12.43

Table 2.3 Stiffened Plate Results

Test No.	Explosive Mass (g)	Impulse (N.s)	PLATES Measured Mid-point Deflection (mm)	PLATES Deflection -Thickness Ratio	BEAMS Measured Mid-point Deflection (mm)	BEAMS Deflection -Thickness Ratio
i) PS-6						
PS1	9,0	14,66	9,48	5,93	10.64	1,77
2	10,0	22,06	15,36	9,60	17.64	2,94
3	11,0	23,77	Not clamped correctly		-	-
4	10,5	25,02	Tearing of plate		-	-
5	10,3	25,51	Tearing of plate		-	-
6	10,15	24,65	Tearing of plate		-	-
7	9,5	25,99	Tearing of plate		-	-
8	10,0	16,46	11,78	7,36	12,84	2,14
9	11,0	21,49	Tearing of plate		-	-
10	11,0	26,31	Tearing of plate		-	-
11	8,5	18,34	11,82	7,39	12,64	2,11
12	7,5	9,18	4,68	2,93	5,88	0,98
13	8,0	20,48	12,63	7,89	13,12	2,19
14	9,0	20,11	13,53	8,46	14,62	2,44
15	9,5	19,15	14,69	9,18	15,54	2,59
87	8,0	21,25	11,98	7,49	13,10	2,18
88	7,0	9,96	5,74	3,59	6,97	1,16
89	7,5	11,58	6,62	4,14	7,63	1,27

Table 2.3 Stiffened Plate Results (continued)

Test No.	Explosive Mass (g)	Impulse (N.s)	PLATES Measured Mid-point Deflection (mm)	PLATES Deflection -Thickness Ratio	BEAMS Measured Mid-point Deflection (mm)	BEAMS Deflection -Thickness Ratio
ii) PS-5						
PS36	7,5	16,06	9,99	6,24	11,02	2,20
37	8,0	20,13	12,90	8,06	14,30	2,86
38	8,5	17,24	13,78	8,61	15,02	3,00
39	9,0	21,88	15,12	9,45	16,06	3,21
40	9,25	22,18	15,14	9,46	16,14	3,23
41	7,0	12,28	7,26	4,54	8,70	1,74
64	11,0	25,31	Tearing of plate		-	-
65	10,5	26,23	16,44	10,28	18,22	3,64
90	7,0	10,92	6,34	3,96	7,48	1,72
91	7,25	9,15	5,18	3,24	6,18	1,46
92	7,75	9,71	5,96	3,73	7,18	1,55

Table 2.3 Stiffened Plate Results (continued)

Test No.	Explosive Mass (g)	Impulse (N.s)	PLATES Measured Mid-point Deflection (mm)	PLATES Deflection -Thickness Ratio	BEAMS Measured Mid-point Deflection (mm)	BEAMS Deflection -Thickness Ratio
iii) PS-4						
PS16	7,5	11,97	8,12	5,08	9,80	2,45
17	8,5	21,18	13,92	8,70	15,24	3,81
18	9,5	24,65	16,81	10,51	Stiffener broke	
19	9,0	18,22	15,45	9,66	16,48	4,12
20	8,0	10,40	6,58	4,11	8,62	2,16
21	9,75	26,48	18,24	11,40	Stiffener broke	
25	8,25	20,09	12,82	8,01	14,30	3,58
49	10,0	10,66	8,04	5,03	9,76	2,44
50	10,0	9,02	6,62	4,14	8,70	2,18
51	12,25	25,97	Tearing of plate		-	-
52	11,0	24,21	16,36	10,23	18,72	4,68
53	11,5	28,96	Tearing of plate		-	-
54	11,25	26,69	Tearing of plate		-	-
55	11,15	10,46	6,82	4,26	8,86	2,22
56	11,15	25,55	16,40	10,25	17,52	4,38
63	11,0	17,81	13,52	8,45	14,68	3,67
66	9,0	9,55	5,98	3,74	7,82	1,96
67	10,0	4,17	3,54	2,21	4,44	1,11
68	10,0	7,27	5,38	3,36	7,16	1,79

Table 2.3 Stiffened Plate Results (continued)

Test No.	Explosive Mass (g)	Impulse (N.s)	PLATES Measured Mid-point Deflection (mm)	PLATES Deflection -Thickness Ratio	BEAMS Measured Mid-point Deflection (mm)	BEAMS Deflection -Thickness Ratio
iv) PS-3						
PS27	7,5	8,83	6,70	4,19	8,50	2,83
28	7,75	18,51	13,08	8,18	14,68	4,89
29	8,0	11,48	10,24	6,40	10,86	3,62
30	7,75	17,95	13,22	8,26	14,94	4,98
31	8,25	10,27	7,52	4,70	8,78	2,93
32	9,0	24,61	19,59	12,24	Stiffener broke	
75	10,0	10,31	6,42	4,01	8,36	2,79
76	11,0	10,40	6,62	4,14	8,82	2,94
77	13,0	32,68	Tearing of plate		-	-
78	11,0	7,03	4,64	2,90	5,74	1,91
86	11,25	7,09	5,50	3,44	5,98	1,99
93	10,0	27,32	20,02	12,51	21,53	7,18
94	9,0	11,27	7,56	4,73	8,97	2,99
95	9,5	25,67	19,42	12,14	20,73	6,91

Table 2.4 Beam Results

Test No.	Explosive Mass (g)	Impulse (N.s)	Measured Mid-point Deflection (mm)	Deflection -Thickness Ratio
i) B-6				
B57	10	15,16	9,24	1,54
B58	13	19,35	13,76	2,29
B59	15	20,72	14,08	2,35
B60	8	12,84	9,14	1,52
B61	6	9,59	5,62	0,94
B62	11,5	15,16	10,76	1,79
B99	16	21,13	Beam slipped	
ii) B-5				
B42	2,5	4,14	2,38	0,48
B43	3,5	5,56	3,46	0,69
B44	5,5	7,5	6,38	1,28
B45	8,5	11,79	10,88	2,18
B46	10,5	12,94	12,44	2,49
B47	12,5	15,57	14,70	2,94
B48	7	9,74	8,26	1,65
B96	13	20,13	Beam broke	
B97	13	17,37	15,74	3,15
B98	14	19,29	19,76	3,95

Table 2.4 **Beam Results (continued)**

Test No.	Explosive Mass (g)	Impulse (N.s)	Measured Mid-point Deflection (mm)	Deflection -Thickness Ratio
iii) B-4				
B69	6	7,71	9,14	2,29
B70	8	11,59	13,02	3,26
B71	10	13,11	14,78	3,69
B72	12	15,24	15,34	3,84
B73	14	17,60	19,68	4,92
B74	4	6,25	6,98	1,75
iv) B-3				
B33	7	No impulse reading		
B34	2,5	No impulse reading		
B35	3,5	4,97	7,70	2,57
B79	4	5,74	9,02	3,01
B80	6	7,66	12,28	4,09
B81	8	11,14	15,22	5,07
B82	10	12,94	Beam broke	
B83	9	12,10	16,66	5,55
B84	9,5	12,67	Beam broke	
B85	9,25	13,11	17,52	5,84

2.5 EXPERIMENTAL OBSERVATIONS

This section describes experimental observations, which are not considered in the analysis in Chapter 4, since they are not within the scope of this thesis. It is however recommended that further investigation be carried out to understand these occurrences.

The first observation that was noted, is the gap which exists between the stiffened plate and the stiffener after the loading has occurred. Fig. 2.11(a) shows this effect. Fig. 2.11(b) shows that it also occurs for negligible deflections of the plate, ie. for very low impulses. The mid-point deflections of the plates and the corresponding mid-point deflections of the stiffeners, as well as their least squares lines, are shown in Figs. 2.12(a,b,c,d). The least squares line equations are given in Appendix E.

The gap appears to be constant across the loading range, ie. it does not increase with increased loading. The average gap distances are:

i) PS-6: gap = 1,12 mm
ii) PS-5: gap = 1,12 mm
iii) PS-4: gap = 1,61 mm
iv) PS-3: gap = 1,41 mm

It appears that this gap is due to a springback effect in the plate. A factor to be studied further is when exactly the separation of the plate and its stiffener takes place. Is it at the initial stage of the response or towards the end?

A second observation noted, is that in three instances the stiffener failed, while the plate showed no indication of tearing. This phenomenon occurred twice for PS-4 tests and once for a PS-3 test. The impulse for these tests was greater than 24 N.s.

Attempts to reproduce this phenomenon were unsuccessful, in that the plate started tearing before the stiffener failed.

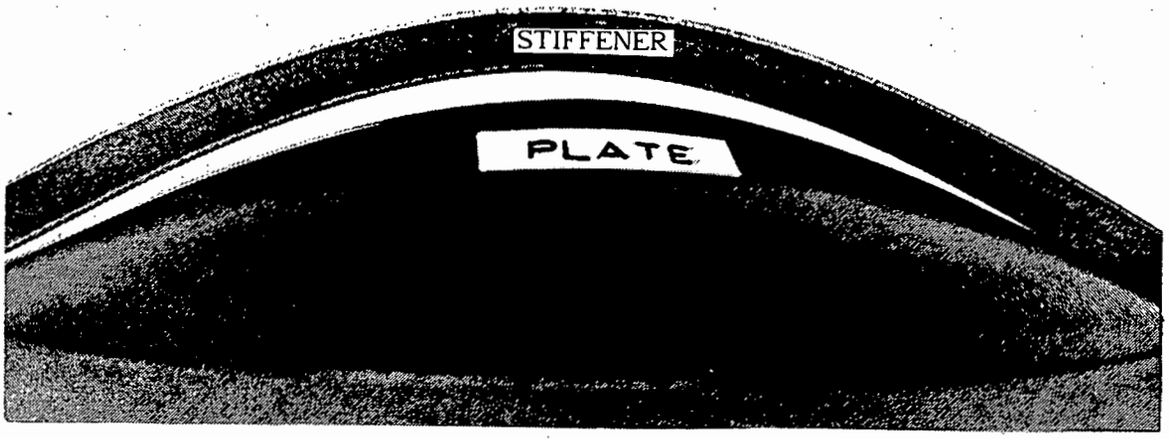

IMPULSE = 22.18 N.s

FIGURE 2.11(a) PHOTOGRAPH OF A STIFFENED PLATE SHOWING THE SPRINGBACK EFFECT

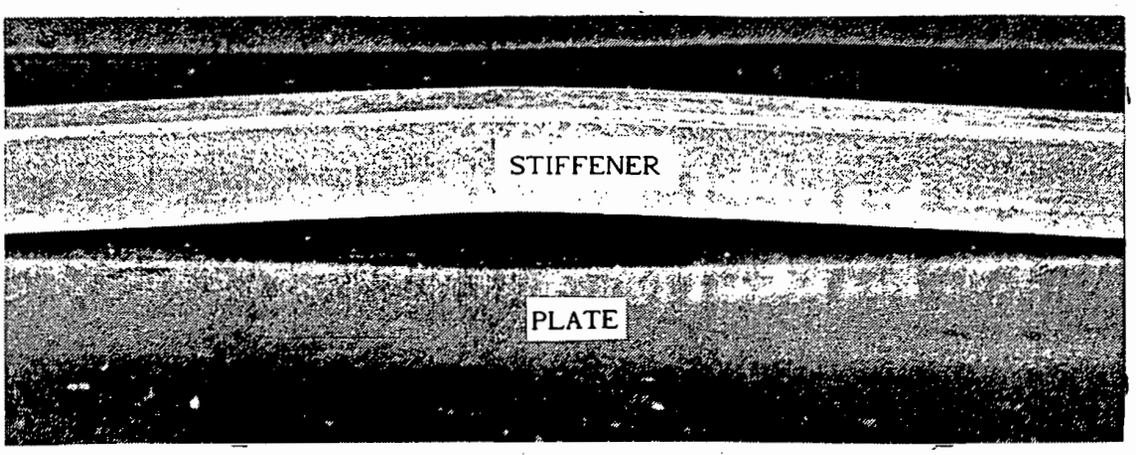

IMPULSE = 1.58 N.s

FIGURE 2.11(b) PHOTOGRAPH OF A STIFFENED PLATE SHOWING THE SPRINGBACK EFFECT

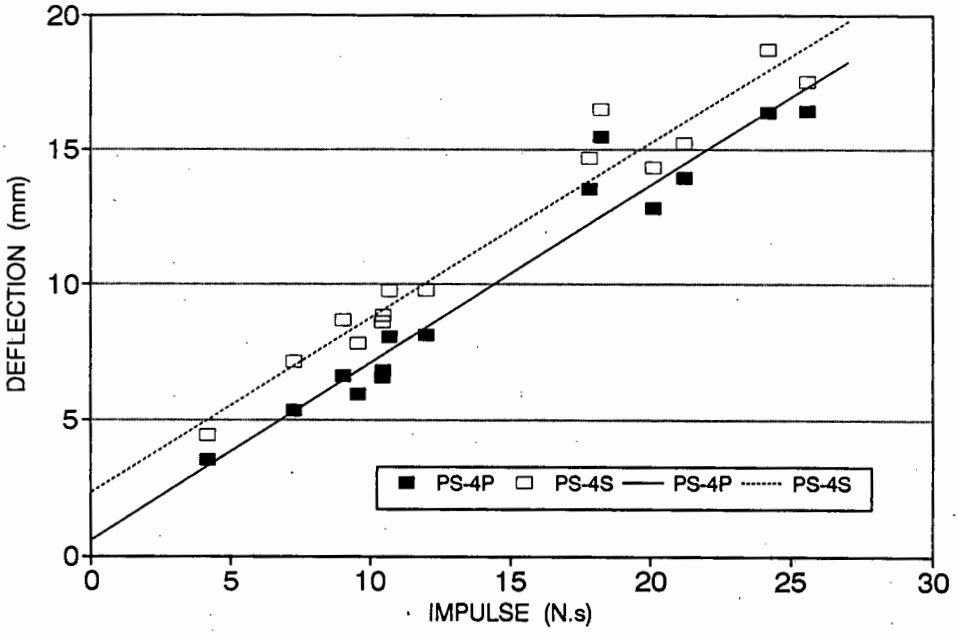

FIGURE 2.12(c) GRAPH SHOWING THE SPRINGBACK EFFECT
(STIFFENER THICKNESS = 4 mm)

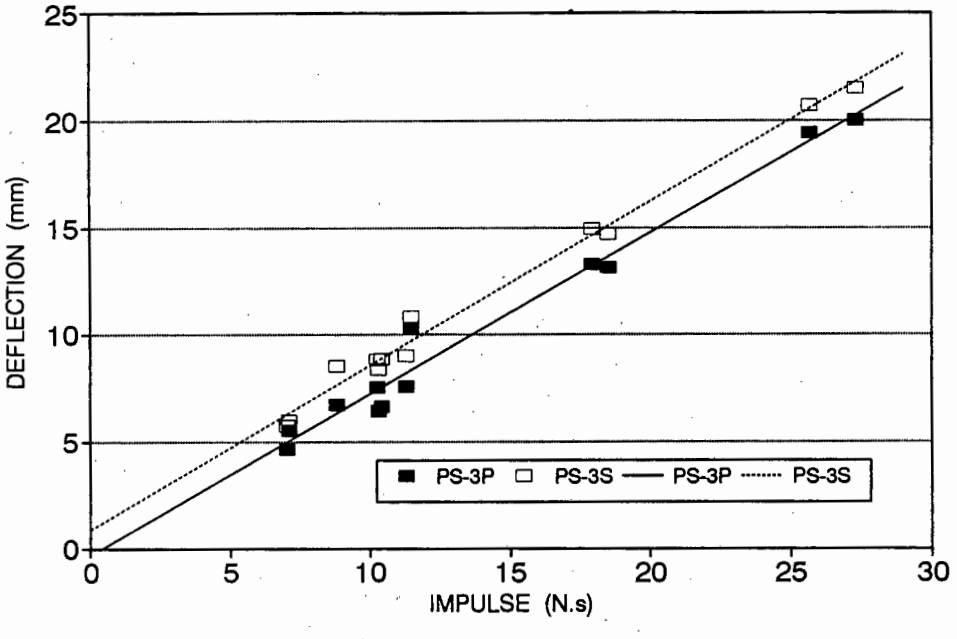

FIGURE 2.12(d) GRAPH SHOWING THE SPRINGBACK EFFECT
(STIFFENET THICKNESS = 3 mm)

CHAPTER 3 - THEORETICAL INVESTIGATION

3.1 Introduction

No work has been found on the impulsive loading of fully-clamped circular stiffened plates. A limited amount of experimental and analytical studies have been done on rectangular warship panels.

Houlston and DesRochers [13] in 1987 performed a finite element analysis to determine the displacement-time history results of stiffened panels subjected to air-blasts. In 1989 Schubak *et al.* [14] developed a simplified analytical procedure to predict the dynamic response of stiffened panels to air-blast loads. Schubak *et al.* [14] report that experimental evidence by Houlston and Slater [5] in 1989 suggested that away from the lateral edges of the structure, the stiffened plate behaves much like a singly-symmetric beam with the plate acting like a large flange. Thus Schubak *et al.* [14] modelled the panels as rigid-plastic, singly-symmetric beams with encastred ends. In their analysis they consider the dynamic response to be an initial plastic hinge mechanism, followed by a final plastic string phase. Also a linear approximation of the yield surface is used, in order to uncouple the nonlinear problem into two separate linear components.

The theoretical work mentioned above is specifically concerned with air-blast loading, where the duration of the applied load is very much longer than that investigated in this study. Houlston and DesRochers [13] use a pressure duration time of approximately 200ms, whereas the response time of circular mild steel plates, as determined by Nurick [9], is 140 - 190 μs. The work is also specifically related to rectangular panels, where the assumption that the stiffened panel essentially behaves like a beam with the panel acting as a large flange.

An energy solution was sought so as to allow comparisons to be made between the stiffened plates in this investigation and similar circular plates investigated by other researchers.

Energy solutions enable procedures for predicting deformations in structures when the transient behaviour is of little interest. The energy absorbed in the deformation of a plate can then be compared to the energy absorbed in a similar stiffened plate.

Lippmann [15] in 1974 developed an energy solution for an axisymmteric rigid-plastic membrane subject to an initial impact. He applied Tresca's yield condition and the associated flow rule and reduced the problem to a single second-order partial differential equation. This equation can be solved numerically in a straightforward manner. From this he derived an approximate analytical solution for a membrane, where the material displaces only transversely and the deformations are not too extensive.

Westine and Baker [16] report that rigid-plastic energy solutions began in the early 1950's when Lee and Symonds used the static plastic-hinge concept, considered beam inertia, and propagated a travelling hinge to analytically obtain the upper bound for the permanent deformation of a beam under a transverse load. Westine and Baker [16] further report that Bodner, Prager, Jones, Martin, Haythornthwaite and others continued this work, while Greenspan pointed out in the 1960's, that solutions could be obtained without propagating a plastic hinge along structural members. Greenspan noted that the residual plastic strain energy stored in a deformed member could be calculated by assuming an appropriate final deformed shape.

Westine and Baker [16] disagree with Greenspan's theory that the plastic strain energy can be equated to the energy flux in an explosive blast wave. They argue that this made deformations independent of the structural orientation relative to the blast wave. They further argue that two separate analytical procedures are

required to calculate the strain energy; one for structures subjected to short duration impulsive loads and another when the load durations are long relative to the structural response time.

It then follows that for short duration loads, ie. impulsive loads, the strain energy of the deformed structure can be equated to the kinetic energy imparted to the structure. While for longer duration loads, a quasi-static loading state is assumed and the strain energy must be equated to the work performed by the peak force deflecting the structure.

Duffey [1] developed a simplified energy method for a rigid-plastic material. This method enables the maximum deflection of a clamped circular plate to be calculated by equating the strain energy of the plate to the initial kinetic energy and assuming a permanent deflected shape.

3.2 ENERGY ANALYSIS

3.2.1 Introduction

A comparison of different energy methods disclosed that Duffey's energy method [1] provides the best correlation with experimental results, see Table 4.2. This is also shown by Teeling-Smith [12] for his experimental results. The energy method as developed by Duffey is based on a rigid-plastic analysis and is described in Section 3.2.2., while Appendix B shows the derivation thereof.

A deformation energy expression for a beam was developed using Duffey's method, however the results give poor agreement with the experimentally determined values.

The strain-rate sensitivity of the test materials is discussed in section 3.2.3., while section 3.2.4. includes the influence of

material strain-hardening and section 3.2.5. dicusses the shape approximation functions, which will be used in the energy analysis in Chapter 4.

3.2.2 Rigid-Plastic Analysis

The assumption is made that the test material is rigid-viscoplastic. This section deals with the rigid-plastic aspect, while the next section discusses the strain-rate effects on the material.

The above assumption is justified if the energy dissipated by the structure in plastic deformation is much larger than the elastic strain energy.

Appendix B contains the detailed analysis of Duffey [1] where the plastic strain energy is

$$E_p = \pi\, t \int_0^R \sigma_{rr} \left(\frac{\partial \omega}{\partial r} \right)^2 r dr \qquad (3.1)$$

The radial yield stress, using the von Mises yield criterion is given by

$$\sigma_{rr} = \frac{\sigma_y}{(1 - \upsilon + \upsilon^2)^{1/2}} \qquad (3.2)$$

A deflection shape for the plate of the following form is assumed

$$\omega = \omega_o \cdot \phi(r) \qquad (3.3)$$

where $\phi(r)$ is the shape function.

Substituting the dynamic yield stress σ_o^1 , as calculated in section 3.2.3, into equation (3.2) and then substituting equations (3.3) and (3.2) into equation (3.1), allows the deformation energy of an

impulsively loaded circular plate to be calculated:

$$E_{deformation} = \pi\, t \int_0^R \frac{\sigma_y}{(1 - \upsilon + \upsilon^2)^{1/2}} \left(\frac{\partial \omega}{\partial r} \right)^2 rdr \qquad (3.4)$$

An energy balance for the plates is given by

$$E_{input} = E_{deformation}$$

and for the stiffened plates

$$E_{input} = E_{deformation\ plate} + E_{deformation\ beam} + E_{losses}$$

where E_{losses} = energy lost due to friction

The input energy is obtained by considering the initial kinetic energy of the structure and using the applied impulse, eqn. (2.6), to give

$$E_{input} = \frac{I^2}{2m} \qquad (3.5)$$

where $m = \rho t \pi r^2$ for plate tests.

and $m = (\rho t \pi r^2 + \rho b h l)$ for the stiffened plate tests.

Thus the energy balance becomes :

i) for plates :

$$\frac{I^2}{2\rho t \pi r^2} = \pi\, t \int_0^R \frac{\sigma_0^1}{(1 - \upsilon + \upsilon^2)^{1/2}} \left(\frac{\partial \omega}{\partial r} \right)^2 rdr \qquad (3.6)$$

ii) for stiffened plates :

$$\frac{I^2}{2(\rho t\pi r^2+\rho bhl)} = \pi\, t \int_0^R \frac{\sigma_0^1}{(1 - \upsilon + \upsilon^2)^{1/2}} \left(\frac{\partial \omega}{\partial r} \right) r dr$$

$$+ E_{\text{deformation beam}} + E_{\text{losses}} \qquad (3.7)$$

An expression for the deformation energy of a beam was derived as shown in Appendix B. However it does not give satisfactory answers and will not be considered in the analysis of the results in Chapter 4.

3.3 STRAIN-RATE SENSITIVITY

The plastic behaviour of mild steel is highly sensitive to strain rate. Thus it is essential to correct the static yield stress obtained from the uniaxial tensile tests to obtain a dynamic yield stress which can be used for an energy analysis.

In previous analyses of impulsive loading, the appropriate dynamic yield stress σ_0^1 was obtained by estimating the maximum strain rates, either empirically, Symonds [17], or analytically, Duffey [18], during an initial phase of the response. Symonds and Wierzbicki [2] omit the early response, involving the elastic-plastic bending, from their analysis.

Symonds and Wierzbicki's [2] mode approximation technique for large deflections of a symmetrically loaded circular plate, which is based on the mode approximation technique by Martin and Symonds [19], gives consideration to the strain rate dependence of the test material in the plastic range. The membrane mode approximation solution enables the use of the dynamic yield stress for the different strain rates

encountered in the experimental work.

Using the rigid-viscoplastic constitutive equation

$$\frac{\sigma_0^1}{\sigma_0} = 1 + \left(\frac{\dot{\varepsilon}}{\dot{\varepsilon}_0} \right)^{\frac{1}{n}} \tag{3.8}$$

where σ_0^1 = dynamic yield stress at plastic strain rate $\dot{\varepsilon}$.

Rearranging gives :

$$\dot{\varepsilon} = \dot{\varepsilon}_0 \left(\frac{\sigma_0^1}{\sigma_0} - 1 \right)^n \tag{3.9}$$

The average strain rate over the response time is given by Symonds and Wierzbicki [2] as

$$\dot{\varepsilon}_r^{ave} = \frac{0,05365\ I^2}{R^5\ t^2 \sqrt{\rho^3\ \sigma_o^1}} \tag{3.10}$$

Substituting the following values into equations (3.9) and (3.10) :

$\dot{\varepsilon}_0$ = 40 s^{-1}
n = 5
ρ = 7850 $kg.m^{-3}$
R = 50 mm
t = 1,6 mm

and equating gives

$$\frac{I^2 \cdot 96421,8}{\sqrt{\sigma_0^1}} = 40 \cdot \left(\frac{\sigma_0^1}{\sigma_0} - 1 \right)^5 \qquad (3.11)$$

where I = applied impulse

σ_0^1 = dynamic yield stress

σ_0 = static uniaxial yield stress

Appendix C gives the dynamic yield stress values for the experiments.

The choice of the material constants n and $\dot{\varepsilon}_o$ requires some justification. Jones [20] notes that most of the available experimental data has been generated at relatively small strains of a few percent, whereas much larger strains are obtained in the experiments in this study. Jones also notes that the strain rate sensitivity of mild steel, is greatest for small strains, with less effect at larger strains and that the dynamic stress-strain curve for mild steel tends towards a perfectly plastic material at high uniaxial strain rates. The constants $\dot{\varepsilon}_0$ and n then become 6844 sec^{-1} and 3,91 respectively, according to Abramowicz and Jones [21]. Abramowicz and Jones [22] report that for another steel, $\dot{\varepsilon}_0$ = 802 sec^{-1} and n = 3,585 for the ultimate tensile stress.

Thus it is clear that there is still some uncertainty as to the value of the constants of equation (3.8), due to the shortage of experimental data. Therefore the most commonly quoted values, $\dot{\varepsilon}_0$ = 40 sec^{-1} and n = 5, are used.

3.4 STRAIN-HARDENING

The influence of material strain-hardening has not been investigated systematically for many structures, mainly because its effect seems to be small.

Symonds and Jones [23] found that the correction required for strain hardening in a rigid perfectly-plastic analysis was relatively unimportant compared to other effects in an impulsively loaded mild steel beam with a transverse deflection-thickness ratio of seven. Marsh and Campbell [24] reported that strain-hardening of viscoplastic materials is less important at high strain rates.

Thus strain-hardening effects are neglected in this study.

3.5 SHAPE APPROXIMATION FUNCTIONS

A deformed shape approximation function needs to be determined in order to establish the deformation energies of the plates and beams.

The shape function must satisfy the appropriate boundary conditions, which for the plates and beams can be assumed to be the same. The boundary conditions are :

i) at $r = 0$, $\omega = \omega_o$

ii) at $r = 0$, $\frac{\partial \omega}{\partial r} = 0$

iii) at $r = R$, $\omega = 0$

where r = radius of plate or length of beam from the centre

ω = transverse displacement of plate or beam

ω_0 = maximum transverse mid-point deflection

Since Westine and Baker [16] consider membrane as well as bending behaviour, an additional boundary condition is introduced:

$$\text{at } r = R, \qquad \frac{\partial \omega}{\partial r} = 0$$

Table 3.1 lists the shape functions used by Westine and Baker [16] and Duffey [1].

Figures 4.8(a,b,c,d) give a comparison between the experimental and theoretical shape functions. From this the most suitable shape function is chosen to be used in the energy analysis.

TABLE 3.1 Predicted Shape Functions

	Shape Function
Westine and Baker [16]	$\omega = \frac{\omega_o}{\omega}\left(1 + \cos\frac{\pi r}{R}\right)$
Duffey [1]	$\omega = \omega_o \cos\left(\frac{\pi r}{2R}\right)$
	$\omega = \omega_o \left(1 - \left(\frac{r}{R}\right)\right)$
	$\omega = \omega_o \left(1 - \left(\frac{r}{R}\right)\right)^2$
	$\omega = \omega_o \left(1 - \left(\frac{r}{R}\right)\right)^3$

CHAPTER 4 - RESULTS

4.1 PLATES

A series of circular plate tests were performed in order to obtain a set of reference data with which the stiffened plate results could be compared. These results were also compared with the circular plate results of Nurick [9] and Teeling-Smith [12].

A dimensionless number ϕ_c, developed by Nurick and Martin [3], is used to compare the results in this investigation and also compare these results with results from the previous studies. This dimensionless number is given by

$$\phi_c = \frac{I\left(1 + \ln\frac{R}{R_o}\right)}{\pi R t^2 (\rho\sigma_o)^{1/2}} \qquad (4.1)$$

where R_o = radius of the loaded area

For the tests presented here, $R_o = R$ and thus equation (4.1) simplifies to

$$\phi_c = \frac{I}{\pi R t^2 (\rho\sigma_o)^{1/2}} \qquad (4.2)$$

The maximum impulse obtained by Teeling-Smith [12] before visible tearing at the plate circumference occurred, was 28 N.s., while that obtained by Nurick [9] was 15,6 N.s. The maximum impulse obtained in this study was 22,2 N.s., however it was not the intention to find the plate tearing threshold and thus this value must not be

interpreted as such. These variations are probably due to the material properties and manufacturing defects.

Fig. 4.1 shows the least squares line for the results performed in this study. The least squares line is bounded by ± 1 deflection-thickness ratio. All the data points lie within these bounds. The least squares line is given by

$$\left(\frac{\delta}{t} \right) = 0{,}330\ \phi_c + 0{,}391 \qquad \text{with } r = 0{,}991 \qquad (4.3)$$

The least squares analysis performed by Nurick and Martin [3] gives

$$\left(\frac{\delta}{t} \right) = 0{,}501\ \phi_c - 1{,}037 \qquad \text{with } r = 0{,}991 \qquad (4.4)$$

and by Teeling-Smith [12] gives

$$\left(\frac{\delta}{t} \right) = 0{,}407\ \phi_c - 0{,}957 \qquad \text{with } r = 0{,}997 \qquad (4.5)$$

while a least squares analysis by Nurick and Martin [3] on experimental work by Bodner and Symonds [25], Wierzbicki and Florence [10] and Nurick [9] gives

$$\left(\frac{\delta}{t} \right) = 0{,}425\ \phi_c + 0{,}277 \qquad \text{with } r = 0{,}974 \qquad (4.6)$$

Fig. 4.2(a) shows a plot of the least squares lines of equations (4.3-4.5). It is shown that the results from this study lie below those from the other tests, particularly for larger values of ϕ_c. A possible reason for this might be the difference in the masses of the ballistic pendulums used.

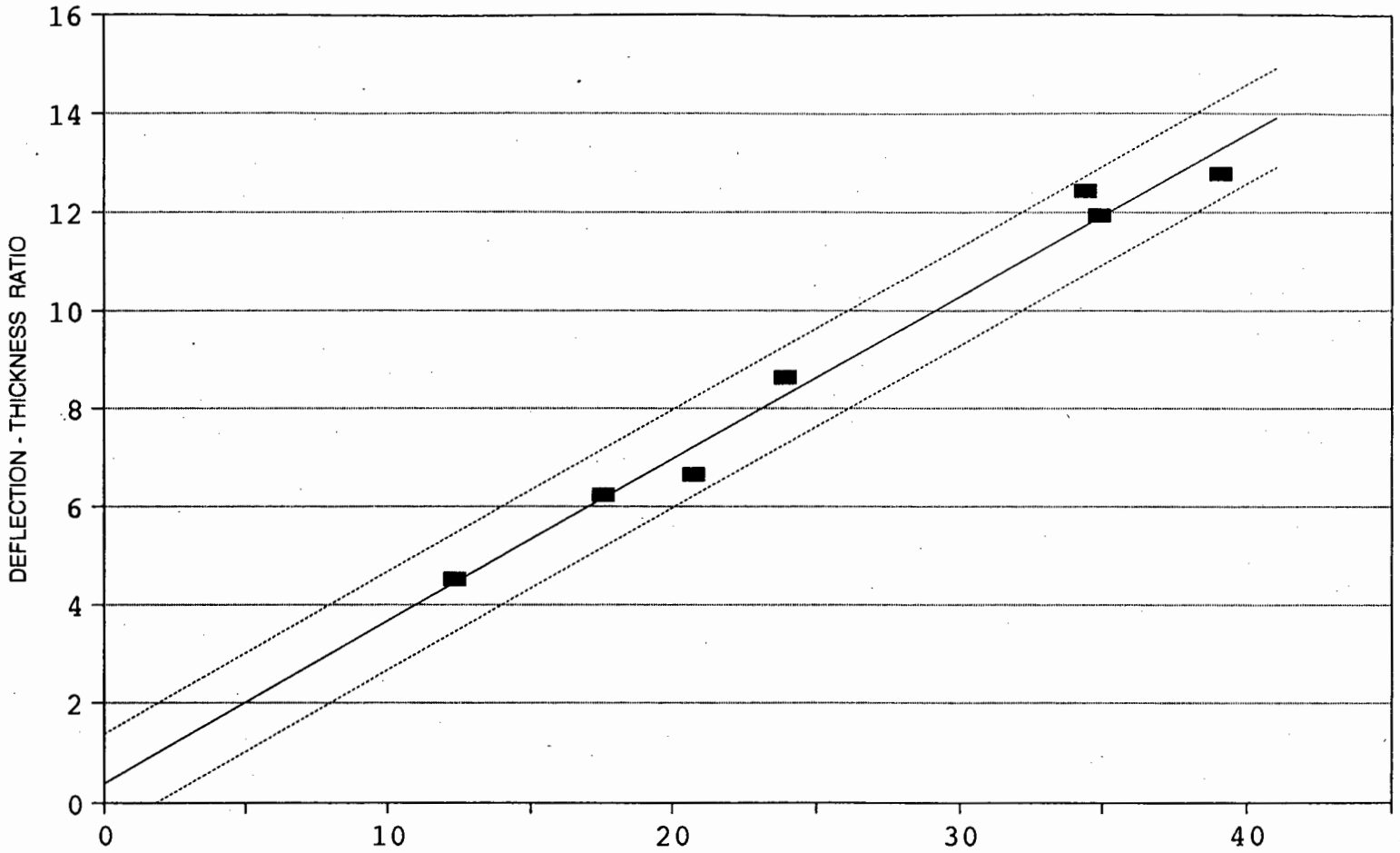

$$\phi_c = \frac{I}{\pi R t^2 \, (\rho \sigma_o)^{1/2}}$$

FIGURE 4.1 GRAPH OF DEFLECTION-THICKNESS RATIO vs. DIMENSIONLESS No. ϕ_c WITH A LEAST SQUARES CORRELATION AND ± 1 DEFLECTION-THICKNESS RATIO

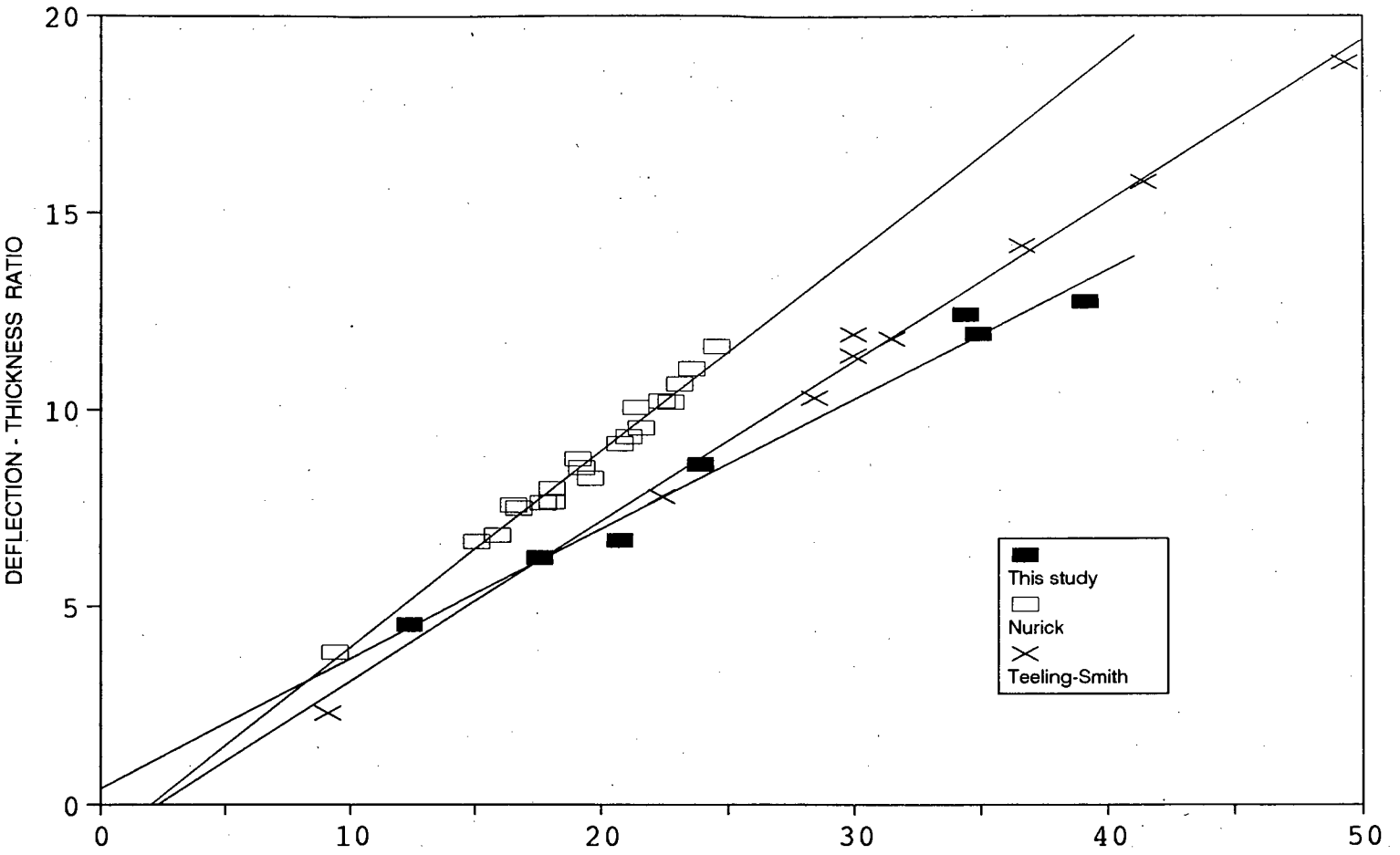

$$\phi_c = \frac{I}{\pi R t^2 (\rho \sigma_o)^{1/2}}$$

FIGURE 4.2(a) GRAPH OF DEFLECTION-THICKNESS RATIO vs. DIMENSIONLESS No. ϕ_c
FOR RESULTS BY NURICK [9], TEELING-SMITH [12] AND THIS STUDY

The masses of the ballistic pendulums used in Nurick's [9], Teeling-Smith's [12] and this study's tests were 66.60 kg, 88.73 kg and 96.06 kg respectively. A plot of the slopes of the least squares lines of these studies (see equations 4.3 - 4.5) against ballistic pendulum mass is shown in Fig. 4.2(b). This graph shows that the slope decreases with increased pendulum mass. This appears to indicate that the impulse measured for a particular plate deflection will be greater for a heavier pendulum.

A mass factor, μ, is introduced to ϕ_c to compensate for this effect. The mass factor is defined as

$$\mu = \frac{m}{M}$$

where m = mass of test specimen
M = mass of ballistic pendulum

and a modified non-dimensional number for circular plates loaded on a ballistic pendulum is given by

$$\phi_c^1 = \mu\phi_c = \frac{I\ R\ \rho^{1/2}}{M\ t\ \sigma^{1/2}} \qquad (4.7)$$

Fig. 4.2(c) gives a plot of deflection-thickness ratio against ϕ_c^1. The data points almost all lie within ± 1 deflection-thickness ratio. The least squares line is given by

$$\frac{\delta}{t} = 358{,}63\ \phi_c^1 - 1{,}19 \qquad \text{with } r = 0{,}983 \qquad (4.8)$$

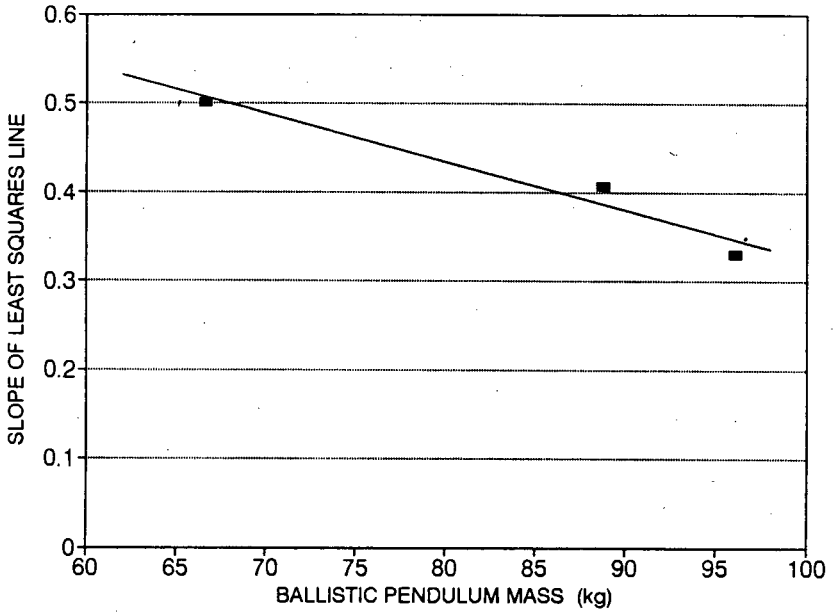

Nurick [9] : $\frac{\delta}{t} = 0{,}501\ \phi_c - 1{,}037$; M = 66,60 kg

Teeling-Smith [12] : $\frac{\delta}{t} = 0{,}407\ \phi_c - 0{,}957$; M = 88,73 kg

This Study : $\frac{\delta}{t} = 0{,}330\ \phi_c + 0{,}391$; M = 96,06 kg

FIGURE 4.2(b) GRAPH OF SLOPES OF LEAST SQUARES LINES vs. BALLISTIC PENDULUM MASS FOR RESULTS BY NURICK'S [9], TEELING-SMITH'S [12] AND THIS STUDY'S RESULTS

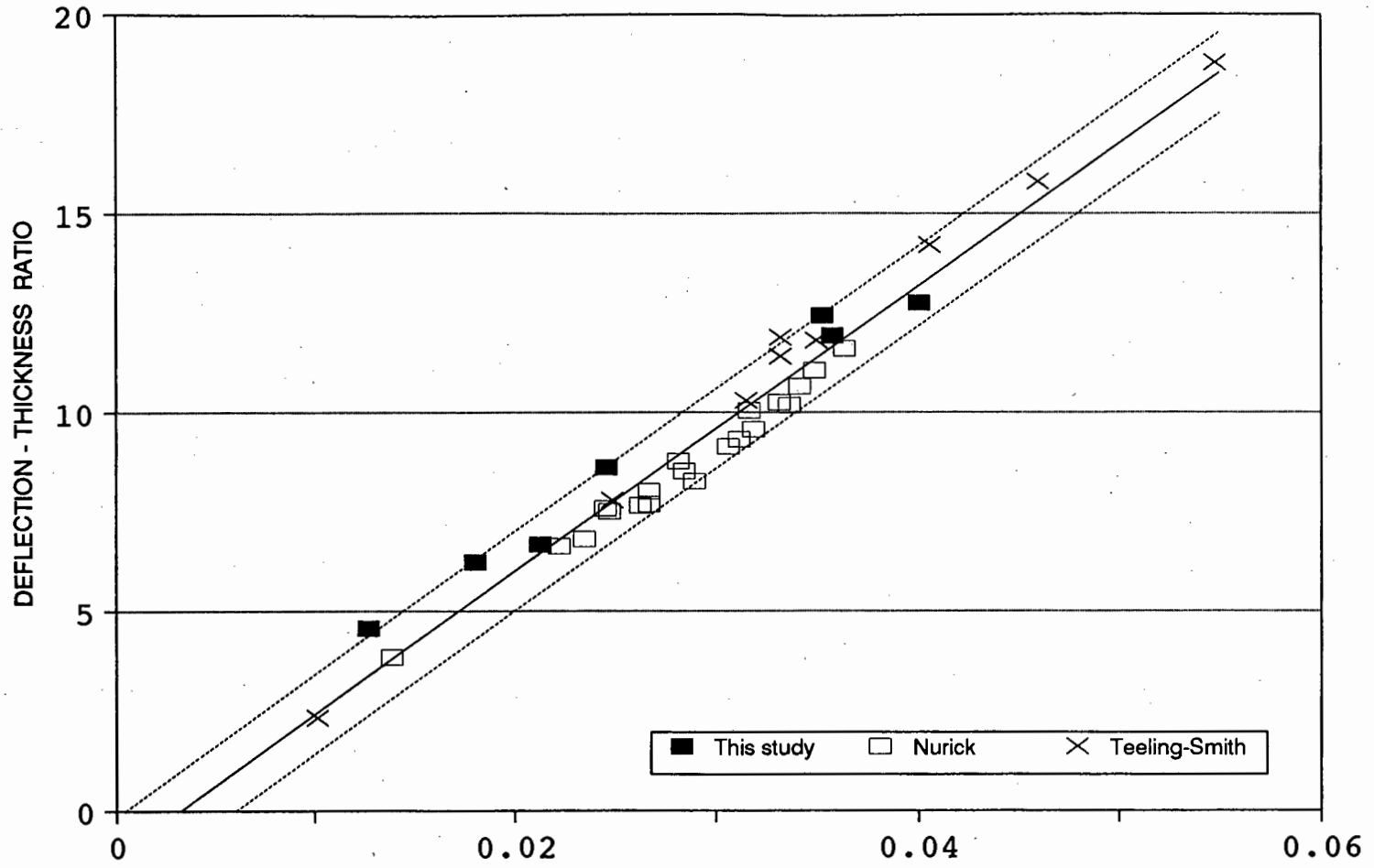

$$\phi_c^1 = \frac{T\ R\ \rho^{1/2}}{M\ t\ \sigma^{1/2}}$$

FIGURE 4.2(c) GRAPH OF DEFLECTION-THICKNESS RATIO vs. MODIFIED DIMENSIONLESS No. ϕ_c^1 FOR RESULTS BY NURICK [9], TEELING-SMITH [12] AND THIS STUDY

4.2 BEAMS

Beams with the same dimensions as the stiffeners used in the Series PS experiments were tested individually. The same clamping rig and ballistic pendulum were used as for the plate experiments.

The experimental results are shown in Fig. 4.3, where the deflection-thickness ratio is plotted against the applied impulse. The least squares equations for deflection against applied impulse are given in Appendix E. Figs. 4.4(a,b,c,d) show the beam results plotted together with the plate results and the plate components of the stiffened plate tests. Here it is observed that for a beam thickness of 6 mm, the beam deflection is essentially the same as for the plate-component only of the stiffened plates. In the preliminary tests, discussed in section 2.2.1, it was noted that stiffeners thicker than 8 mm caused the plates to tear for relatively low applied impulses. Thus it seems that above a certain thickness, the stiffener behaviour becomes the dominant factor in the stiffened plate response.

The results were compared with tests done on similar dimension mild steel beams by Symonds and Jones [23], who also used a ballistic pendulum. In an attempt to compare results, Johnson's dimensionless damage number [26] given as

$$\alpha = \frac{\rho V_o^2}{\sigma_d} = \frac{I^2}{(lbt)^2\ \rho\sigma} \qquad (4.9)$$

was used. Here ρ is material density, V_o is impact velocity and σ_d is the damage yield stress. Fig. 4.5(a) gives the plot of deflection-thickness ratio against $\alpha^{1/2}$.

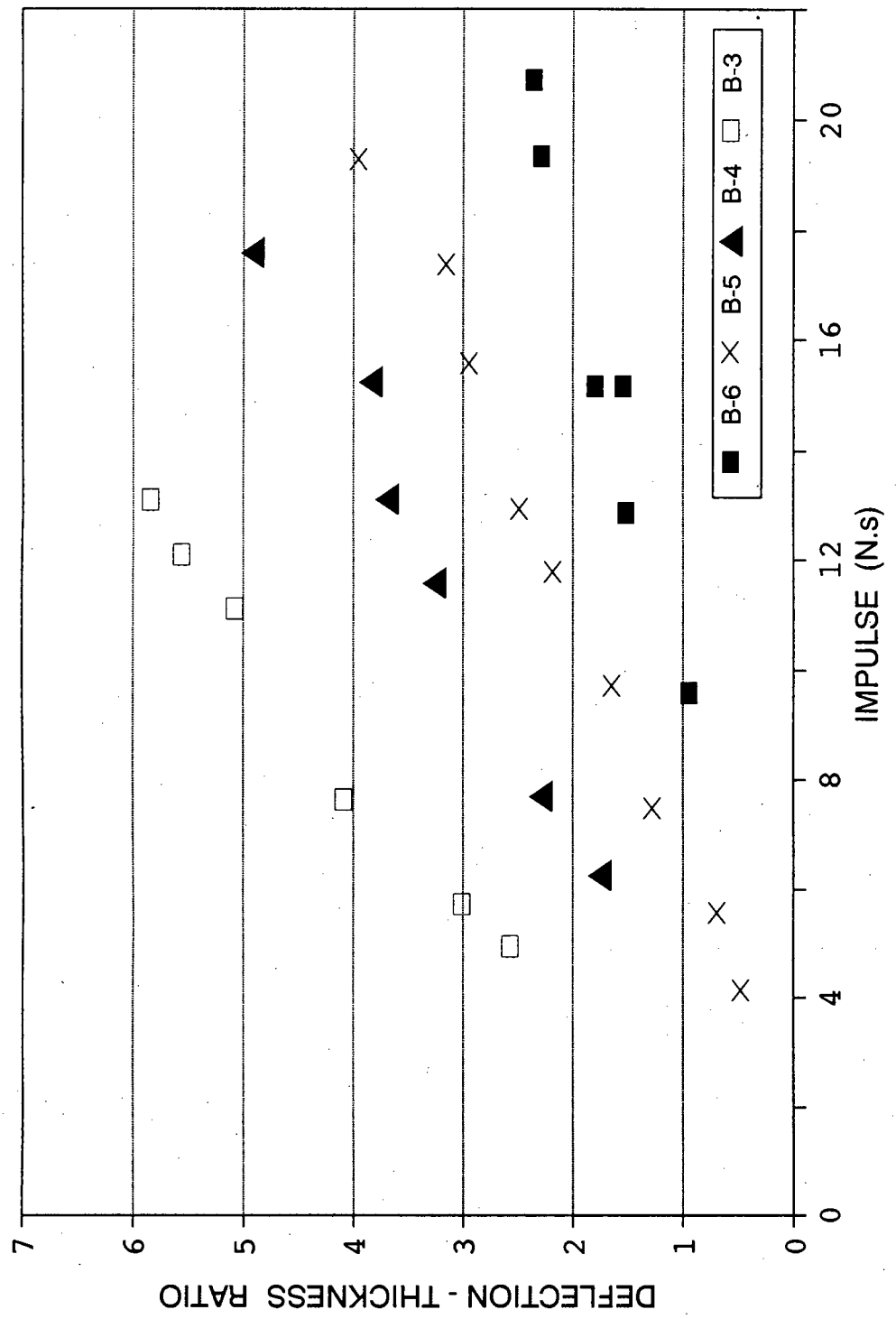

FIGURE 4.3 GRAPH OF DEFLECTION-THICKNESS RATIO vs. IMPULSE FOR ALL BEAM TESTS

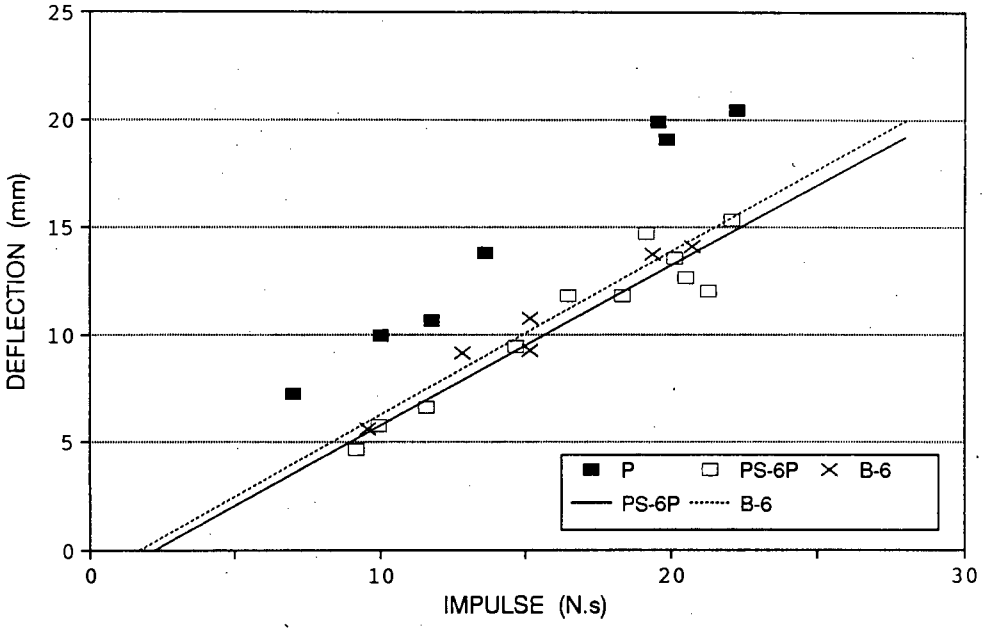

FIGURE 4.4(a) GRAPH OF DEFLECTION-THICKNESS RATIO vs. IMPULSE FOR BEAM TESTS (thickness = 6 mm)

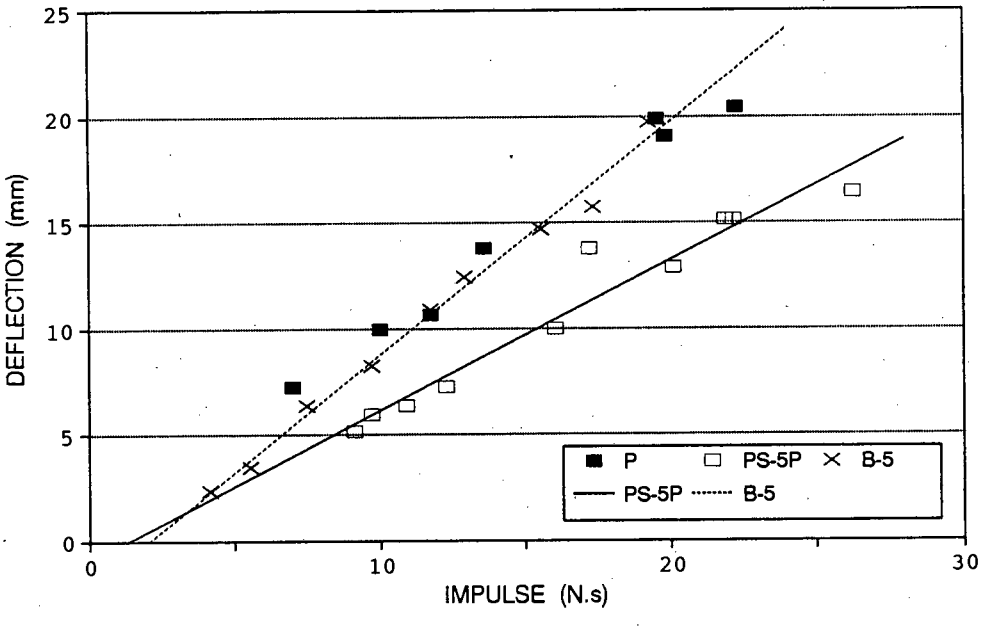

FIGURE 4.4(b) GRAPH OF DEFLECTION-THICKNESS RATIO vs. IMPULSE FOR BEAM TESTS (thickness = 5 mm)

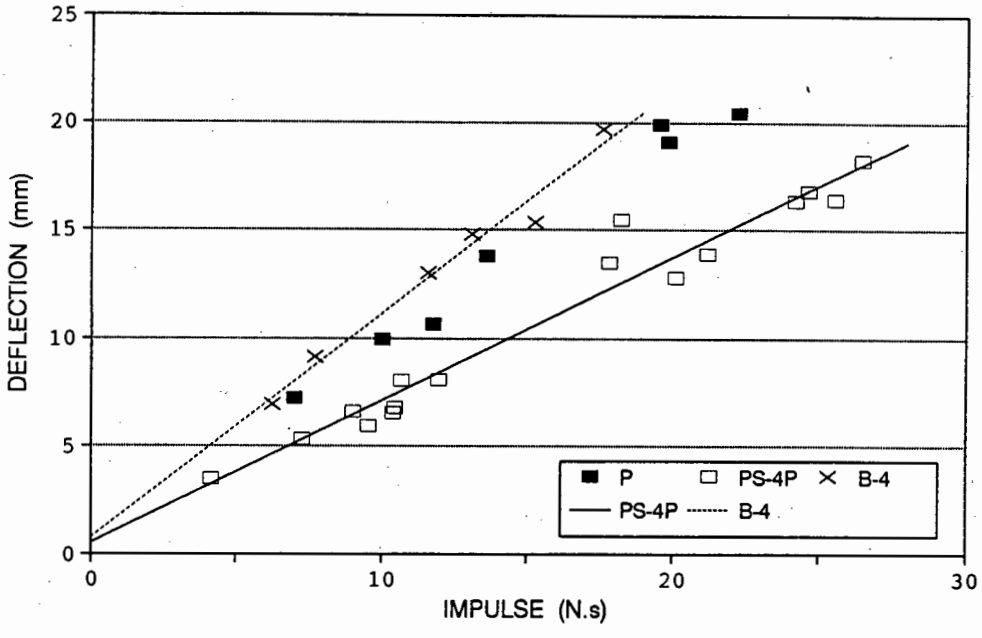

FIGURE 4.4(c) GRAPH OF DEFLECTION-THICKNESS RATIO vs. IMPULSE FOR BEAM TESTS (thickness = 4 mm)

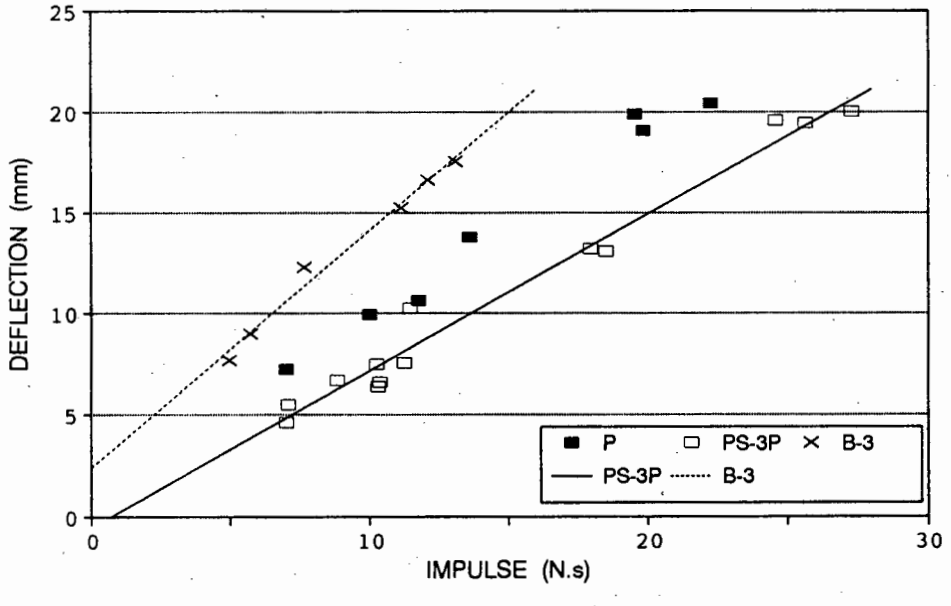

FIGURE 4.4(d) GRAPH OF DEFLECTION-THICKNESS RATIO vs. IMPULSE FOR BEAM TESTS (thickness = 3 mm)

Symonds and Jones [23] plotted their beam results against a non-dimensionalised form of the initial kinetic energy given as

$$\lambda = \frac{m\ V_o^2\ L^2}{M_o\ t} \tag{4.10}$$

where M_o = static fully plastic bending moment of the beam

Symonds and Jones [23] measured impact velocities which were approximately a factor of ten higher than those recorded in this study. Appendix D shows how the impact velocity of the beam was derived. The mass of the ballistic pendulum used by Symonds and Jones [23] was 21,77 kg. It should also be noted that the static yield stress of the beam material in this study is approximately double that used in [23].

A geometry number, used to modify equation (4.9), is defined as

$$\beta = \frac{l}{t} \times \frac{b}{t} \tag{4.11}$$

where l = length of beam

b = breadth of beam

Figure 4.5(b) gives a plot of the deflection-thickness ratios for this study's results against a non-dimensional number γ, which includes the geometry number β, given by

$$\gamma = (\alpha\beta)^{1/2} = \frac{I}{t^2\ \sqrt{\rho b l \sigma}} \tag{4.12}$$

Figure 4.5(c) shows a similar plot, including Symonds and Jones' results [23].

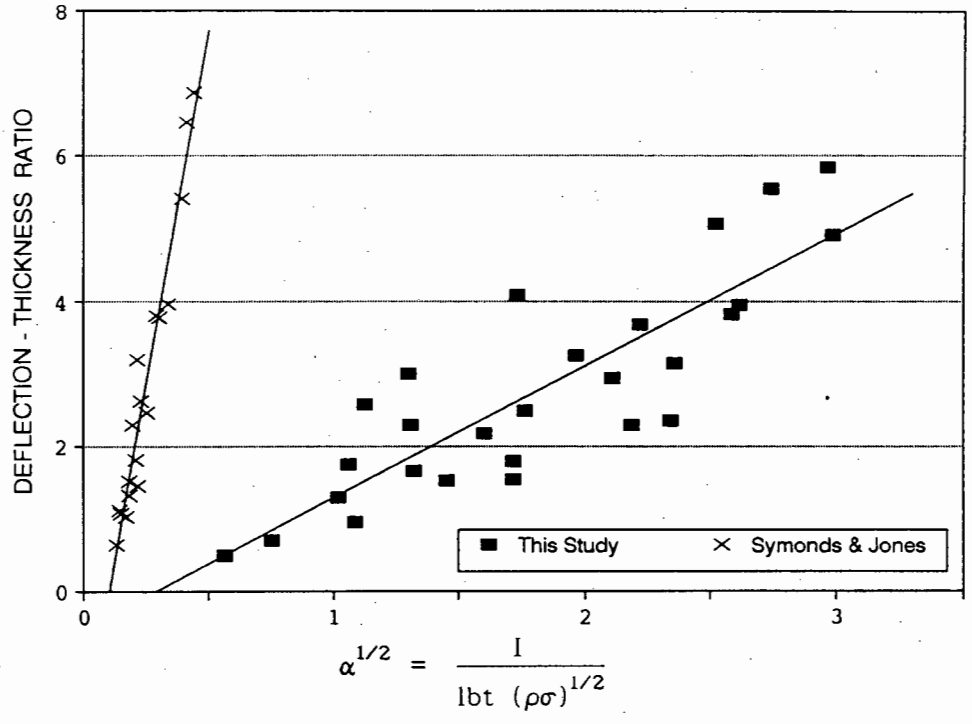

FIGURE 4.5(a) GRAPH OF BEAM DEFLECTION-THICKNESS RATIO vs. $\alpha^{1/2}$

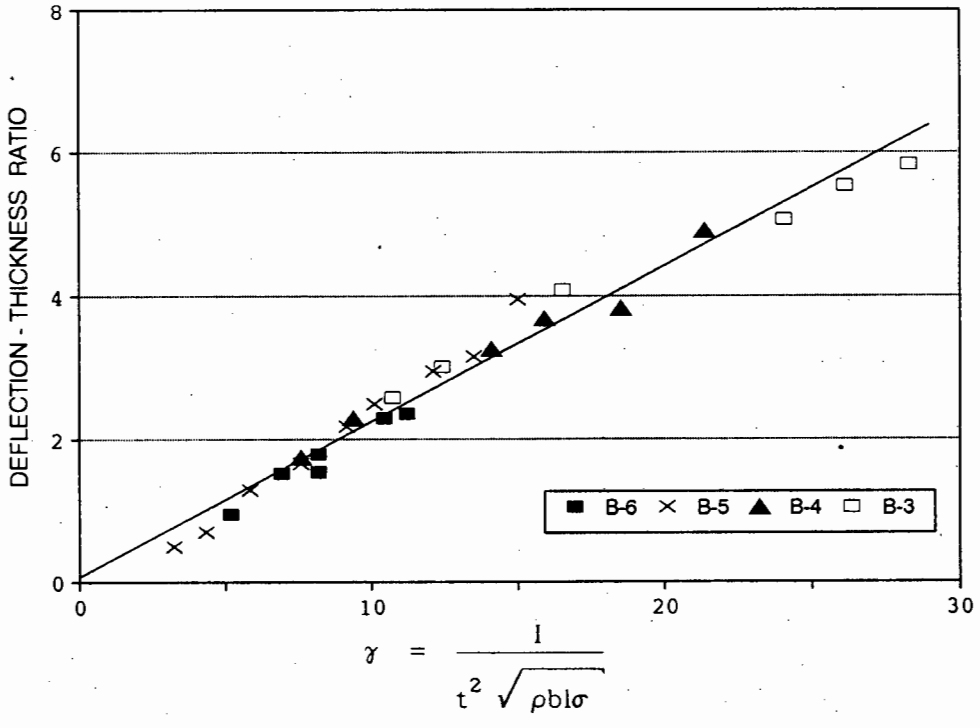

FIGURE 4.5(b) GRAPH OF DEFLECTION-THICKNESS RATIO vs. γ FOR THIS STUDY

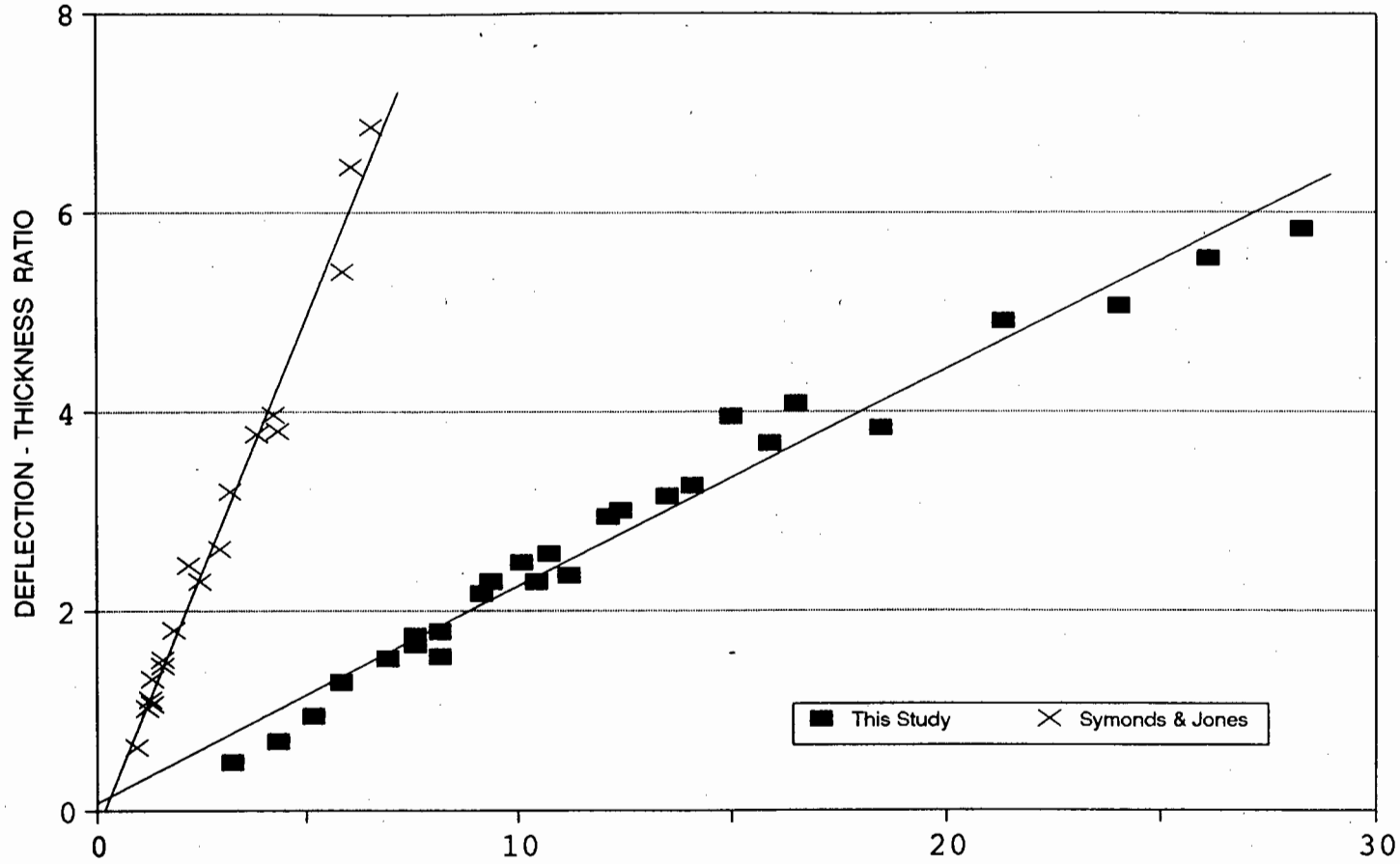

$$\gamma = \frac{I}{t^2 \sqrt{\rho b l \sigma}}$$

FIGURE 4.5(c) GRAPH OF DEFLECTION-THICKNESS RATIO vs. γ
RESULTS FOR SYMONDS AND JONES [23] AND THIS STUDY

The introduction of the mass factor, μ, (see section 4.1) gives a non-dimensional number of the form

$$\phi_b = \gamma \mu = \frac{I}{Mt} \sqrt{\frac{\rho b l}{\sigma}} \qquad (4.13)$$

Figs. 4.5(d) and 4.5(e) gives plots of deflection-thickness ratio against ϕ_b for this study's and Symonds and Jones' results respectively. Fig. 4.5(f) shows a combined graph of the results from this study and Symonds and Jones' work. A plot of deflection-thickness ratio against ϕ_b/t is given in Fig. 4.5(g). Figs. 4.5(d,e,f,g) all show the least squares lines bounded by ± 1 deflection-thickness ratio.

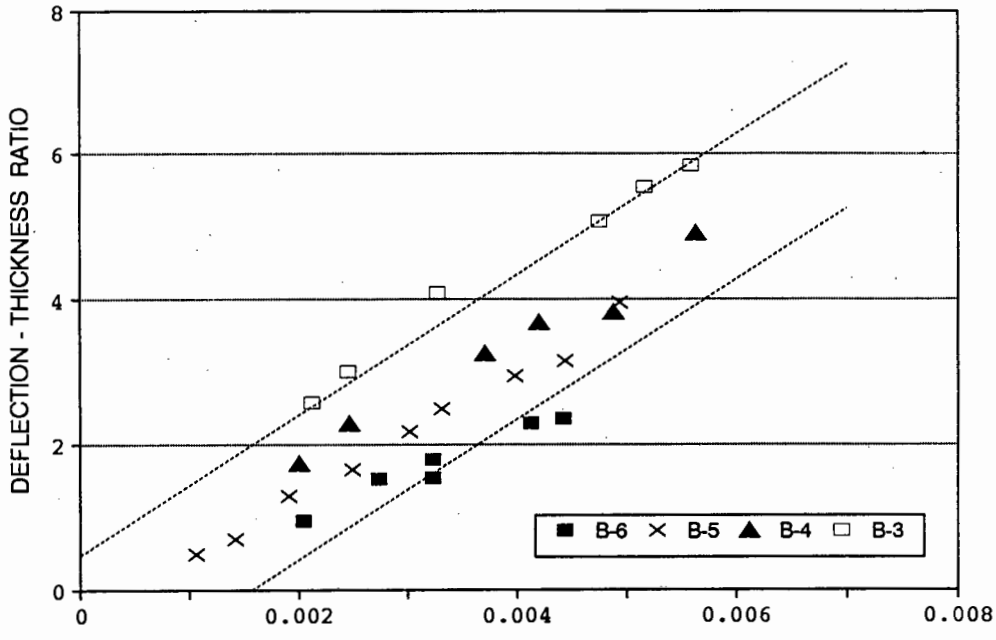

$$\phi_b = \frac{I}{Mt}\sqrt{\frac{\rho bl}{\sigma}}$$

FIGURE 4.5(d) GRAPH OF BEAM DEFLECTION-THICKNESS RATIO vs. ϕ_b FOR THIS STUDY

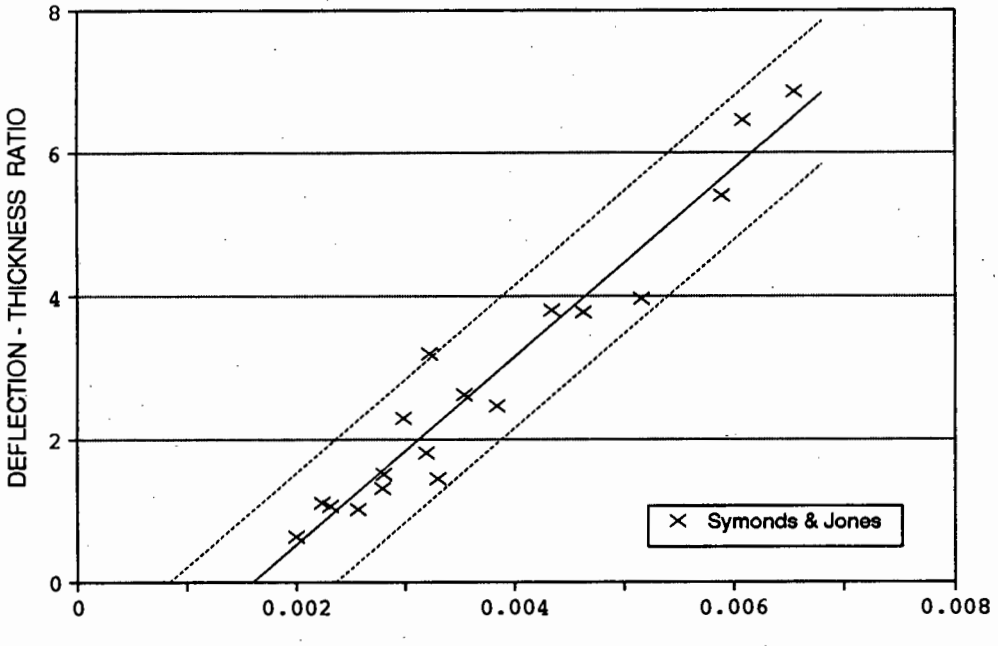

$$\phi_b = \frac{I}{Mt}\sqrt{\frac{\rho bl}{\sigma}}$$

FIGURE 4.5(e) GRAPH OF BEAM DEFLECTION-THICKNESS RATIO vs. ϕ_b FOR SYMONDS AND JONES [23]

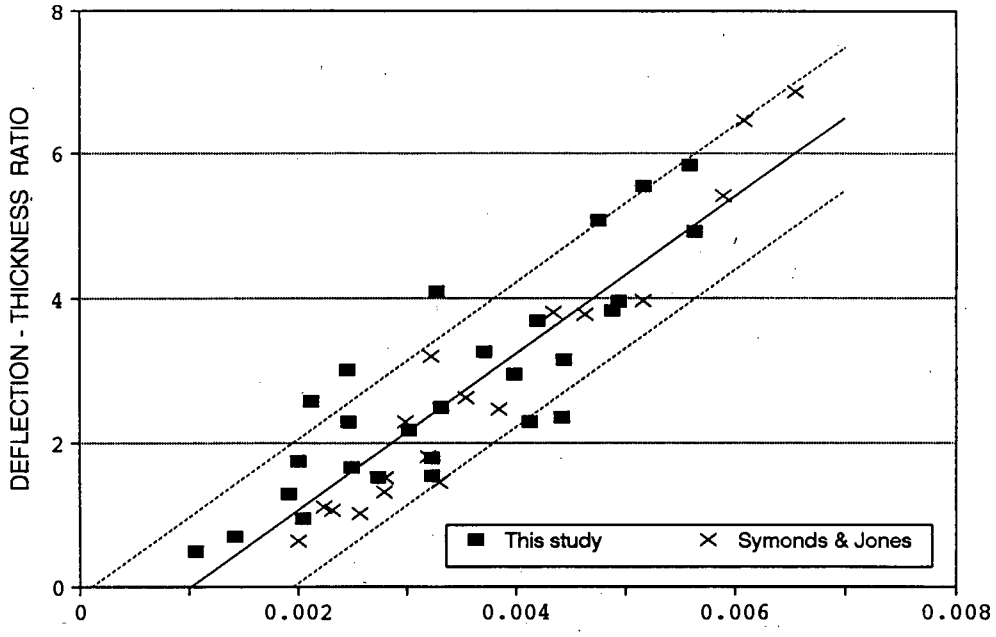

$$\phi_b = \frac{I}{Mt}\sqrt{\frac{\rho b l}{\sigma}}$$

FIGURE 4.5(f) GRAPH OF BEAM DEFLECTION-THICKNESS RATIO vs. ϕ_b FOR SYMONDS AND JONES [23] AND FOR THIS STUDY

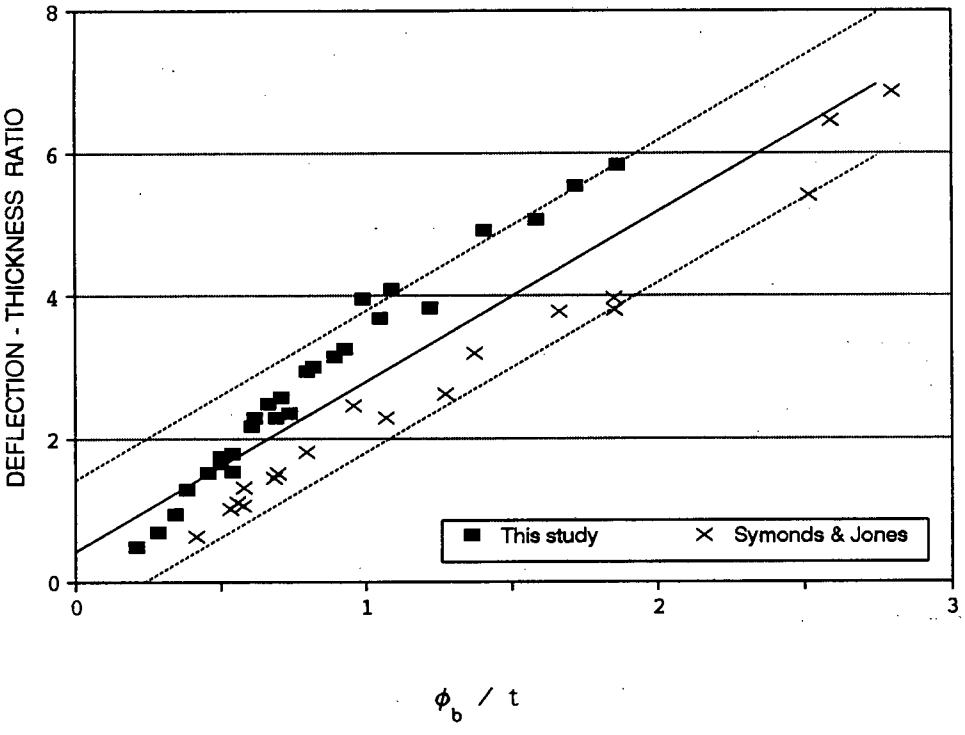

FIGURE 4.5(g) GRAPH OF DEFLECTION-THICKNESS RATIO vs. ϕ_b / t FOR SYMONDS AND JONES [23] AND FOR THIS STUDY

4.3 STIFFENED PLATES

The experimental results for the stiffened plates, ie. Series PS tests, are presented in this section.

Fully-clamped circular plates were stiffened using beams of four different thicknesses, ie. 3, 4, 5 and 6 mm. The experimental results are shown in Figs. 4.6 (a, b, c, d), where the deflections of the plates are plotted against the applied impulse. Also plotted in the same graph are the results for the Series P tests; where these are given as reference values. Fig. 4.7(a) gives the results for all the stiffened plate tests on the same graph. A plot showing the upper and lower bound least squares lines, ie. the least squares lines for the PS-3 and PS-6 tests respectively is given in Fig. 4.7(b).

The general trend in the stiffened plate deformation behaviour is that the thicker the stiffener, the smaller the plate deflection for equal impulses. Also, the thicker the stiffener, the smaller the maximum impulse with which the structure can be loaded, before tearing of the plate occurred. Table 4.1 below gives the maximum applied impulse, which was measured for each plate-stiffener combination.

The least squares lines for the stiffened plate results are given in Appendix E.

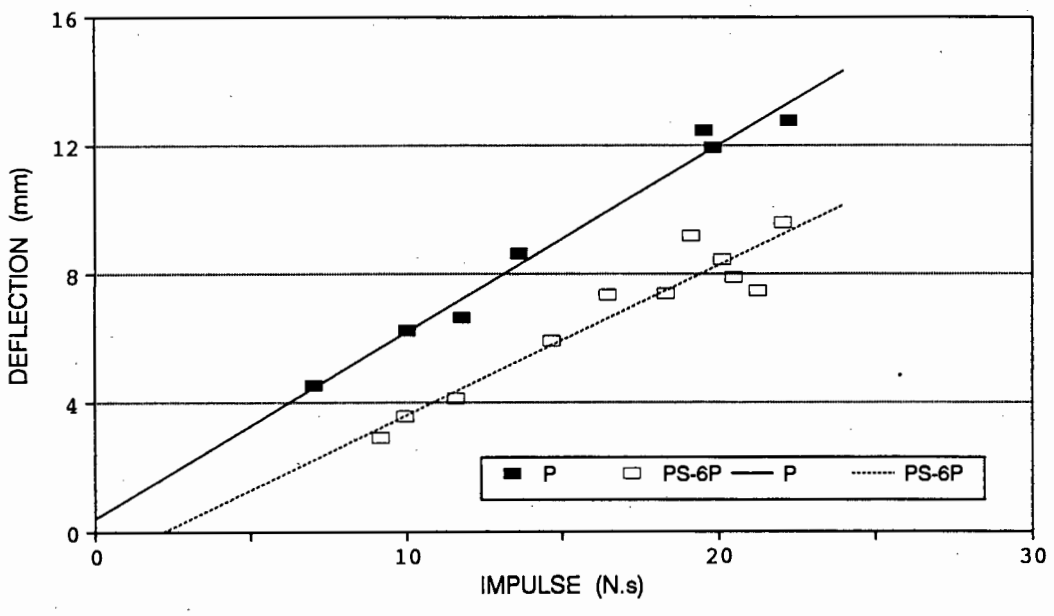

FIGURE 4.6(a) GRAPH OF DEFLECTION-THICKNESS RATIO vs. IMPULSE FOR STIFFENED PLATES (stiffener thickness = 6 mm)

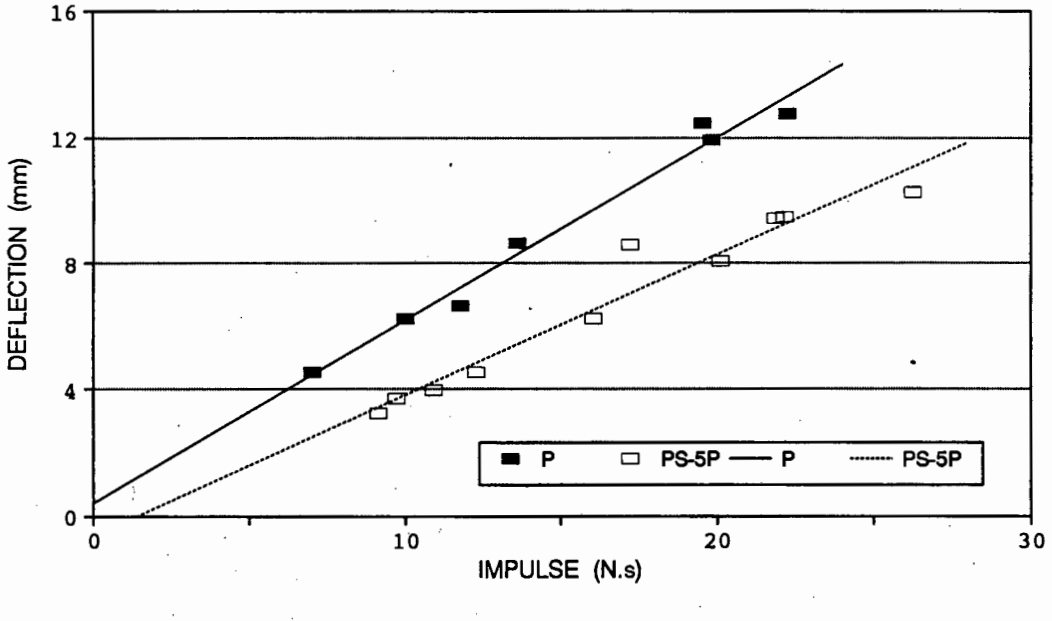

FIGURE 4.6(b) GRAPH OF DEFLECTION-THICKNESS RATIO vs. IMPULSE FOR STIFFENED PLATES (stiffener thickness = 5 mm)

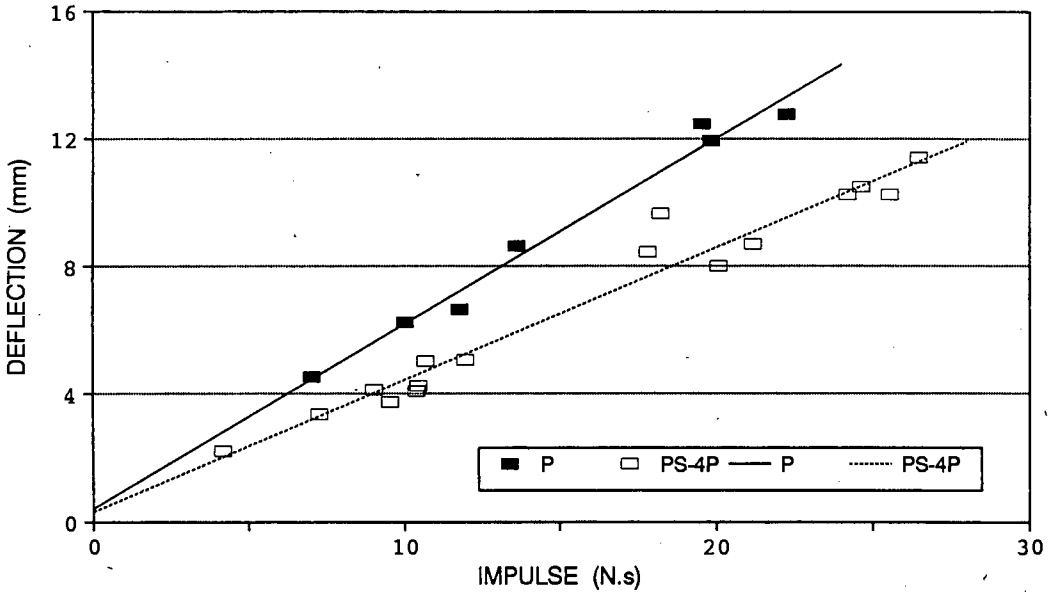

FIGURE 4.6(c) GRAPH OF DEFLECTION-THICKNESS RATIO vs. IMPULSE FOR STIFFENED PLATES (stiffener thickness = 4 mm)

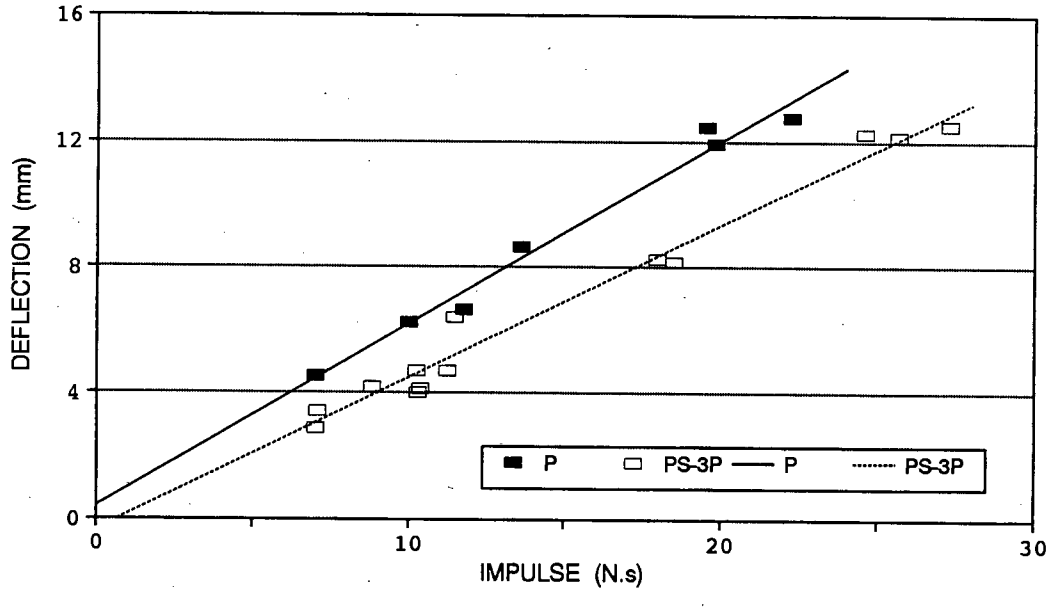

FIGURE 4.6(d) GRAPH OF DEFLECTION-THICKNESS RATIO vs. IMPULSE FOR STIFFENED PLATES (stiffener thickness = 3 mm)

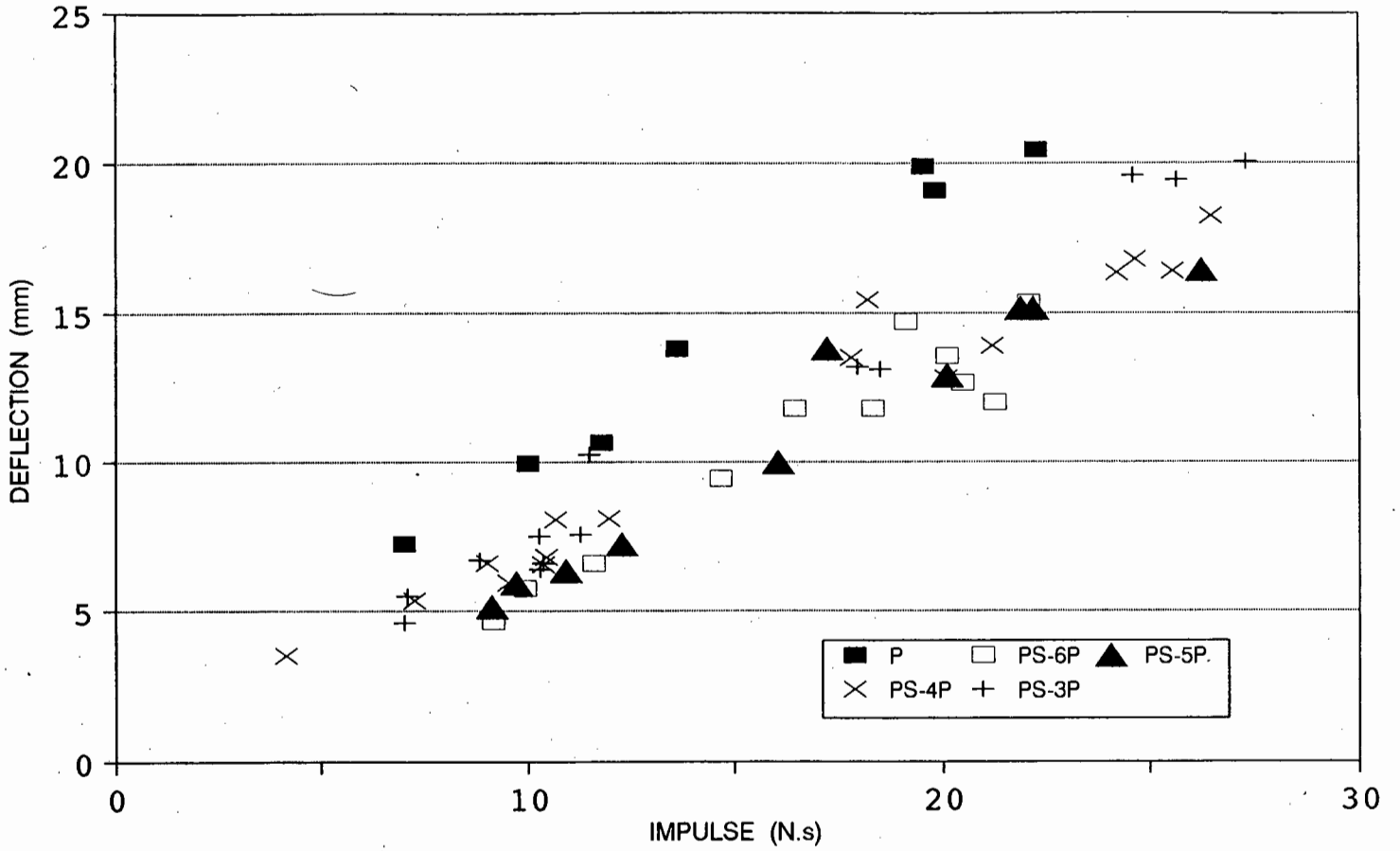

FIGURE 4.7(a) GRAPH OF DEFLECTION-THICKNESS RATIO vs. IMPULSE FOR ALL STIFFENED PLATE TESTS

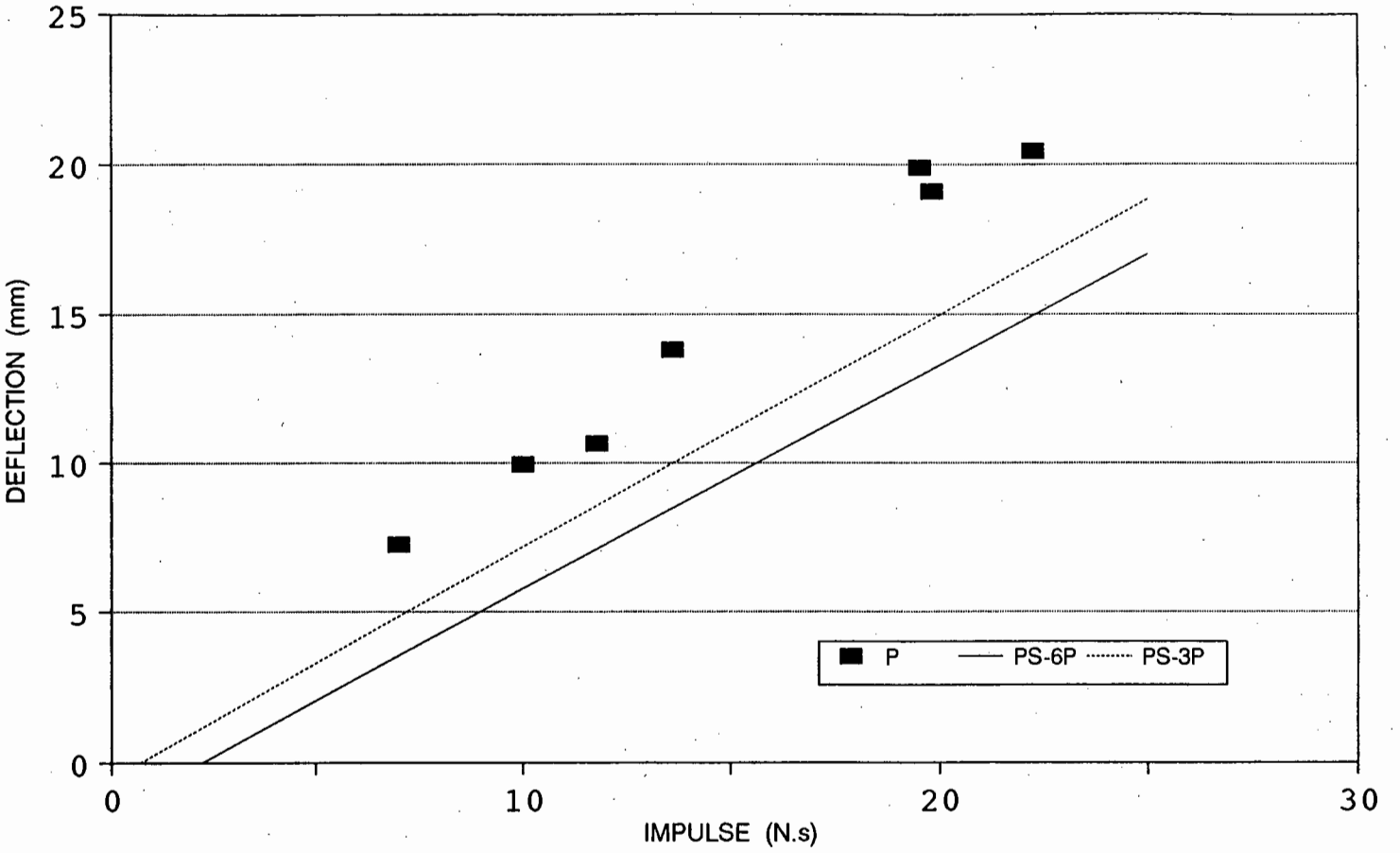

FIGURE 4.7(b) GRAPH OF DEFLECTION-THICKNESS RATIO vs. IMPULSE FOR ALL STIFFENED PLATE TESTS SHOWING UPPER AND LOWER LIMITS

TABLE 4.1 MAXIMUM APPLIED IMPULSES MEASURED BEFORE TEARING OF PLATE OCCURRED

Stiffener Thickness (mm)	Maximum Applied Impulse (N.s)
3	27.32
4	26.48
5	26.43
6	22.06

The elastic force-deflection equations for the stiffened plate components are :

a) stiffeners: $$P = y \left(\frac{32\ E\ b\ t_s^3}{l^3} \right) \qquad (4.14)$$

b) plates: $$P = y \left(\frac{16\ \pi\ E\ t_p^3}{3\ R^2\ (1 - \upsilon^2)} \right) \qquad (4.15)$$

where P = total uniformly applied force

t_s = stiffener thickness

t_p = plate thickness

The elastic bending stiffness ratio is obtained by dividing equation (4.14) by equation (4.15) and is given by

$$K_{s/p} = \frac{6\ b\ t_s^3\ R^2\ (1 - \upsilon^2)}{\pi\ l^3\ t_p^3} \tag{4.16}$$

The ratios for the stiffened plates are :

a) PS-6 : 1.83
b) PS-5 : 1.06
c) PS-4 : 0,54
d) PS-3 : 0.23

4.4 ENERGY ANALYSIS

A comparative study of the shape approximation functions, discussed in section 3.5, determined that the most suitable function for the energy analysis is the one given by Duffey [1] :

$$w = w_o \cos\left(\frac{\pi r}{2R} \right) \tag{4.17}$$

This function is the most suitable for Series P, PS and B experiments, as can be seen in Figs. 4.8(a,b,c,d,e). Fig. 4.8(a) shows the comparison for a plate-only test. Fig. 4.8(b) gives the comparative plot for the plate component of a stiffened plate, where the deformed profile is shown in the same orientation as the stiffener placement, while Fig. 4.8(c) shows the comparison for an orientation at 90° to the stiffener. Fig. 4.8(d) shows the plot for the stiffener beam only. Fig 4.8(e) compares the experimentally determined deformed shapes shown in Figs. 4.8(b) and 4.8(c). This plot shows that the deformed shape is not noticeably changed by the presence of a stiffener for the particular plate-stiffener geometry

used in this investigation.

Substituting the shape function equation (4.9) into the deformation energy equation (3.4) for a plate, gives

$$E_{deformation} = \frac{\pi^3 \, t \, \sigma_y \, w_o^2}{(1 - \upsilon + \upsilon^2)^{1/2}} \left(\frac{1}{4} + \frac{1}{\pi^2} \right) \qquad (4.18)$$

Table 4.2 lists the deformation energy formulations for a plate as given by Duffey [1], Westine and Baker [16] and Lippman [15]. Table 4.2 also lists the deformation energy formulations for a fully-clamped plate as given by Duffey [15], Westine and Baker [14] and Lippmann [13]. The table also gives a comparison of deformation energy values obtained using these formulae, for two typical plate-only tests; one for a deflection-thickness ratio of 6.67 and the other for a ratio of 12,77. The use of the static yield stress shows quite different results to those obtained using the dynamic yield stress. Note that hereafter only the energy formulation of Duffey will be referred to, since it gave the closest input energy - deformation energy correlation.

Ideally the deformation energy should equal the input energy. From the results in Table 4.2 it is observed that for the smaller deformation, the deformation energy is 54% of the input energy, while for the larger deformation it is 65%. These values are obtained using Duffey's modified formula, ie. with dynamic yield stress, which shows the closest correlation and is thus used for further analysis.

Fig. 4.9 shows the graph of the input and the deformation energies for the plate tests plotted against Nurick's damage number ϕ_c. Also shown is the percentage differences between the input and the deformation energies.

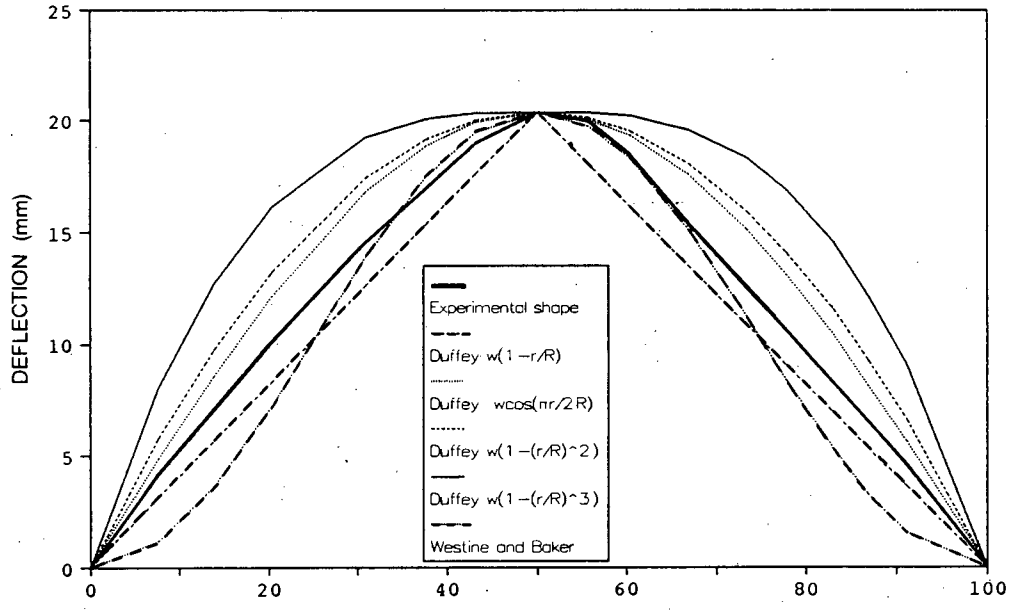

FIGURE 4.8(a) COMPARISON BETWEEN EXPERIMENTAL AND PREDICTED SHAPE FUNCTIONS FOR A PLATE

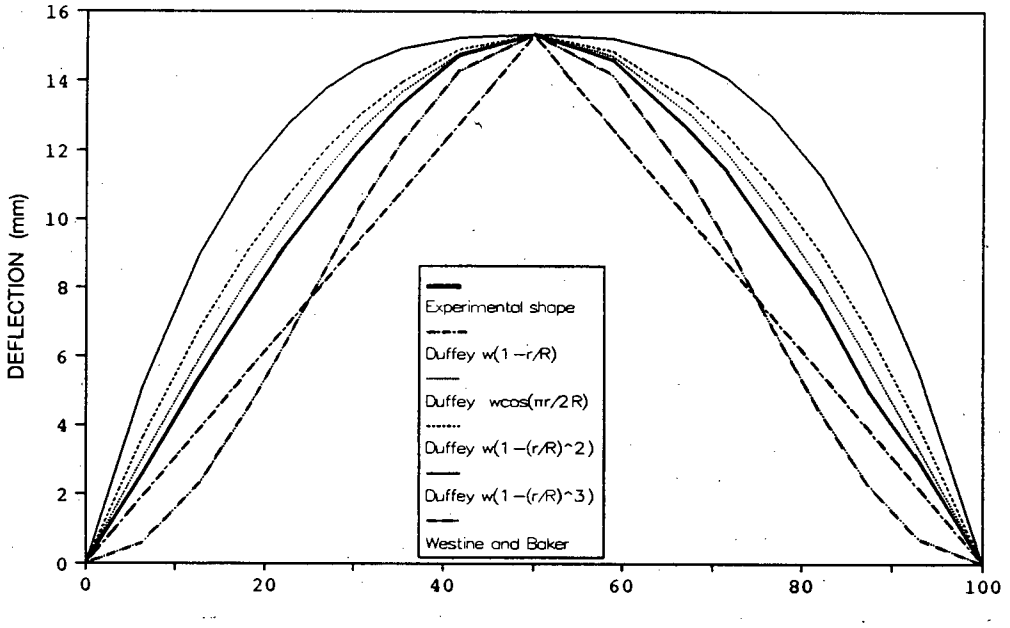

FIGURE 4.8(b) COMPARISON BETWEEN EXPERIMENTAL AND PREDICTED SHAPE FUNCTIONS FOR A STIFFENED PLATE
(orientation parallel to stiffener)

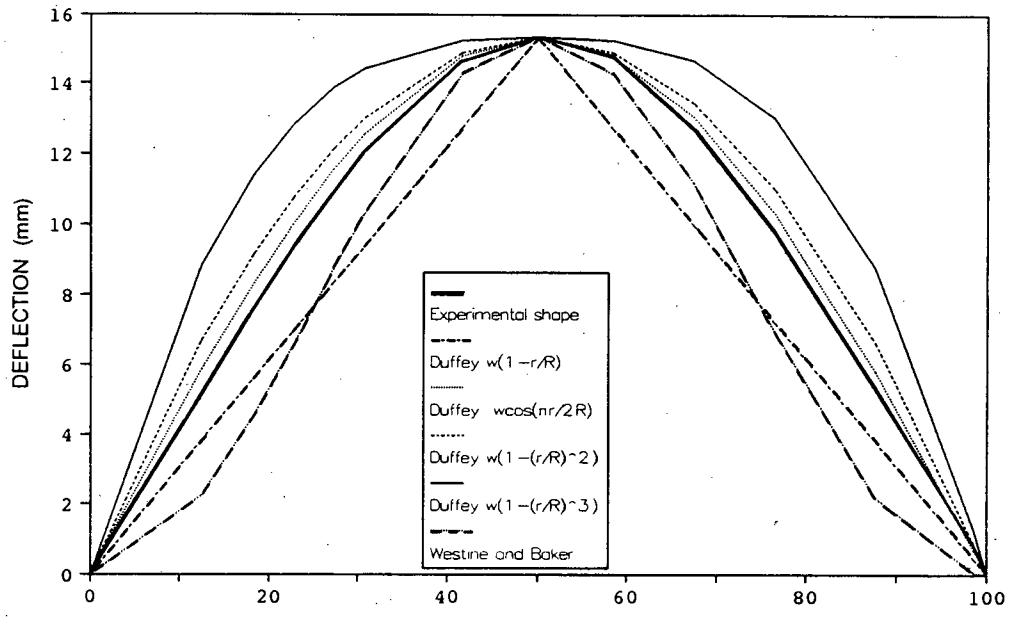

FIGURE 4.8(c) COMPARISON BETWEEN EXPERIMENTAL AND PREDICTED SHAPE FUNCTIONS FOR A STIFFENED PLATE
(orientation perpendicular to stiffener)

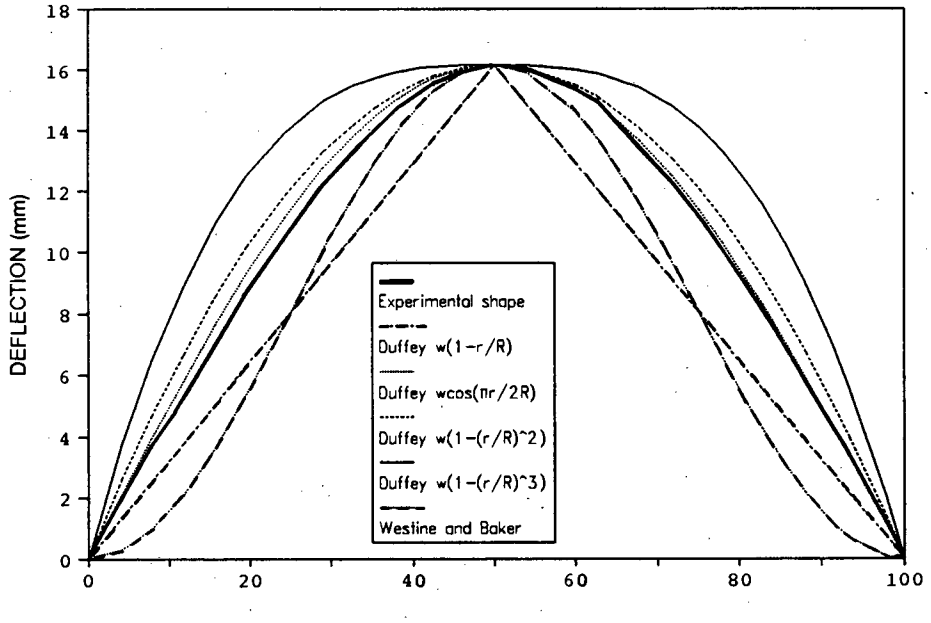

FIGURE 4.8(d) COMPARISON BETWEEN EXPERIMENTAL AND PREDICTED SHAPE FUNCTIONS FOR A STIFFENER

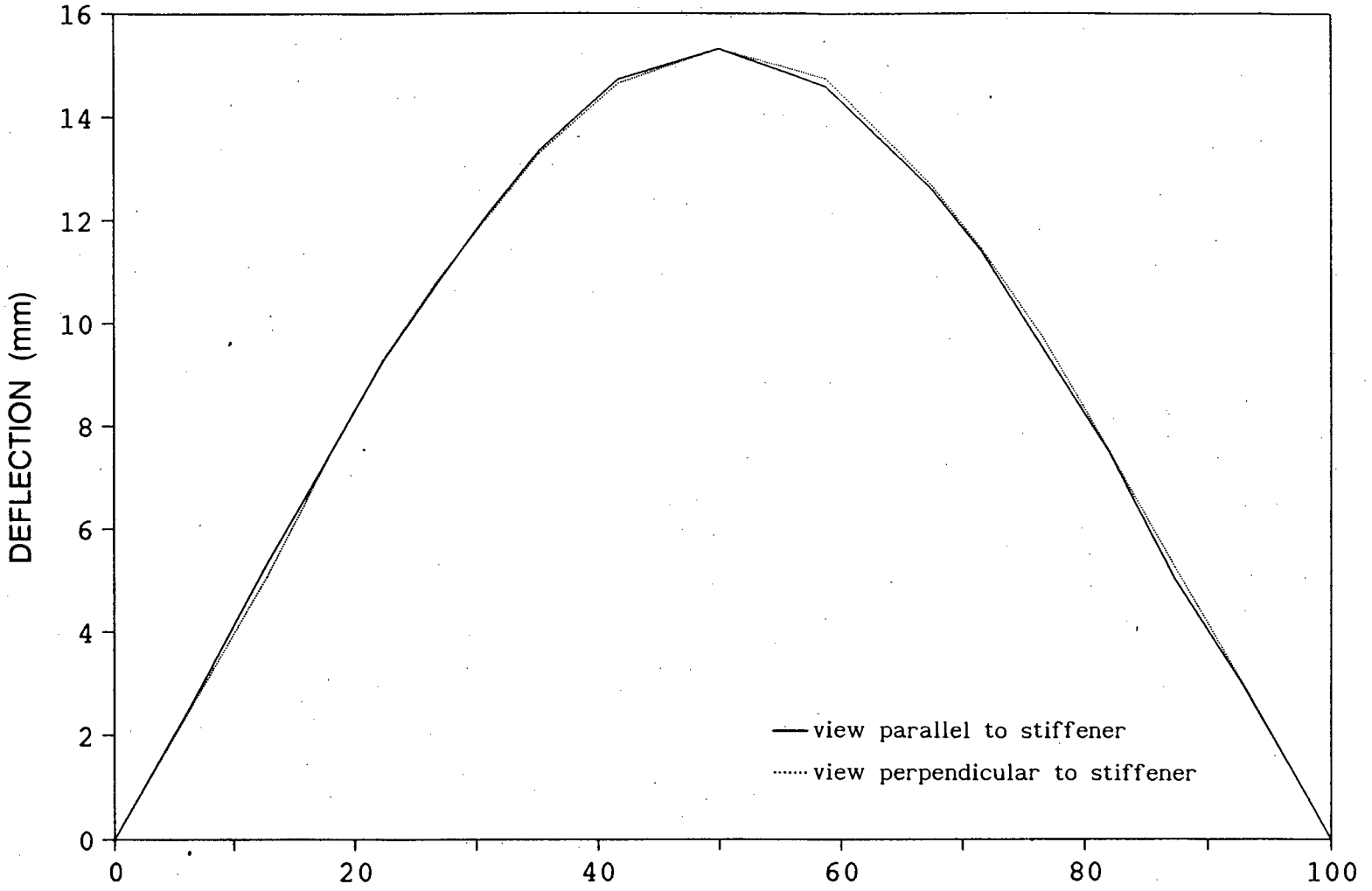

FIGURE 4.8(e) COMPARISON BETWEEN EXPERIMENTALLY DETERMINED DEFORMED SHAPES PERPENDICULAR TO ONE ANOTHER FOR A STIFFENED PLATE

<- Pg 80

TABLE 4.2 DEFORMATION ENERGY FORMULAE AND DEFORMATION ENERGIES FOR PLATES

Deformation Energy Formulae :

a) Duffey [1] $$E_{def} = \frac{\pi^3 \, t \, \sigma_y \, \omega_o^2}{4(1 - \upsilon + \upsilon^2)^{1/2}} \left(\frac{1}{4} + \frac{1}{\pi^2} \right)$$

b) Westine and Baker [16] $$E_{def} = \frac{\pi^2 \, \sigma_y \, \pi^2 \, \omega_o}{4} + \frac{\pi^3 \, \sigma_y \, t \, \omega_o}{16}$$

c) Lippman [15] $$E_{def} = 0{,}423 \, \rho t R^2 \left(\frac{\omega_o \, \pi}{1{,}306} \times R \left(\frac{\rho}{\sigma_y} \right)^{1/2} \right)^2$$

Test P1 : I = 11,79 N.s ; ω_o = 10,65 mm ; σ_o^1 = 679,21 MPa ; E_{input} = 704,56 J

	$E_{def}(\sigma_o)$	% of E_{inp}	$E_{def}(\sigma_o^1)$	% of E_{inp}
Duffey [1]	142,63	20,24	380,34	53,98
Westine & Baker [16]	106,71	15,15	284,56	40,39
Lippman [15]	113,14	16,06	301,70	42,82

Test P2 : I = 22,24 N.s ; ω_o = 20,43 mm ; σ_o^1 = 793,44 MPa ; E_{input} = 2507,03 J

	$E_{def}(\sigma_o)$	% of E_{inp}	$E_{def}(\sigma_o^1)$	% of E_{inp}
Duffey [1]	524,86	20,94	1634,99	65,22
Westine & Baker [16]	362,50	14,46	1129,23	45,04
Lippman [15]	416,35	16,61	1296,95	51,73

Table 4.3 lists typical deformation energy values for the plate components of the stiffened plate tests. As was noted for Table 4.2, the use of the dynamic yield stress gives better results than the static yield stress.

Figs. 4.10(a,b,c,d) show the deformation energies of the plate components of the stiffened plates plotted against the applied impulse. Plate-only results are plotted as a reference. The plots also show the percentage difference in deformation energies of the plate-only tests and of the plate components of the stiffened plates.

The difference between the deformation energy curves in Figs. 4.10(a, b,c,d) is due to the the energy absorbed by the stiffener, see Fig. 4.11. However this could not be verified because of the poor analytical results obtained for the beam deformation energies.

TABLE 4.3 INPUT AND DEFORMATION ENERGIES FOR STIFFENED PLATES

Test No.	E_{inp}	$E_{def}(\sigma_o)$	$E_{def}(\sigma_o^1)$
PS-1	788,24	113,01	317,45
PS-2	1784,85	296,69	921,90
PS-41	579,79	66,28	178,45
PS-40	1891,46	288,25	897,30
PS-16	578,84	82,91	221,89
PS-52	2367,87	336,58	1068,84
PS-31	448,87	71,11	183,63

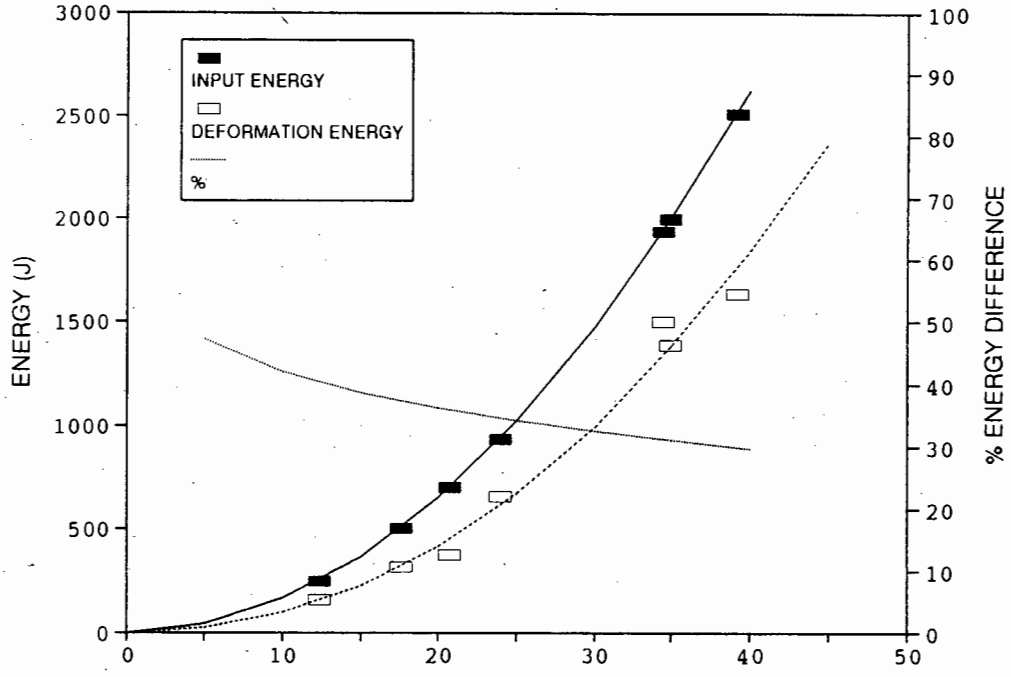

$$\phi_c = \frac{I}{\pi R t^2 (\rho\sigma)^{1/2}}$$

FIGURE 4.9 GRAPH OF THE INPUT AND DEFORMATION ENERGIES vs. ϕ_c FOR PLATE TESTS (also shown is the % difference in energies)

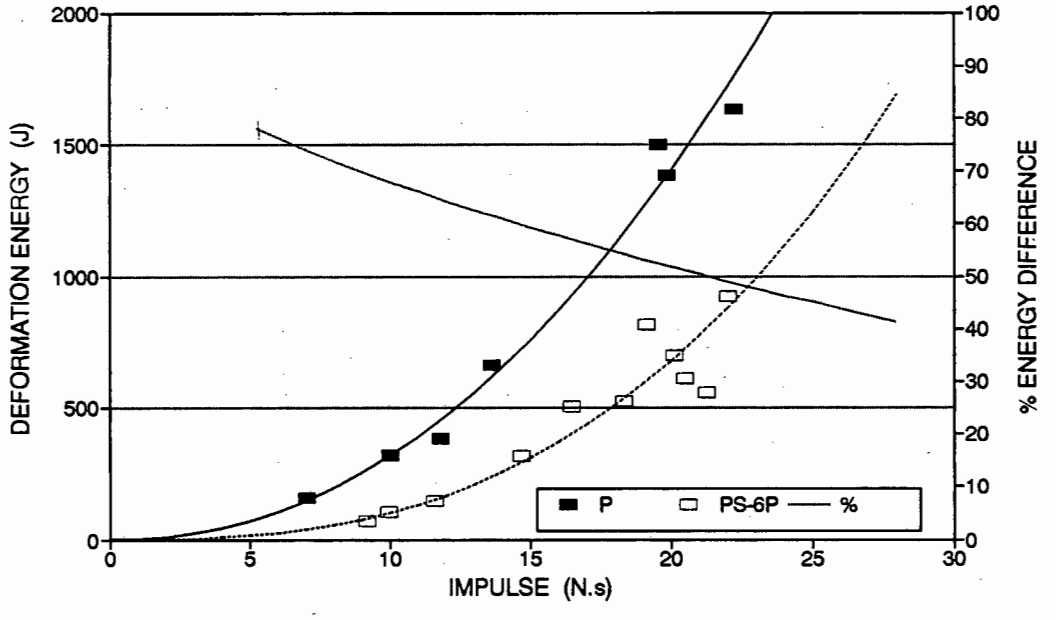

FIGURE 4.10(a) GRAPH OF DEFORMATION ENERGIES vs. IMPULSE FOR PLATES AND STIFFENED PLATES (stiffener thickness = 6 mm) (also shown is the % difference in deformation energies)

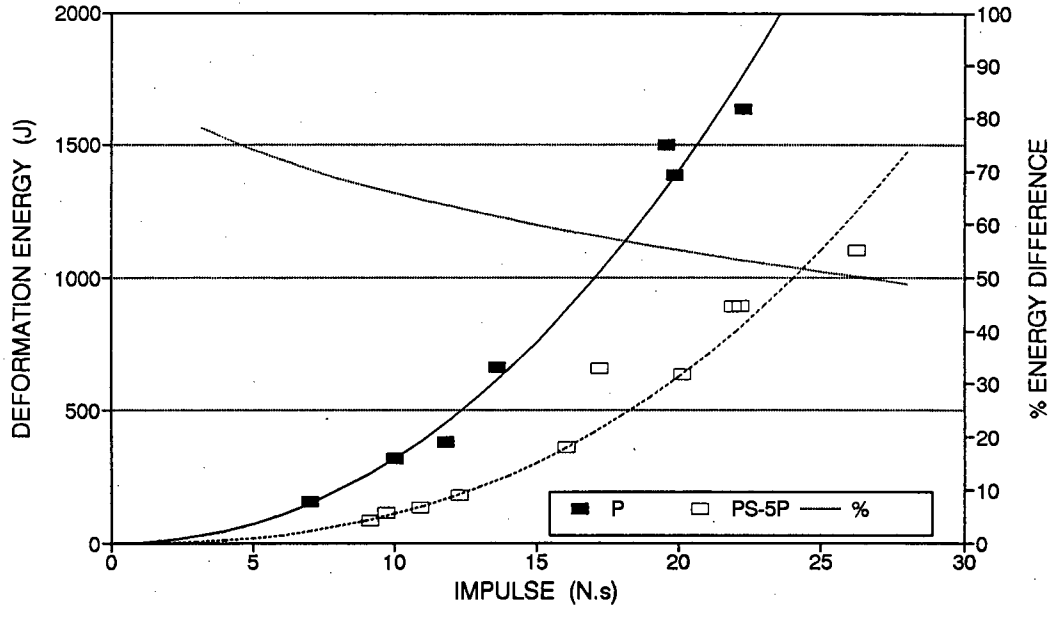

FIGURE 4.10(b) GRAPH OF DEFORMATION ENERGIES vs. IMPULSE FOR PLATES AND STIFFENED PLATES (stiffener thickness = 5 mm) (also shown is the % difference in deformation energies)

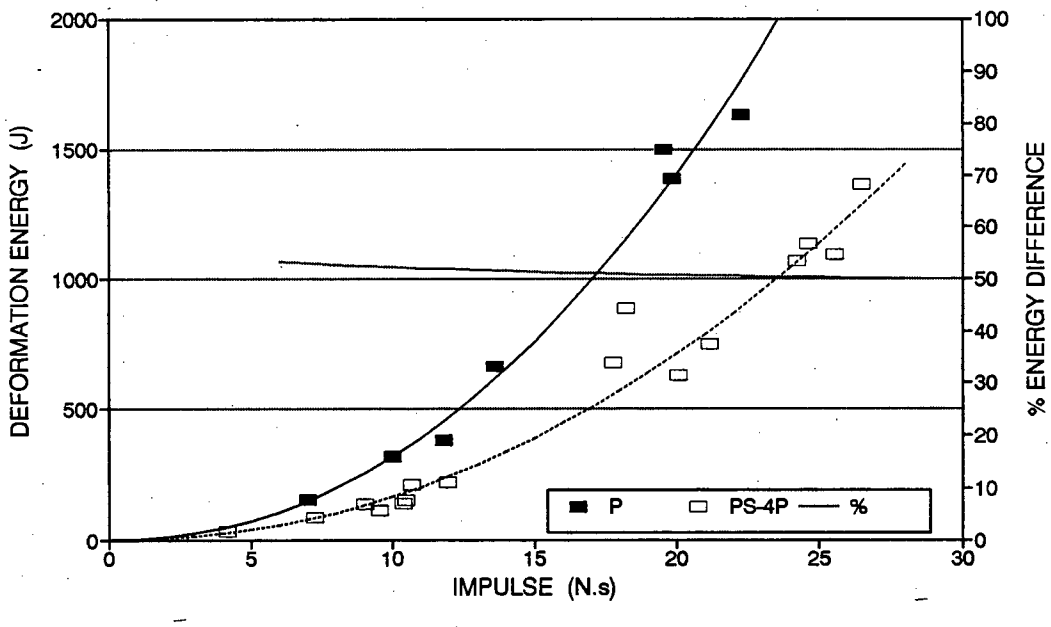

FIGURE 4.10(c) GRAPH OF DEFORMATION ENERGIES vs. IMPULSE FOR PLATES AND STIFFENED PLATES (stiffener thickness = 4 mm) (also shown is the % difference in deformation energies)

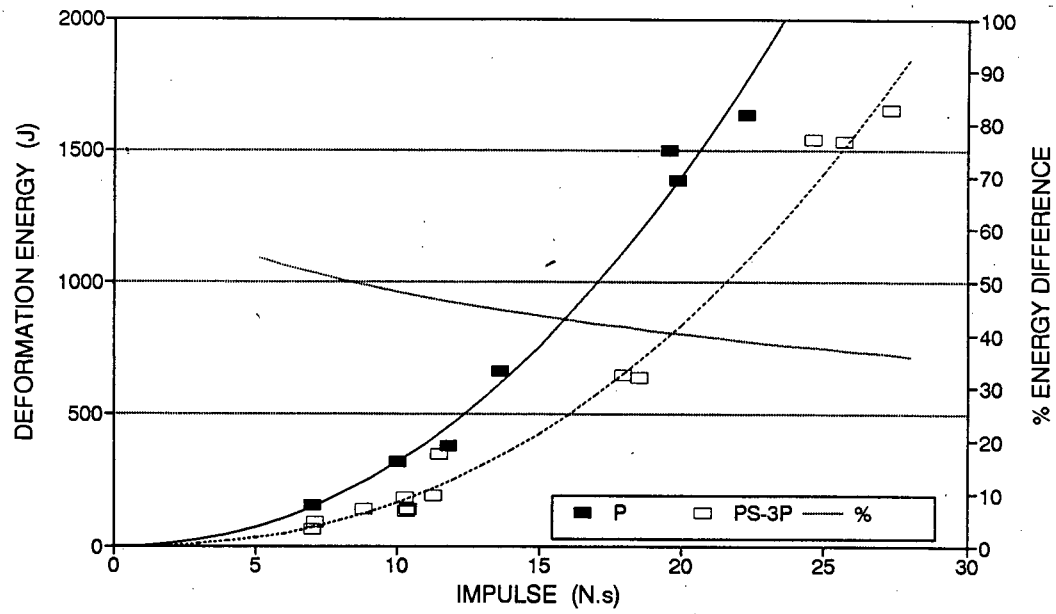

FIGURE 4.10(d) GRAPH OF DEFORMATION ENERGIES vs. IMPULSE FOR PLATES AND STIFFENED PLATES (stiffener thickness = 3 mm) (also shown is the % difference in deformation energies)

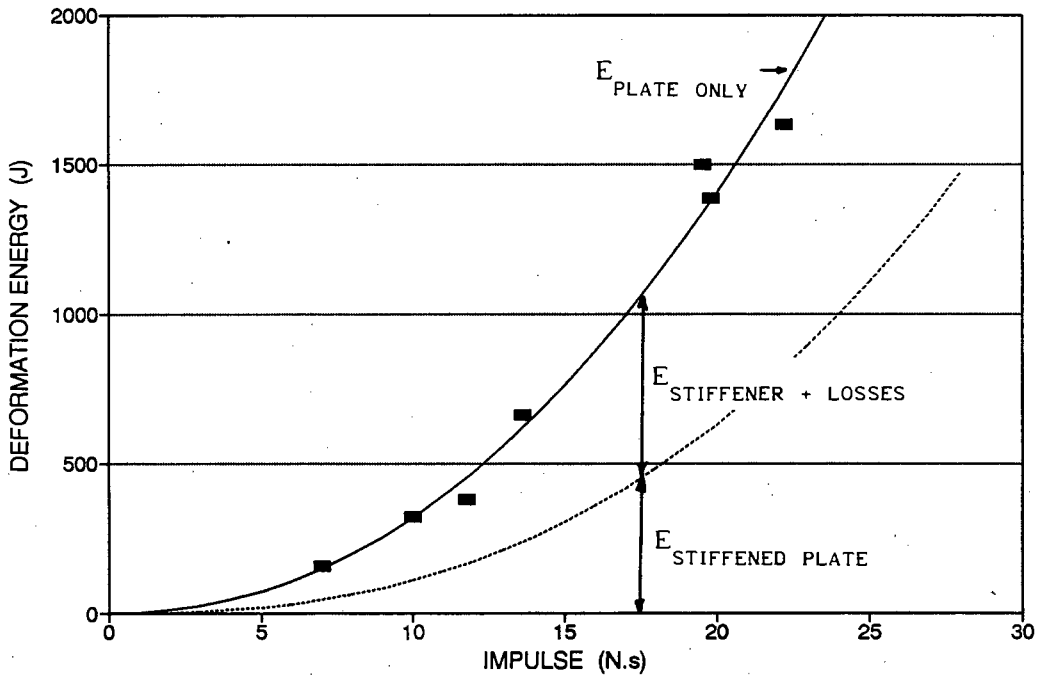

FIGURE 4.11 DESCRIPTIVE GRAPH OF DEFORMATION ENERGY vs. IMPULSE

CHAPTER 5 - DISCUSSION

This thesis presents an experimental investigation into the dynamic response of fully-clamped stiffened circular plates subjected to impulsive loading. Experiments were also performed on fully-clamped circular plates and fully-clamped beams.

The results of the circular plate experiments were compared with those of similar experiments performed by Nurick [9] and Teeling-Smith [12]. The least squares line for the deflection-thickness versus Nurick's damage number ϕ_c for the plates from this study is given by

$$\frac{\delta}{t} = 0{,}330\ \phi_c + 0{,}39 \qquad \text{with } r = 0{,}991 \qquad \text{where } \phi < 40$$

Fig 4.2(a) shows that the slope of this line is lower than for the other two sets of experimental results mentioned above. Since the masses of the ballistic pendulums used in Nurick's [9], Teeling-Smith's [12] and this study's experiments were 66,60 kg, 88,73 kg and 96,06 kg respectively, this difference in mass could be a possible reason for the difference in slopes. By introducing an experimental mass scaling factor μ to the non-dimensional number ϕ_c, the data points converge when plotted against this modified number ϕ_c^1, as is shown in Fig 4.2(c).

The non-dimensional damage number for fully-clamped circular plates, including the experimental mass scaling factor, is given by

$$\phi_c^1 = \frac{I\ R\ \rho^{1/2}}{M\ t\ \sigma^{1/2}}$$

The least squares line for the deflection-thickness ratio against ϕ_c^1 for this study is given by

$$\frac{\delta}{t} = 321{,}887\ \phi_c^1 + 0{,}391 \qquad \text{with } r = 0.991 \qquad \text{and } \phi_c^1 < 0.041$$

and for the combined results of Nurick [9], Teeling-Smith [12] and this study it is

$$\frac{\delta}{t} = 358{,}634\ \phi_c^1 - 1{,}195 \qquad \text{with } r = 0.983 \qquad \text{and } \phi_c^1 < 0.058$$

Fig. 4.2(c) shows that the results almost all lie within ± 1 deflection-thickness ratio of the least squares line.

The experimental beam results were compared with those obtained by Symonds and Jones [23], who also used a ballistic pendulum. The results however did not compare well when the beam deflection-thickness ratios were plotted against a non-dimensional kinetic energy value λ, which was developed by Symonds and Jones [23]. Symonds and Jones [23] measured impact velocities which were approximately a factor of ten higher than those recorded in this study. The static yield stress of the beam material in this study was a factor of two greater and the ballistic pendulum mass for this study was approximately a factor of 4,5 greater.

A non-dimensional number ϕ_b, based on Johnson's damage number [26], was developed. Johnson's damage number was modified by incorporating a beam geometry factor and an experimental mass scaling factor to give

$$\phi_b = \frac{I}{Mt}\sqrt{\frac{\rho b l}{\sigma}}$$

A plot of deflection-thickness ratio against ϕ_b for Symonds and Jones [23] and this study, as shown in Fig. 4.5(f), shows that most of the results lie within ± 1 deflection-thickness ratio of the least squares line, which is given by

$$\frac{\delta}{t} = 1087{,}897\ \phi_c^1 - 1{,}128 \qquad \text{with } r = 0{,}905$$

The least squares line for this study is given by

$$\frac{\delta}{t} = 969{,}004\ \phi_c^1 - 0{,}539 \qquad \text{with } r = 0{,}857$$

The stiffened plates were strengthened using four different thickness stiffeners. The general trend observed when plotting the plate mid-point deflections against applied impulse, is that the thicker the stiffener, the smaller the plate deflections for equal impulses. Fig. 4.7(a) shows this trend.

It was also observed that too thick a stiffener causes the plate components to tear at lower impulses than for plate-only tests. Thus a thinner stiffener, which allows greater plate deflections for equal impulses than a thicker stiffener, enables the structure to sustain a greater impulse. It appears that the plate component must be allowed to dissipate sufficient plastic deformation energy through deflecting, or else the plate starts tearing at the clamping boundaries. It appears that for an elastic bending stiffness ratio of the stiffener to the plate greater than about 1.8, the stiffener behaviour dominates the response, see Fig 4.4(a). Fig. 4.4(b) shows that for an elastic bending stiffness ratio of approximately unity, the deflection behaviour of the plate only and the beam only are very similar.

An energy study was done on the plates and on the stiffened plates. The energy balance for the plate tests is given by

$$E_{input} = E_{deformation\ plate}$$

and for the stiffened plates by

$$E_{input} = E_{deformation\ plate} + E_{deformation\ stiffener} + E_{losses}$$

The input energy is calculated by considering the applied impulse. The deformation energy of the plate and the plate component of the stiffened plate is calculated by measuring the maximum mid-point deflection and assuming a deformed shape function.

Figs. 4.10(a,b,c,d) show that as the impulse increases, the plate component of the stiffened plate structure tends to dissipate a greater fraction of the deformation energy than the stiffener component.

The deformation energy values found for the stiffeners and beams were very poor, and thus the energy equation could not be verified. Therefore the magnitude of the energy lost, eg. due to friction, could not be determined.

CHAPTER 6 - RECOMMENDATIONS

The experimental observations mentioned in Section 2.5 were beyond the scope of this thesis. It is thus recommended that further investigation be done into the following :

1. The springback effect which occurs between plate and stiffener. A displacement-time history analysis might reveal at what time during the deformation this separation takes place. Also, what effect would the bonding of the stiffener to the plate have on the response?

2. The failure of the stiffener beam before the failure of the plate.

3. The effect the mass of the ballistic pendulum has on the measured impulsive loading of the plate.

REFERENCES

1 DUFFEY TA, 1967, **The large deflection dynamic response of clamped circular plates subjected to explosive loading,** Sandia Laboratories Research Report, SC-RR-67532.

2. SYMONDS PS, WIERZBICKI T, 1978, **Membrane modes for impulsively loaded plates,** J. Appl. Mech., Vol.46, pp.58 - 64.

3. NURICK GN, MARTIN JB, 1989, **Deformation of thin plates subjected to impulsive loading - A Review, Part II: Experimental Studies,** Int. J. Impact Eng., Vol. 8, No. 2, pp.171 - 186.

4. CHONG CC, HETHERINGTON JG, LOK TS, SMITH PD, 1989, **Response of panels subject to simultaneous in-plane compressive loading and transverse blast loading,** Presented at SUSI 89, First International Conference on Structures under Shock and Impact, 11-13 July, Cambridge, Massachusetts.

5. HOULSTON R, SLATER JE, 1989, **The response and damage of a stiffened panel subjected to force-field and confined air-blast loading,** Presented at SUSI 89, First International Conference on Structures under Shock and Impact, 11-13 July, Cambridge, Massachusetts.

6. SLATER JE, HOULSTON R, RITZEL DV, 1990, **Air-blast studies on naval steel panels: Final Report, Task DMEM-53,** Defence Research Establishment Suffield, Ralston, Alberta, Suffield Report No. 505.

7. HUMPHREYS JS, 1965, **Plastic deformation of impulsively loaded straight clamped beams,** J. Appl. Mech., Vol.32, pp.7 - 10.

8. HALLIDAY D, RESNICK R, **Fundamentals of Physics,** Second Edition, John Wiley & Sons.

9. NURICK GN, 1987, **Large deformations of thin plates subjected to impulsive loading,** Phd, University of Cape Town.

10. WIERZBICKI T, FLORENCE AL, 1970, **A theoretical and experimental investigation of impulsively loaded clamped circular viscoplastic plates,** Int. J. Solids. Structs., Vol. 6, pp. 553 - 568.

11. GHOSH SK, BALENDRA R, TRAVIS FW, 1978, **Inertial forming of circular and annular diaphragms,** Adv. Mech. Tool Des. Res., pp.845 - 854.

12. TEELING-SMITH RG, NURICK GN, 1991, **An investigation into the deformation and tearing of thin circular plates subjected to impulsive loads,** Int. J. Impact Eng. (to appear)

13. HOULSTON R, DESROCHERS CG, 1987, **Non-linear structural response of ship panels subjected to air-blast loading,** Computers and Structures, Vol.26, pp.1 - 15.

14. SCHUBAK RB, OLSON MD, ANDERSON DL, 1989, **Non-linear analysis of one-way stiffened plates under blast loads,** Presented at SUSI 89, First International Conference on Structures under Shock and Impact, 11-13 July, Cambridge, Massachusetts.

15. LIPPMAN H, 1974, **Kinetics of the axi-symmetric rigid-plastic membrane subject to initial impact,** Int. J. Mech. Sci., Vol.16, pp.297 - 303.

16. WESTINE PS, BAKER WE, 1974, **Energy solutions for predicting deformations in blast loaded structures,** Proc. 16 th. Explosive Safety Seminar, Hollywood Beach, Florida, U.S.A., pp.849 - 878.

17. SYMONDS PS, 1965, **Viscoplastic behaviour in response of structures to dynamic loading,** Proc. Coll. Behaviour of Materials under Dynamic Loading, ASME, NY, pp.106 - 129, Ed. N. J. Huffington, Jr.

18. DUFFEY TA, 1972, **An elastic-viscoplastic solution for impulsively loaded rings,** Int. J. Solids Structures, Vol.8, pp.913 - 921.

19. MARTIN JB, SYMONDS PS, 1966, **Mode approximations for impulsively loaded rigid-plastic structures,** J. Eng. Mech. Div., Proc. ASCE, Vol. 92, No. EM5, pp.43 - 66.

20. JONES N, 1986, **Some comments on the dynamic plastic behaviour of structures,** Keynote address, Proceedings of the International Symposium on Intense Dynamic Loading and its Effects, Beijing, China, pp.49 - 71.

21. ABRAMOWICZ W, JONES N, 1984, **Dynamic axial crushing of square tubes,** Int. J. Impact Eng., 2(2), pp.179 - 208.

22. ABRAMOWICZ W, JONES N, 1985, **Dynamic progressive buckling of circular and square tubes,** Liverpool University, Dept. Mech. Eng., Report ES/23/85.

23. SYMONDS PS, JONES N, 1972, **Impulsive loading of fully clamped beams with finite plastic deflections and strain-rate sensitivity,** Int. J. Mech. Sci., Vol. 14, pp.49 - 69.

24. MARSH KJ, CAMPBELL JD, 1963, **The effect of strain rate on the post-yield flow of mild steel,** J. Mech. Phys. Solids, Vol. 11, pp.49 - 63.

25. BODNER SR, SYMONDS PS, 1979, **Experiments on viscoplastic response of circular plates to impulsive loading,** J. Mech. Phys. Solids, Vol. 27, pp.91 - 113.

26. JOHNSON W, 1972, **Impact Strength of Materials,** Edward Arnold, London.

APPENDIX A - TENSILE TESTS

The specimen size was selected from ASTM designation E8M were the standard test specimen sizes are given. The Cowper-Symonds rigid-viscoplastic constitutive equation

$$\frac{\sigma_o^1}{\sigma_o} = 1 + \left(\frac{\dot{\varepsilon}}{\dot{\varepsilon}_o} \right)^{\frac{1}{n}}; \qquad n = 5 ; \qquad \dot{\varepsilon}_o = 40\ s^{-1}$$

is used to calculate the uniaxial static yield stress.

$$\sigma = \frac{F}{A} ; \qquad \dot{\varepsilon} = \frac{CHS}{L} \times \frac{1}{60} \qquad \text{where } L = \text{gauge length} = 62 \text{ mm}$$

1) Plate Material

Dimensions (mm)	CHS (in)	Chart Speed (in/m)	Yield σ_o^1 (MPa)	Strain Rate $\dot{\varepsilon}$ (s^{-1})	Uniaxial Yield Stress σ_o (MPa)
12,6 x 1.6	0,05	0,5	259,59	$3,414 \times 10^{-4}$	236,57
12,6 x 1,6	0,05	0,5	302,34	$3,414 \times 10^{-4}$	275,64
12,6 x 1,6	0,2	2	263,49	$1,366 \times 10^{-3}$	233,62
12,6 x 1,6	0,2	2	271,66	$1,366 \times 10^{-3}$	240,87
12,6 x 1,6	0,2	2	321,49	$1,366 \times 10^{-3}$	285,05
12,5 x 1,6	1	10	277,55	$6,828 \times 10^{-3}$	235,94
12,6 x 1,6	1	10	277,69	$6,828 \times 10^{-3}$	236,06
12,6 x 1,6	1	10	313,78	$6,828 \times 10^{-3}$	266,73
12,6 x 1,6	5	50	287,29	$3,414 \times 10^{-2}$	231,06
12,6 x 1,6	5	50	279,81	$3,414 \times 10^{-2}$	225,04
12,5 x 1,6	20	50	389,06	0,137	294,49
12,5 x 1,6	20	50	390,27	0,137	295,41

Average yield stress σ_o = 254,71

APPENDIX B - RIGID PLASTIC ANALYSIS OF DUFFEY [1]

The maximum deflection of a clamped circular plate is calculated by a simplified energy method for rigid-plastic material behaviour, while assuming a permanent deflection shape.

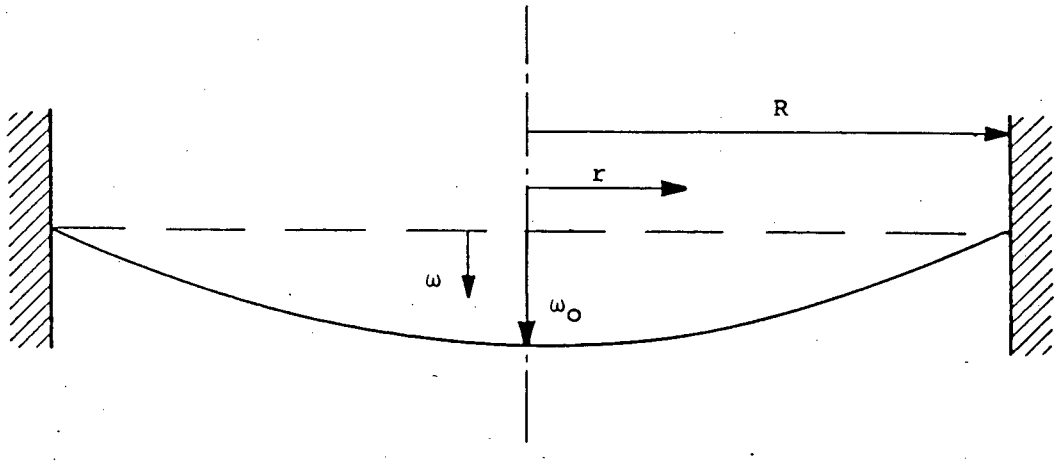

FIGURE B.1 CLAMPED CIRCULAR PLATE AFTER DEFORMATION

The strain energy is calculated as follows:

$$E_p = \int_V \left(\int \sigma_{ij}\, d\varepsilon_{ij} \right) dV \qquad (B.1)$$

From the Kirchoff assumption, ε_{13} and ε_{23} are zero. In addition, using the plane stress assumption, $\sigma_{33} = 0$. Since $\sigma_{ij} = \sigma_{ji}$, the integrand in (B.1) reduces to

$$\sigma_{ij}\, d\varepsilon_{ij} = \sigma_{11}\, d\varepsilon_{11} + 2\sigma_{12}\, d\varepsilon_{12} + \sigma_{22}\, d\varepsilon_{22}$$

Due to symmetry, the shear stress in cylindrical coordinates is zero,

$$\sigma_{12} = \sigma_{r\theta} = 0$$

leaving

$$\sigma_{ij}\, d\varepsilon_{ij} = \sigma_{11}\, d\varepsilon_{11} + \sigma_{22}\, d\varepsilon_{22}$$

Evaluating (B.1), assuming rigid-plastic material behaviour and a proportional stress state,

$$E_p = \int_{\frac{-t}{2}}^{\frac{t}{2}} \int_0^{2\pi} \int_0^R \left(\sigma_{\theta\theta}\, \varepsilon_{\theta\theta} + \sigma_{rr}\, \varepsilon_{rr} \right) r\, dr\, d\theta\, dz \qquad (B.2)$$

Strains in the radial and circumferential directions, respectively, are

$$\varepsilon_{rr} = \varepsilon_{rr_0}(r,\theta) + z\chi_r(r,\theta) \qquad (B.3)$$

and

$$\varepsilon_{\theta\theta} = \varepsilon_{\theta\theta_0}(r,\theta) + z\chi_\theta(r,\theta) \qquad (B.3)$$

For axisymmetric deformations, the terms in equations (B.3) become functions only of r. Thus equations (B.2) and (B.3) become

$$E_p = \int_0^{2\pi} \int_0^R \int_{\frac{-t}{2}}^{\frac{t}{2}} \sigma_y \left(\sigma_{rr}\, \varepsilon_{rr_0} + \sigma_{\theta\theta}\, \varepsilon_{\theta\theta_0} \right) r\, dz\, dr\, d\theta \qquad (B.4)$$

Integrating (B.4) over θ and z, while assuming $\sigma_{\theta\theta}$ and σ_{rr} are constant, gives

$$E_p = 2\pi t \int_0^R \left(\sigma_{rr}\, \varepsilon_{rr_0} + \sigma_{\theta\theta}\, \varepsilon_{\theta\theta_0} \right) r\, dr \qquad (B.5)$$

Thus the bending component cancels out of the equation.

For very large deflections

$$\varepsilon_{rr_0} = \frac{\partial u}{\partial r} + \frac{1}{2}\left[\left(\frac{\partial u}{\partial r}\right)^2 + \left(\frac{\partial w}{\partial r}\right)^2\right] \qquad (B.6)$$

and

$$\varepsilon_{\theta\theta_0} = \frac{u}{r} + \frac{1}{2}\left(\frac{u}{r}\right)^2 \qquad (B.6)$$

For simplicity it is assumed that u = 0, ie. there is no displacement in the radial direction

$$\varepsilon_{rr_0} = \frac{1}{2}\left(\frac{\partial w}{\partial r}\right)^2 \qquad (B.7)$$

and

$$\varepsilon_{\theta\theta_0} = 0 \qquad (B.7)$$

By substituting equations (B.7) into equation (B.5), the plastic strain energy then becomes

$$E_p = \pi t \int_0^R \sigma_{rr}\left(\frac{\partial w}{\partial r}\right)^2 r\,dr \qquad (B.8)$$

Utilising the Hencky deformation theory of plasticity that there is a one to one correspondence between stress and strain, the location on the yield surface in stress space can be determined as the intersection of the elastic radial line from the origin of stress space and the yield surface.

In the elastic region,

$$\varepsilon_{\theta\theta_0} = \frac{1}{E}\left(\sigma_{\theta\theta} - \upsilon\sigma_{rr}\right) \qquad (B.9)$$

But $\varepsilon_{\theta\theta_0}$ is assumed to be zero, see equation (B.7). Thus equation (B.9) becomes

$$\sigma_{\theta\theta} = \upsilon\sigma_{rr} \tag{B.10}$$

Invoking the von Mises yield condition that

$$\sigma_{rr}^2 - \sigma_{rr}\sigma_{\theta\theta} + \sigma_{\theta\theta}^2 = \sigma_y^2 \tag{B.11}$$

where σ_y is the yield stress in simple tension, and substituting (B.10) into (B.11)

$$\sigma_{rr} = \frac{\sigma_y}{\left(1 - \upsilon + \upsilon^2 \right)^{1/2}} \tag{B.12}$$

Equation (B.12) is substituted into equation (B.8) to give

$$E_p = \frac{\pi t\, \sigma_y}{\left(1 - \upsilon + \upsilon^2 \right)^{1/2}} \int_0^R \left(\frac{\partial w}{\partial r} \right)^2 r dr \tag{B.13}$$

A shape approximation function is then substituted into this equation and the plastic strain energy, ie. energy of deformation, of a plate will be obtained.

For a beam the following initial assumption is made

$$\sigma_{ij}\, d\varepsilon_{ij} = \sigma_{11}\, d\varepsilon_{11}$$

The radial yield stress then simply becomes

$$\sigma_{rr} = \sigma_y$$

Thus for a beam the plastic strain energy is given by

$$E_p = \frac{1}{2} B\ t\ \sigma_y \int_0^L \left(\frac{\partial w}{\partial r} \right)^2$$

where B = width of beam

L = length of beam

t = thickness of beam

APPENDIX C - DYNAMIC YIELD STRESS VALUES

$$\frac{I^2 \cdot 96421,8}{\sqrt{\sigma^1}} = 40 \cdot \left(\frac{\sigma^1_o}{\sigma_o} - 1 \right)^5$$

Note : The dynamic yield stresses have been calculated for plates, therefore the results refer only to the plate tests and the plate components of the stiffened plate tests.

Test No.	Impulse (N.s)	Dynamic Yield Stress σ^1_o (MPa)
P1	11,79	679,21
P2	7,03	603,97
P3	19,83	770,78
P4	10,00	653,67
P5	22,24	793,44
P6	13,61	702,77
P8	19,55	768,03
PS1	14,66	715,46
PS2	22,00	791,80
PS8	16,46	735,94
PS11	18,34	755,88
PS12	9,18	641,01
PS13	20,48	777,05
PS14	20,11	773,49
PS15	19,15	764,07
PS16	11,97	681,63
PS17	21,18	783,67
PS18	24,65	814,59
PS19	18,22	754,65
PS20	10,40	659,62
PS21	26,48	829,80
PS25	20,09	773,30
PS27	8,83	635,38
PS28	18,51	757,62

Test No.	Impulse (N.s)	Dynamic Yield Stress σ_o^1 (MPa)
PS29	11,48	674,97
PS30	17,95	751,85
PS31	10,27	657,70
PS32	24,61	814,26
PS36	16,06	731,52
PS37	20,13	773,69
PS38	17,24	704,86
PS39	21,88	790,16
PS40	22,18	792,89
PS41	12,28	685,76
PS49	10,66	663,4
PS50	9,02	638,45
PS52	24,21	810,84
PS55	10,46	660,49
PS56	25,55	822,16
PS63	17,81	750,39
PS65	26,23	827,77
PS66	9,55	646,81
PS67	4,17	541,25
PS68	7,27	608,43
PS75	10,31	658,29
PS76	10,40	659,62
PS78	7,03	603,97
PS86	7,09	605,09
PS87	21,25	784,33
PS88	9,96	653,07
PS89	11,58	676,34
PS90	10,92	667,13
PS91	9,15	640,53
PS92	9,71	649,27
PS93	27,32	836,56
PS94	11,27	672,06
PS95	25,67	823,16

APPENDIX D - IMPACT VELOCITY OF BEAM SPECIMEN

M = mass of ballistic pendulum

m = mass of beam test specimen

V = initial velocity of ballistic pendulum

V_0 = impact velocity of beam

s = distance between centre of gravity of ballistic pendulum and its suspension plane

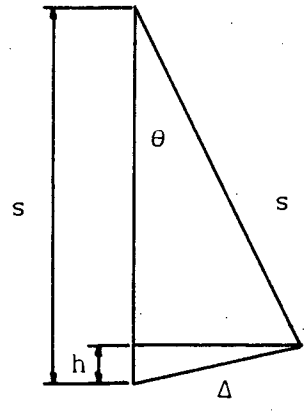

FIGURE B.2 MOTION OF BALLISTIC PENDULUM

i) from Conservation of Momentum:

$$MV = mV_o \quad \Rightarrow \quad V_o = \frac{M}{m} V \tag{1}$$

ii) from Conservation of Energy:

$$\frac{1}{2} MV^2 = Mgh \quad - \quad (2)$$

where $h = s - s \cdot \cos\theta$

$$= s \cdot \left(2\sin^2 \frac{\theta}{2} \right)$$

$$\Rightarrow \quad V^2 = 2gh = 4gs \cdot \sin^2 \frac{\theta}{2} \tag{3}$$

substituting (3) into (1) : $V_o = \frac{M}{m} \sqrt{4gs \cdot \sin^2 \frac{\theta}{2}}$

for small angles $\sin\theta \approx \theta$

$$\Rightarrow \quad V_o = \frac{M}{m}\,\theta\,\sqrt{gs}$$

now want V_o in terms horizontal displacement Δ :

$$V_o = k\Delta \quad \therefore k = \frac{M}{m}\sqrt{\frac{g}{s}} \qquad \text{because } \Delta = s\theta$$

$$\underline{\Rightarrow \quad V_o = \frac{M}{m}\sqrt{\frac{g}{s}}\,\Delta}$$

APPENDIX E - LEAST SQUARES LINES

P :	$\delta = 0.929\ I + 0,622$	$r = 0,991$
PS-6P :	$\delta = 0,744\ I - 1,651$	$r = 0,952$
PS-6S :	$\delta = 0,754\ I - 0,679$	$r = 0,942$
PS-5P :	$\delta = 0,719\ I - 0,989$	$r = 0,973$
PS-5S :	$\delta = 0,726\ I - 0,009$	$r = 0,977$
PS-4P :	$\delta = 0,657\ I + 0,555$	$r = 0,973$
PS-4S :	$\delta = 0,647\ I + 2,317$	$r = 0,976$
PS-3P :	$\delta = 0,775\ I - 0,557$	$r = 0,989$
PS-3S :	$\delta = 0,765\ I + 0,889$	$r = 0,995$
B-6 :	$\delta = 0,941\ I - 3,677$	$r = 0,938$
B-5 :	$\delta = 1,101\ I - 2,269$	$r = 0,995$
B-4 :	$\delta = 1,037\ I + 0,796$	$r = 0,988$
B-3 :	$\delta = 1,172\ I + 2,377$	$r = 0,993$

APPENDIX F

Courses completed for the partial fulfilment of the requirements for the degree of Master of Science.

		CREDITS
END 520Z -	APPLIED MECHANICS I	3
END 521Z -	APPLIED MECHANICS II	3
END 522Z -	AN INTRODUCTION TO FINITE ELEMENTS	3
END 523Z -	FINITE ELEMENT ANALYSIS	4
CIV 593Z -	ENGINEERING SOFTWARE DESIGN AND DEVELOPMENT	3
CIV 525Z -	CONTRACT LAW	2
AMA 367Z -	CONTINUUM MECHANICS	3
	TOTAL :	21